REGULATION OF DROSOPHILA NEURAL CIRCUIT ASSEMBLY BY CELL SURFACE MOLECULES

by

EMILY CELESTINA SALES

A DISSERTATION

Presented to the Department of Biology
and the Graduate School of the University of Oregon
in partial fulfillment of the requirements
for the degree of
Doctor of Philosophy

September 2019

DISSERTATION APPROVAL PAGE

Student: Emily Celestina Sales

Title: Regulation of Drosophila Neural Circuit Assembly by Cell Surface Molecules

This dissertation has been accepted and approved in partial fulfillment of the requirements for the Doctor of Philosophy degree in the Department of Biology by:

Bruce Bowerman	Chairperson
Chris Doe	Advisor
Adam Miller	Core Member
Shawn Lockery	Core Member
Tory Herman	Core Member
Matt Smear	Institutional Representative

and

Janet Woodruff-Borden	Vice Provost and Dean of the Graduate School

Original approval signatures are on file with the University of Oregon Graduate School.

Degree awarded September 2019

DISSERTATION ABSTRACT

Emily Celestina Sales

Doctor of Philosophy

Department of Biology

September 2019

Title: Regulation of Drosophila Neural Circuit Assembly by Cell Surface Molecules

Nervous systems assemble with remarkable organization and precision. Developmental mechanisms ensure that neurons identify and form specific synapses with the correct set of neurons at the appropriate subcellular locations. This precise connectivity determines how information flows within circuits and defines key aspects of neural circuit function. Understanding the molecular mechanisms that underlie synapse specificity has the potential to provide insight into neurodevelopmental disorders and their etiology, and to inform the development of treatments. Cell surface molecules (CSMs) are well positioned to regulate synaptic partner choice and have emerged as key regulators of axon guidance, cell recognition, and synapse formation. To better understand synapse specificity, it is critical to characterize CSM function and their roles in neural development. Here, I describe a model system designed to identify CSMs, or other classes of genes, that regulate synapse specificity in pairs of larval *Drosophila* neurons. Using this model system, I investigated the role of Dpr/DIP genes, cell adhesion molecules in the immunoglobulin family, in synapse formation. Furthermore, I explored the role of axon guidance molecules, Robo-2 and Unc-5, in the subcellular positioning of synapses in these neurons, and explored the contribution of dendritogenesis in the

regulation of synapse specificity. This dissertation contains previously published co-authored material (Chapter IV).

CURRICULUM VITAE

NAME OF AUTHOR: Emily Celestina Sales

GRADUATE AND UNDERGRADUATE SCHOOLS ATTENDED:

University of Oregon, Eugene, OR
University of California, Santa Cruz, CA

DEGREES AWARDED:

Doctor of Philosophy, Neuroscience, 2019, University of Oregon
Bachelor of Science, Neuroscience, 2013, University of California, Santa Cruz

AREAS OF SPECIAL INTEREST:

Developmental Biology
Cellular Neuroscience

PROFESSIONAL EXPERIENCE:

Operations Assistant, Adipogen International, 1 year

GRANTS, AWARDS, AND HONORS:

Gilliam Fellowship for Advanced Study, Establishing synaptic specificity in the *Drosophila* Central Nervous System: the role of Dpr/DIP proteins, Howard Hughes Medical Institute, 2016

Graduate Research Fellowship Honorable Mention, Establishing synaptic specificity in the *Drosophila* Central Nervous System: the role of Dpr/DIP proteins, National Science Foundation, 2016

Promising Scholar Award, University of Oregon Graduate School, 2014

PUBLICATIONS:

Sales, E. C., Heckman, E. L., Warren, T. L., and Doe, C. Q. (2019), Regulation of dendritic synapse specificity by axon guidance cues. Elife

Sweeney, N. T., James, K. N., **Sales, E. C.**, and Feldheim, D. A. (2015), Ephrin-As are required for the topographic mapping but not laminar choice of physiologically distinct RGC types. Devel Neurobio, 75: 584–593. doi:10.1002/dneu.22265

TABLE OF CONTENTS

LIST OF FIGURES

Figure Page

LIST OF TABLES

CHAPTER I

INTRODUCTION

Assembling neural circuits with cellular and subcellular precision

Nervous systems function to control animal behavior and are composed of many interconnected neurons. Throughout development, genetic programs ensure nervous systems assemble properly. Neural stem cells generate many different types of neurons, which then incorporate into neural circuits by forming specific synapses, specialized junctions that facilitate cell communication, with particular sets of neurons. Neural circuits also show remarkable subcellular synaptic specificity, where neurons form synapses on particular subcellular domains of their synaptic partners. The connectivity between neurons, or neural circuit architecture, dictates key aspects of information processing within neural circuits.

Specific neural circuit functions are determined, in part, by the specific patterns of connectivity between neurons. For example, in vertebrates, the reflex arc circuit mediates a quick behavioral response to avoid a noxious stimulus. First, a sensory neuron detects a painful stimulus and sends information to small interneuron in the spinal cord. The interneuron then activates a motor neuron, which then pulls the limb away from the stimulus. This connectivity pattern, by avoiding higher processing centers in the brain, ensures a rapid and specific behavioral output. A second example shows that the subcellular positioning of synapses across neurons also impacts neural function. The CA1 pyramidal neurons in mice receive input from several neuron types, with certain inputs localized to particular subcellular domains. Modeling work has shown that inputs to different subcellular domains of CA1 differentially affect firing rate, with distal synapses having a larger impact compared to proximal synapses (Bloss et al., 2016). Functioning neural circuits rely upon synaptic connectivity with precision on the cellular and subcellular scales.

When neural connectivity is established improperly, aberrant behaviors can emerge. Many neural developmental disorders, such as Autism Spectrum Disorders (ASD) and schizophrenia, are related to synapse formation (Washbourne, 2015). Many

genes associated with ASD have synaptic functions (Giovedí et al., 2014). For example, members of the neuroligin and cadherin gene families, which function as synaptic cell adhesion molecules, and potassium gated voltage channel genes, which regulate neuronal excitability, have been associated with ASD. While these complex neural developmental disorders etiologies are not yet clearly defined, the genetic and behavioral changes associated with these disorders suggest that synaptic connectivity is abnormal. Further, therapies to effectively treat neural developmental disorders are currently lacking, as the genetic programs underlying normal neural connectivity are not well understood.

Significance

Understanding the genetic basis of neural circuit assembly has medical and social importance. It is critical for alleviating the burden of neural disorders on patients, caregivers and on society. For example, in a 2014 study, students with intellectual disabilities were 9% less likely to graduate from United States high schools (Allensworth et al., 2016), a well described predictor of health and life expectancy (Rostron et al., 2010). People with mental illness are overrepresented in prisons and jails, with three times more persons incarcerated than in hospitals (Fuller et al., 2010). The homeless population in the United States also has an overrepresentation of people with mental disorders, with 26.2% of sheltered people with a severe mental illness compared to the national average of 4.5% (Merikangas et al., 2010; Samhsa, 2009). Mental illness healthcare expenditures are costly, with an estimated $57.5 billion spent nationally in 2006 and individuals spending a 25% rate of out-of-pocket expenses, a remarkable burden for caretakers and families (Soni, 2009). Better understanding of the underlying disease mechanisms, both genetic and environmental factors such as education and judicial systems, could lead to better disease treatment through the identification of drug targets, novel biomarkers for early disease detection or progression.

Furthermore, understanding developmental mechanisms of circuit assembly could lead to the treatment of non-developmental circuit related conditions, such as traumatic brain injury or neurodegenerative disease. For example, encouraging developmental genetic programs may allow for regeneration of a neural circuit to replace one that has been lost due to an injury (i.e. spinal cord trauma followed by regeneration). Encouraging

early developmental synaptogenesis programs could also stifle deleterious effects of neurodegeneration. A thorough understanding of the relationship between genetic programs that instruct nervous system assembly and overall neural circuit function will lead to a better understanding of both developmental and regenerative processes.

Once the relationships between genetic programs and neural circuit function are defined, the generation of novel neural networks, either biological or computational, would be feasible, transforming technology, medicine, and society. The discipline of artificial intelligence, which is rooted in neuroscience, continues to apply neuroscience principles to generate more robust artificial neural networks. For example, advancements in artificial neural networks, such as deep learning algorithms, have enabled novel robust image recognition (i.e. self-driving cars and skin cancer diagnoses) and have impacted the analyses of financial markets (i.e. capital asset pricing models). Science fiction media has explored futures in which humans have the knowledge to generate biological neural circuits. For example, the movie "Blade Runner 2049" (2017) comments on the impacts of bio-engineered humans and explores ideas of perception, identity, power, and what it means to be human. While understanding neural circuit assembly has the potential to improve quality of life through the transformation of technology and medicine, it is critical to consider the ethical and biological implications of neural circuit generation, and its use by individuals, corporations, and governments.

Despite the dangerous potential of bioengineering, better characterization of neural circuit assembly can help individuals and society. This knowledge has the potential to describe the etiologies of nervous system related disorders and aid in the generation of novel therapeutics. The basic understanding of nervous system development can also lead to societal changes; such as informing police enforcement practices, developing effective education programs, or improving healthcare related practices. Defining the relationship between genetic programs and neural circuits will transform society, inform humans understanding of themselves, and redefine human advancement.

Towards the identification of synapse specificity genes

The assembly of neural circuits requires that developing neurons interact with their environment. Neurons must navigate through complex biological territories to reach and form synapses with the correct synaptic partners. Cell surface molecules (CSMs) are the interface between neurons and their surroundings, positioned to allow neurons to 'sense' their environment, communicate with neighboring cells, and traverse biological landscapes. Not surprisingly, the evolution of complex multicellular organisms was accompanied by the vast expansion of CSM genes, allowing for the development of morphologically sophisticated heterogeneous tissues, such as neural circuits (Cheng et al., 2019; Vogel & Chothia, 2006). CSMs have emerged as regulators of neural circuit assembly by playing critical roles in axon guidance, cell recognition, and synapse formation (reviewed in Washbourne, 2004; Yogev & Shen, 2014).

It has been challenging to comprehensively characterize how CSM genes regulate synapse specificity. Eliminating gene function completely using whole animal mutants, risks compromising overall neural circuit development and function making it difficult to parse out the gene's distinct role in cellular mechanisms. For example, without temporal resolution to eliminate gene function at particular developmental stages, it is difficult to determine if genes are required for axon guidance, initial synapse assembly, or maintenance of established synapses. And because neural circuits are highly interconnected, loss of gene expression could lead to compensatory mechanisms across the entire circuit, obscuring gene function.

It can also be difficult to label cells of interest and observe their synaptic connectivity preferences. Many studies rely upon dye labeling or genetic labeling techniques that mark massive populations of unidentified, and often uncharacterized neuron types. Often without single cell resolution, researchers are left to assay general synaptic target regions (e.g., layers in the optic lobe of *Drosophila*, or general brain regions in the mouse cortex). Additionally, the inability to label specific synapses, especially in the central nervous system when neuronal processes are packed and intermingled, has limited studies. Due to these technical limitations, the genetic programs underlying synaptic connectivity (e. g., synaptic partner choices or synapse numbers) remain elusive.

Despite these technical challenges, some mechanisms that govern synapse specificity have emerged in recent years. Work in *C. elegans* and *Drosophila* has pioneered the identification of specificity genes through rigorous genetic analyses in defined populations of cells (Christensen et al., 2013). Many of these studies took advantage of peripheral neurons (e. g., motor neurons), whose morphology and synaptic connectivity can be easily identified due to their physical isolation from other neurons. Laminated structures, such as the optic lobe in *Drosophila*, have also been fruitful in identifying synapse specificity genes due to the ability to observe changes to a neuron's innervation layer upon gene manipulation. While these model systems are advantageous in many ways, peripheral nervous system assembly or laminated circuit assembly may not recapitulate circuit assembly in other types of circuit architectures, such as spinal cord assembly or cortical assembly.

Here, with the aim of identifying additional synapse specificity genes, I define a model system in the larval ventral nerve cord of *Drosophila* that allows for the identification of genes that are necessary or sufficient for synapse formation in defined, single-pair, pre- and post-synaptic partners. By combining the genetic labeling of individual neurons and their synapses, light microscopy image acquisition and analyses, and gene manipulation, I was able to assess the role of genes in synapse formation and neuronal morphology. Using this system, I investigated the role of *defective in proboscis extension response (dpr)* genes in synapse formation and did not identify a synaptic function for these genes. Then, using the same model system, I investigated the role of axon guidance cues in subcellular synaptic specificity, and report that axon guidance cues, Robo-2 and Unc-5, are major determinates of synaptic specificity within the dendrites of my model neurons, dbd and A08a.

CHAPTER II

METHODOLOGY TO IDENTIFY SYNAPSE SPECIFICITY GENES

Rationale and strategy:

The achievement of synapse specificity in developing neural circuits requires the orchestration of many biological processes, including axon guidance and activity dependent pruning of synapses. Synapse specificity genes, regardless of which step in the biological process they may participate, are necessary for synapse formation. For example, if a gene is required for synapse specificity between a pair of neurons, then removal of that gene should lead to a loss of synapse formation between those neurons. Importantly, while some genes may be important for the development of all synapses, others may regulate synapse formation between a neuron and only one of its synaptic partners; thus, loss of gene function would result in a specific loss of those synapses, while the remaining synapses are left intact. The ability to screen for this phenotype, instead of screening for genes that impact overall synapse formation likely due to defects in overall cell health, would be helpful in identifying genes that are specific for synaptic partner choice.

Axon guidance cues are necessary for neurons to traverse an immensely complex nervous system to the same location as their synaptic partners; but once there, how do they recognize one another? One might predict that there is a cell-recognition event between a pair of neurons where neurons identify their appropriate synaptic partners preceding synapse formation. For example, binding of "matching" CSMs could result in the recruitment of synaptic proteins to the site of membrane contact, much like the chemoaffinity hypothesis proposed by Sperry (reviewed in Meyer, 1998; Sperry, 1963). If this were the case, then one might predict that misexpression of "matching", or binding, CSMs in pairs of non-synaptically coupled neurons would act like a "lock and key" and result in ectopic synapse formation.

I designed a model system to screen candidate genes for their requirement in synaptic specificity during CNS development. The requirements for this model system were to: 1) genetically access individual neurons to enable the visualization of neuron

membranes and synapses and manipulate CSM expression, and 2) quickly visualize and quantify changes in synaptic connectivity upon gene manipulation. To this end, using a pair of synaptically coupled neurons in the *Drosophila* ventral nerve cord, I can test which genes are necessary for synapse formation. If I knockdown gene expression from either the pre- or post-synaptic partner neurons (A or B) by expressing RNA interference (RNAi) constructs and then observe a loss of synapse formation, then that gene is required for synapse formation between neurons A and B (Figure 2.1, left). On the other hand, using a pair of non-synaptically coupled neurons (A and C), I can test which genes are sufficient for synapse formation by misexpressing genes in either neuron (Figure 2.1, right). If I misexpress genes in either neuron A or C, and observe an artificial synaptic coupling of these neurons, then that gene is sufficient for synapse formation. Using these complementary approaches, I can identify genes that are either necessary or sufficient for synapse formation.

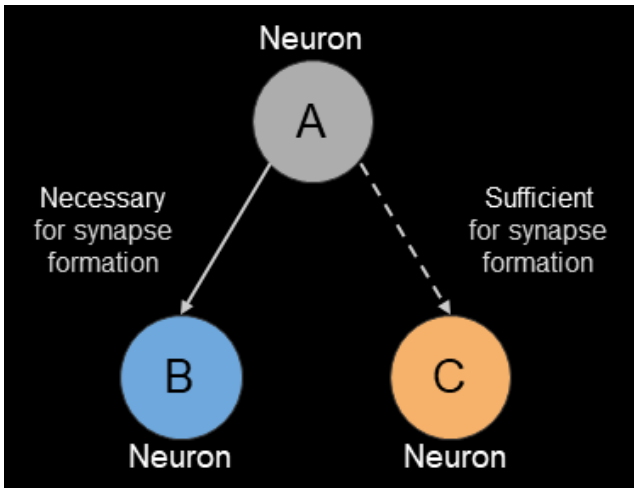

Figure 2.1. A model system to identify synapse specificity genes. Synaptically coupled neurons (A and B, left) can be utilized to identify genes necessary for synapse formation. If knockdown of a particular gene in neuron A or B via expression of an RNAi construct results in loss of synapse formation, then that gene can be identified as necessary for synapse formation between neurons A and B. Non-synaptically coupled neurons (A and C) can be utilized to identify genes that are sufficient for synapse formation. If misexpression of a particular gene via expression of a cDNA construct results in artificial synapses between neurons A and C, then that gene can be identified as sufficient for synapse formation.

Gaining genetic access to individual neurons

The first step in generating the model system was identifying neurons with the appropriate connectivity and sufficient genetic tools. I needed to identify pairs of synaptically coupled and non-synaptically coupled neurons, where each individual neuron had available genetic tools, including Gal4 and LexA binary expression systems. These Gal4 and LexA tools would enable the labeling of two different neurons with distinct fluorophores. The larval *Drosophila* ventral nerve cord was an attractive system because of the existence of an electron microscopy (EM) reconstruction database (Saalfeld et al., 2012), which described the connectivity between neurons within an early larval central nervous system, and the large collection of Gal4 and LexA lines to genetically access neurons. This strategy allowed me to identify one pair of synaptically coupled neurons (dbd→A08a) (Figure 2.2) and four pairs of non-synaptically coupled neurons (dbd-A27j, dbd-A27l, A08a-A27j, and A08a-A27l) that are in close proximity but are not synaptically coupled (Figure 2.3). The morphology of these neurons observed at the light microscopic level qualitatively matched the morphology in the electron microscopy dataset (Figure 2.4).

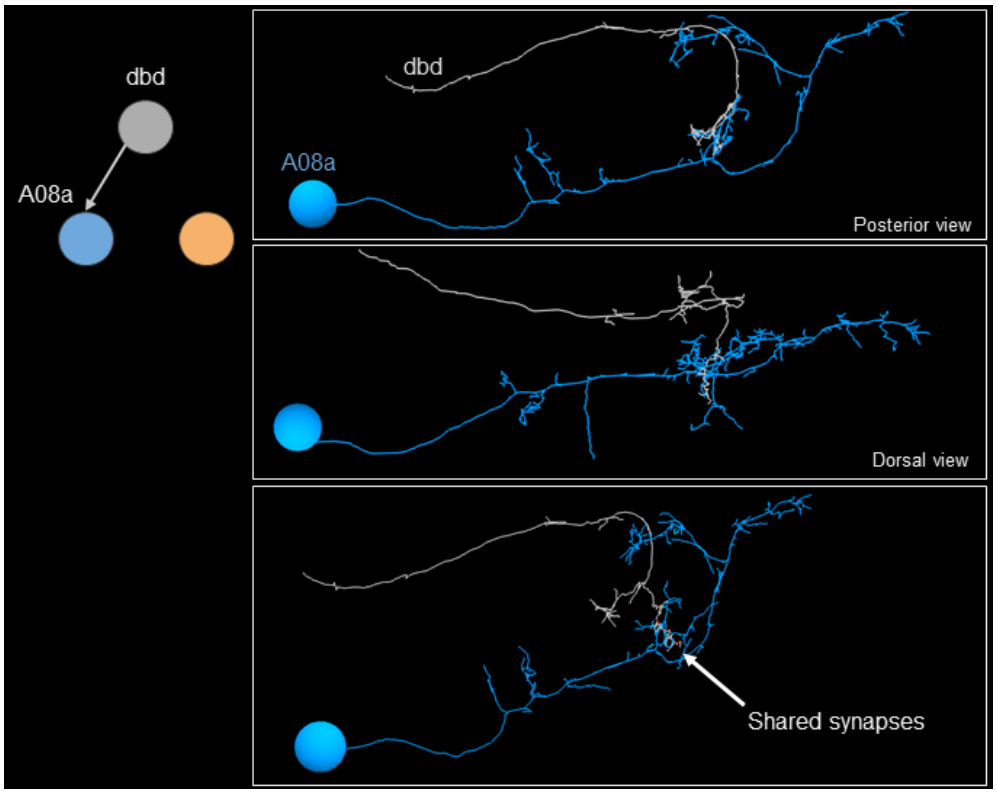

Figure 2.2. dbd and A08a are synaptic partners. Electron microscopy reconstructions show the dbd sensory neuron contacts the membrane of A08a interneurons (posterior view, top panel; dorsal view, middle panel). dbd-A08a synapses are labeled by red ticks (bottom panel).

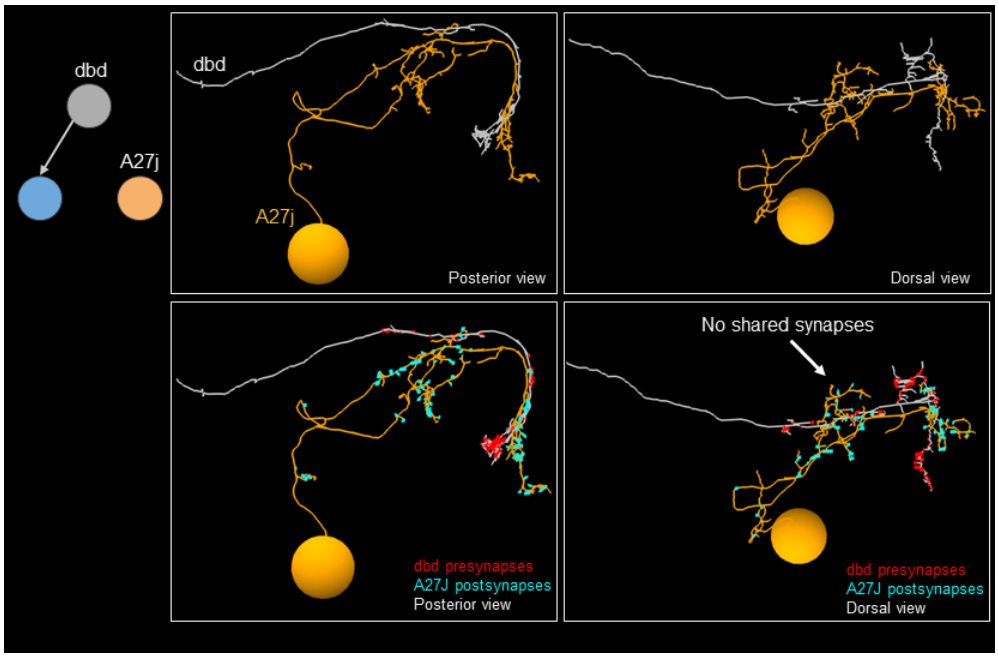

Figure 2.3. dbd and A27j are not synaptic partners. Electron microscopy reconstructions show the dbd and A27j neuron membranes are in close proximity, but not touching (top left panel, posterior view; top

right panel, dorsal view). dbd pre-synapses are in close proximity to A27j postsynapses (bottom panels), which makes them a good neuron pair to artificially induce synapse formation.

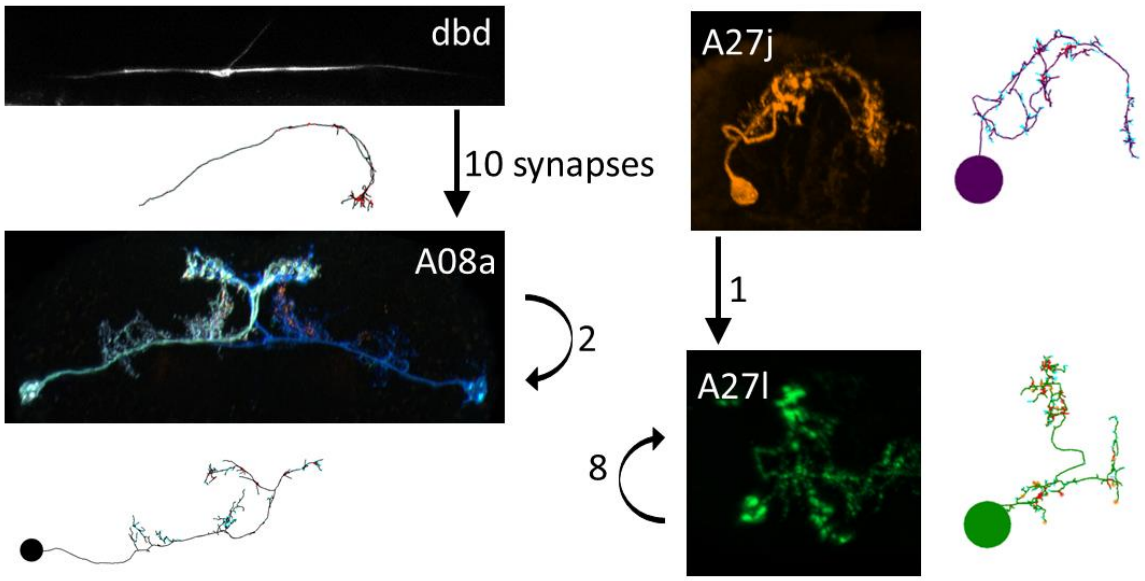

Figure 2.4. Morphology and synaptic connectivity of model neurons dbd, A08a, A27j, and A27l. dbd neurons form ~10 synapses with A08a in each hemisegment (left). A08a neurons from the left hemisegments form ~2 synapses with A08a on the right hemisegments (lower right). A27j forms ~1 synapse with A27l (right). A27l forms ~8 synapses with A27l in an anterior hemisegment. Light micrographs show morphology of neurons are similar to the morphology of neurons in the EM reconstruction.

Labeling neuron membranes and synapses

To quantify synaptic connectivity between pairs of neurons, I sought to label individual neurons and their shared synaptic contacts. I labeled the individual neuron membranes and the pre-synaptic neurons' sites, then I assayed for proximity between the pre-synaptic sites and the post-synaptic neurons membranes. Although the proximity of these two signals does not ensure there is actual synaptic connectivity between these neurons, it allows for a faster identification of potential synapse specificity genes.

In order to label the neuron membranes, I used the neuron Gal4 and LexA lines to drive expression of myristolated epitope tags, namely *UAS-myr::mGDP-HA* and *LexAop-myr::smGDP-V5* tags respectively (Figure 2.5). The advantage to this strategy is that the covalently linked myristolated tag will localize the chimeric protein to the inner leaflet of

the plasma membrane (Van't Hof & Resh, 2000), which might be less disruptive to cell surface molecule binding than if placed on the outside of the cell. The myristolated sequence is attached to a *spaghetti monster Green Dark Protein (smGdP)* sequence, a variant of green fluorescent protein that does not have a fluorophore but localizes well to fine neural processes (Pfeiffer et al., 2010; Viswanathan et al., 2015). And finally, the *HA* and *V5* tags are short polypeptide sequences with high-affinity antibodies readily available.

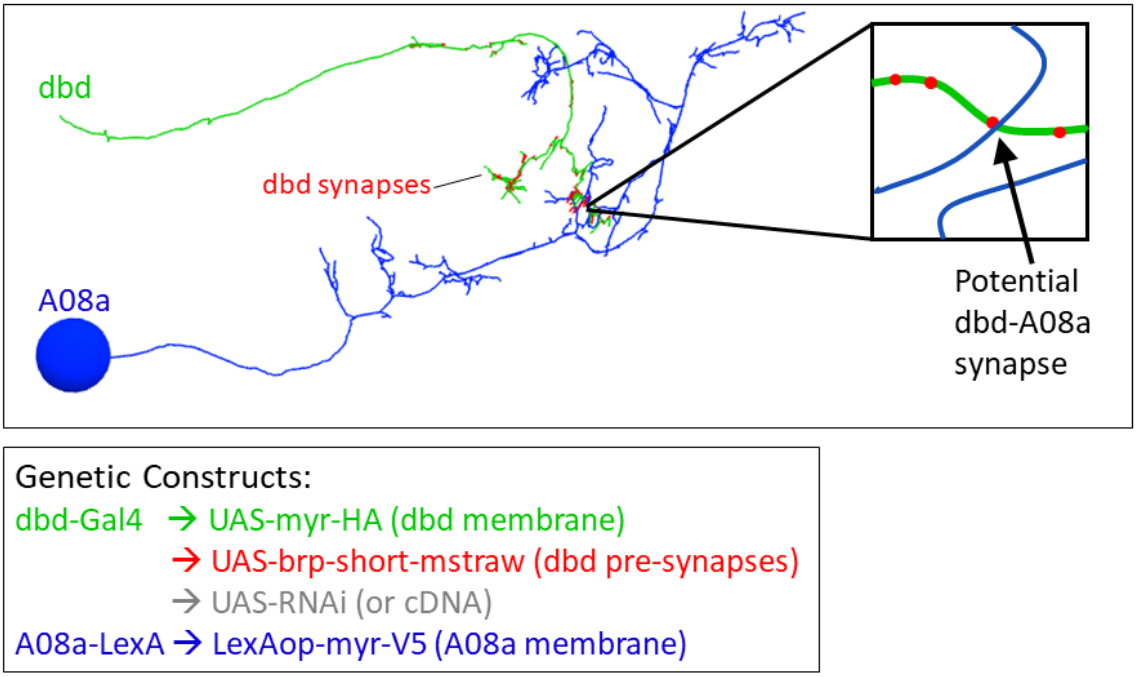

Figure 2.5. Genetic strategy to label A08a membrane, dbd pre-synapses, and dbd membrane. EM reconstruction shows dbd neuron skeleton (green), dbd presynaptic sites (red), and A08a skeleton (blue). Inset (top panel, right) shows a schematic of potential dbd-A08a synapses, where dbd presynaptic sites are in close proximity to A08a membrane. Genetic constructs (bottom panel) can be used to label these structures for subsequent light microscopy image acquisition.

In order to label the pre-synaptic neuron sites, I used the neuron *Gal4* and *LexA* lines to drive expression of a truncated presynaptic protein gene construct labeled with a fluorophore, namely *UAS-bruchpilot-short-mstrawberry (brp-short-mstraw)* and *LexAop-brp-short-mcherry* respectively. The advantage to this system is that the truncated form of Brp can still localize to presynaptic sites, but expression of this construct in a *brp* null

background does not rescue synapses, suggesting that it is not functional (Fouquet et al., 2009). This is an important feature because if a gene required for synapse formation is removed, then overexpression of a functional synaptic protein may rescue the phenotype and therefore obscure the role of that gene in synapse formation. Notably, while the Brp-short-mstraw localized to pre-synaptic sites, there also was faint expression in the cytosol of dbd neurons, suggesting that some proteins were not targeted properly. This localization pattern could be due to an overabundance of Brp-short-straw resulting from overexpression, or possibly, newly synthesized proteins getting transported to the synaptic terminals. This faint expression was mostly disregarded in the image analyses pipeline (see below).

In summary, these genetic strategies enable the synaptic and membrane labeling of neuron pairs, either synaptically coupled or non-synaptically coupled. This strategy is also amendable to gene manipulation, allowing for the identification of genes that not only instruct synapse specificity, but more generally regulate synapse formation.

Manipulating gene expression in individual neurons

As aforementioned, the goal of this model system was to identify genes that are necessary or sufficient for synapse formation between pairs of neurons. My strategy was to a) artificially couple normally non-coupled neurons and b) to uncouple normally coupled neurons by manipulating expression of genes that are key to synapse formation. In order to manipulate gene expression, I expressed *UAS* controlled *RNAi* and *cDNA* constructs in individual neurons (Figure 2.5). The advantage to this strategy is that I can manipulate gene expression in individual neurons, while leaving the rest of the nervous system relatively intact. The *Gal4* and *LexA* drivers used in these studies were quite sparse, though there was sometimes 'off-target' expression in other neurons or different cell types in the animal. The other advantage to this system is temporal control of gene expression. Depending on when the enhancers or promoters are active, Gal4 will be produced which can then drive expression of RNAi or complementary DNA constructs. For example, the *dbd-Gal4* driver is expressed in dbd before axon extension, while the A08a driver is expressed after the final cell morphology has been determined. In addition to timing of these drivers, it is possible to couple the heat shock controlled Gal80 to the

Gal4-UAS system prevent UAS activity and further control temporal expression of genetic constructs.

Assembling the genetic toolkit

Once I identified neurons that had the appropriate connectivity and genetic tool requirements for the model system, I assembled the genetic components into the fly genome. In order to identify synapse specificity genes rapidly, I needed to add all of the genetic components to one fly, then outcross this fly to either a fly stock containing *UAS-RNAi* or *UAS-cDNA* (overexpression constructs). For example, for the synaptically coupled pair, dbd and A08a, I put all five genetic constructs into one fly, then in one cross, could add the RNAi or overexpression construct (Figure 2.5, bottom panel). In order to test gene function in the context of all neuron pairs (both synaptically and non-synaptically coupled), I generated flies containing all possible combinations of neuron Gal4 and LexA with membrane and synaptic reporters.

Preparing tissue for imaging

After dissecting animals with RNAi or overexpression constructs, I needed to label the neuron membranes and synapses with fluorescently tagged antibodies. Once the tissue was stained, I needed to clear the tissue for imaging, as biological structures are difficult to resolve in the dense, thick, larval nerve cord neuropil. I used the DPX tissue clearing strategy, which involves tissue dehydration, to bring the refractive index of the nerve cords to 1.52, similar to the refractive index of glass. The DPX tissue clearing process does result in changes in tissue size, namely non-isomorphic shrinkage, and results in fluorescence quenching. Despite these downsides, the DPX protocol permitted the high-resolution imaging of neurons and synapses in the larval ventral nerve cord.

Imaging the nerve cords on the microscope

Once the tissue was cleared, I imaged the samples on a point scanning confocal microscope, which allowed me to take thin optical sections throughout the sample and assemble a 3D image of the nerve cords. A critical component of the image acquisition was to assign the appropriate pixel size, which informs the image analyses pipeline (see

below). As mentioned before, I wanted to identify the amount of presynaptic material in close apposition to the post-synaptic neuron membranes. In other words, I wanted to ask, how many voxels containing pre-synaptic material are near voxels containing post-synaptic membrane material? This required me to set a distance threshold between the pre-synaptic marker and the post-synaptic membrane, to assign potential sites of synaptic connectivity, which I termed "putative synapse voxels" (Figure 2.6). Assigning this distance threshold required me to consider two important aspects, the size of the synaptic cleft and the amount of chromatic aberration between the two colors that label the pre-synaptic sites and the post-synaptic membrane (Figure 2.6A, B). The sum of these two distances would be a reasonable threshold to assign putative synapse voxels. Previous electron microscopy studies have shown that the synaptic cleft is about 20nm (Zhan et al., 2016). In order to measure the chromatic aberration between the two channels I was imaging in the ventral nerve cord, I labeled the pre-synaptic sites with two fluorescently labeled secondary antibodies, 488nm and 555nm. Although I labeled the same structures with the two different wavelengths, they appear to be in different locations due to chromatic aberration in the microscope (Figure 2.6C, D). I performed a line scan across individual synaptic sites, fitted a curve to estimate the location of peak signal intensity, and measured the distance between these two peaks to be around 70nm (Figure 2.6D', D''). Taken together with the size of the synaptic cleft, I assigned a distance threshold criterion of 90nm to assign putative synapse voxels. Therefore, I assigned a pixel size of 90nm on the image acquisition settings to support the image analyses pipeline.

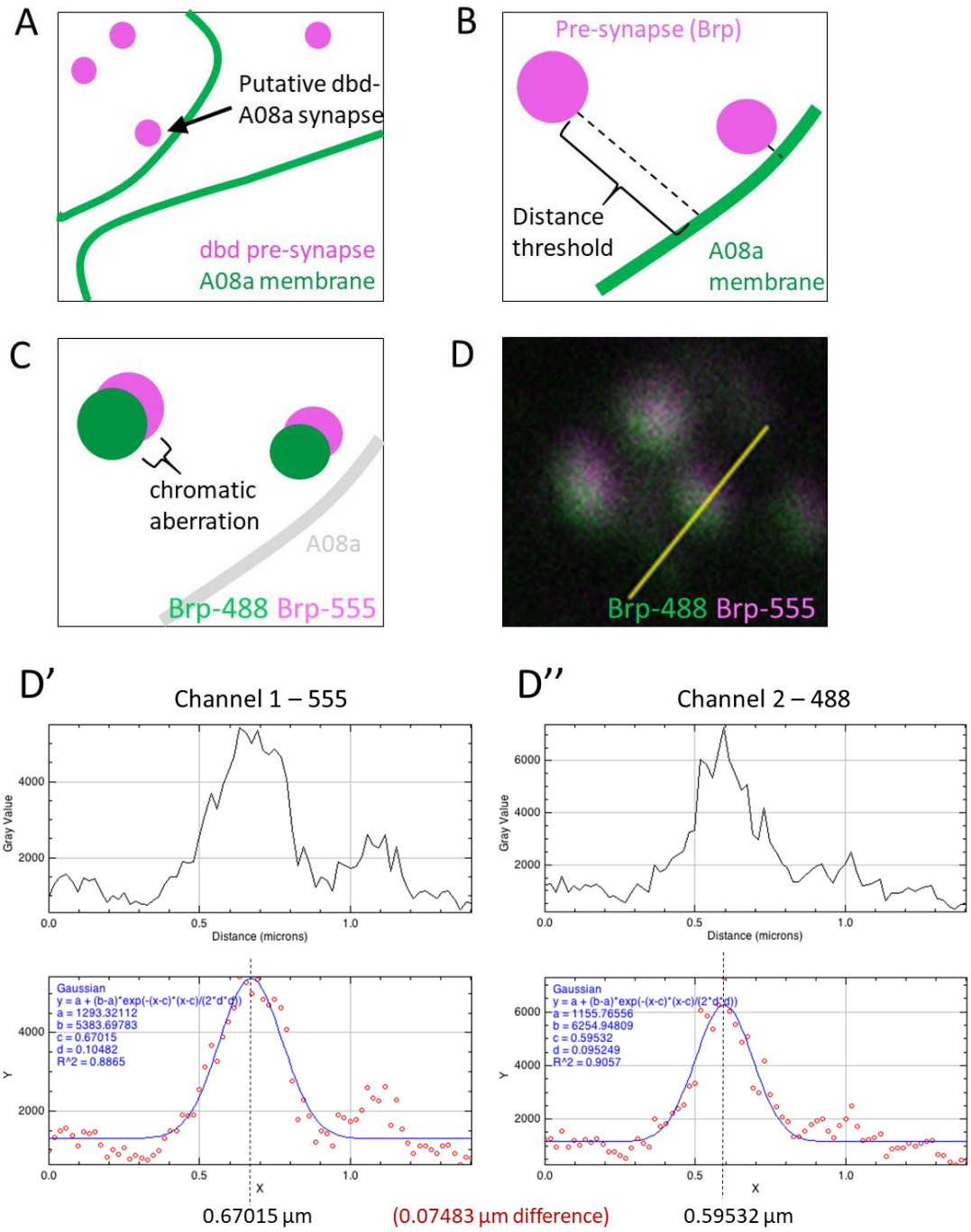

Figure 2.6. Measurement of chromatic aberration between 488nm and 555nm fluorophores. A) Schematic showing dbd pre-synapses (Brp, magenta) and A08a membrane (green). Some dbd synapses are far away from A08a membrane, suggestive of synaptic contacts with other neurons. Some dbd synapses are in very close proximity to A08a, suggestive of a putative dbd-A08a synaptic contact. B) The appropriate distance threshold between dbd pre-synapses and A08a membrane labels must be assigned to identify putative dbd-A08a synaptic contacts. C) Schematic showing chromatic aberration between the channels (488nm and 555nm) used to label the dbd pre-synapses and the A08a membrane. To measure the amount of aberration, Brp-short-mstraw was labeled by both 488nm and 555nm. D) Micrograph showing diffraction

limited Brp-short-mstraw positive pre-synapses labeled in 488nm and 555nm. D'-D'') A line scan was performed across an individual Brp-short-mstraw positive pre-synapse (top panels). To identify the location of each diffraction limited spot, a gaussian curve was fitted to estimate the location of maximum voxel intensity (bottom panels). The distance between these two maxima was calculated (~70nm).

Quantification of putative synapse voxels

In order to determine if changes in gene expression resulted in changes in synaptic connectivity, I needed to measure the amount of putative synapse voxels across different experimental conditions for each synaptic pair (Figure 2.7). I first identified the voxels, or 3D pixels, that contain intensity in the pre-synaptic channel by assigning a threshold (Figure 2.8A, C). The FIJI thresholding toolkit (ImageJ 1.50d, https://imagej.net/Fiji) was not suitable for assigning relevant thresholds (data not shown), most likely due to the nature of the pixel intensity distribution (i.e. not binary in nature), so manual thresholding was required. Then, I assigned a threshold to the post-synaptic membrane channel (Figure 2.8B, D). In order to identify the amount of pre-synaptic containing voxels within 90nm, or one voxel length away from the post-synaptic membrane containing voxels, I dilated the segmented pre-synaptic channel one iteration (Figure 2.8E) and then asked how many of the voxels in this channel overlapped with voxels in the segmented post-synaptic membrane channel (Figure 2.8F). This gave me the putative synapse voxel count for each synaptic pair (Figure 2.8G-H).

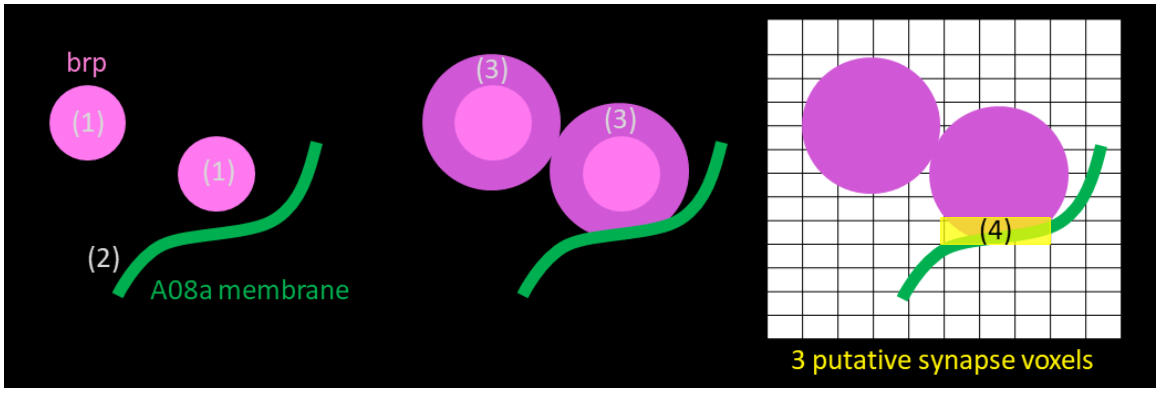

Figure 2.7. Image analyses pipeline to quantify putative synapse voxels. (1) Identify voxels containing brp intensity (mask), (2) Identify voxels containing A08a membrane (mask), (3) Dilate brp mask by one iteration (90nm), (4) Identify the number of voxels where the dilated brp mask and the A08a membrane mask colocalize.

It is important to note that putative synapse voxels analysis is not a replacement for EM level analyses; it only describes the number of voxels containing presynaptic material within a close distance (less than 90nm) from the post-synaptic membrane. Since both the pre-synapse and post-synaptic neuron membrane channel were made binary through the assignment of a threshold, information regarding the amount of pre-synaptic material revealed by voxel intensity was lost. Furthermore, in *Drosophila*, many synapses are polyadic (i.e., each pre-synaptic site can have several post-synaptic sites), oftentimes with several synaptic partners. For example, a pre-synaptic site on dbd connects to A08a and several other neurons. It is also important to note that although the distance threshold of 90nm is much below the resolution limit of light microscopy (about 200nm depending on the wavelength), distances smaller than the resolution limit can be resolved by comparing measurements using two different wavelengths, in this case between 488nm and 555nm.

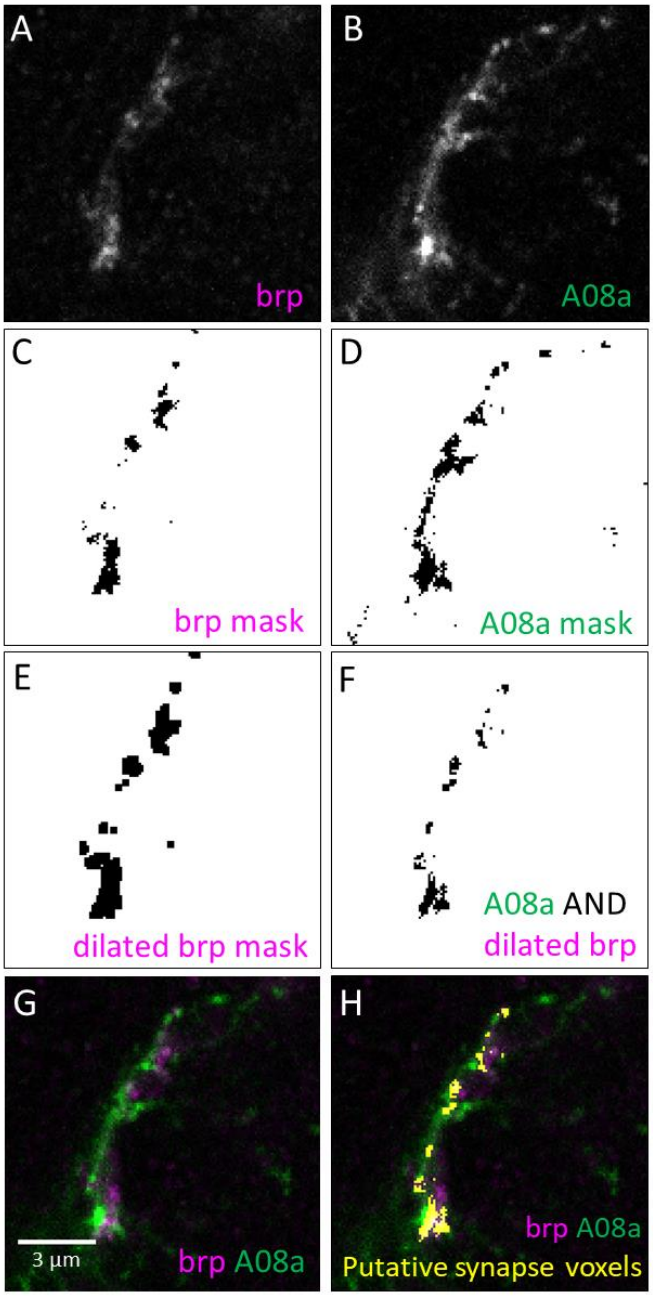

Figure 2.8. Example of image analyses pipeline to quantify putative synapse voxels. A) Micrograph of Brp-short-mstraw (single z-slice). B) Micrograph of A08a membrane (single z-slice). C) Binary image of brp mask after manual thresholding. D) Binary image of A08a mask after manual thresholding. E) Image of of brp mask after dilation (expansion of voxels by 90nm). F) Image of voxels containing intensity in the A08a mask channel and the dilated Brp mask channel (putative synapse voxels). G) Merge of original Brp-short-mstraw and A08a membrane channels. H) Overlay of putative synapse voxels onto original micrograph shows voxels where Brp-short-mstraw is within 90nm of voxels containing A08a membrane.

Limitations and advantages of the putative synapse voxel analyses

There are many limitations with this model system. The variability of Gal4 and LexA systems results in variability in the amount of neuron membrane and pre-synapse marker expression, which in turn effects the putative synapse voxel analyses by making it difficult to segment channels. The tissue clearing process also leads to shrinkage in nerve cord size, complicating distance measurements. Also, it is difficult to identify specific synapses between defined synaptic partners because the neuropil is so dense, and many synapses are polyadic.

Despite these challenges, the model system I describe here has great value because of its speed. Although EM reconstruction provides more detailed information on synaptic connectivity and morphology, it does not allow for a high throughput method to test gene function. While this model system is useful to identify CSMs that regulate synapse specificity, it also allows for the investigation of genes in any class, including genes that are upstream or downstream from CSM interactions. This model system, aiming to identify synapse specificity genes, takes advantage of the *Drosophila* genetic toolkit to label individual pre and postsynaptic neurons, manipulate gene expression in those neurons, and the light microscopy acquisition and analyses enables the rapid quantitation of putative synapse voxels.

CHAPTER III

TOWARDS IDENTIFYING SYNAPSE SPECIFICITY GENES IN DROSOPHILA

One approach to identify synapse specificity genes would be to perform an unbiased RNAi screen using the model system. Namely, one could express RNAi constructs that would knock down individual genes in synaptically coupled neurons, dbd or A08a, to determine which genes are required for synapse formation. Alternatively, one could misexpress individual gene cDNAs in non-synaptically coupled neurons, dbd and A27j, to determine which genes are sufficient for synapse formation. This approach would be a costly and time intensive endeavor, however, because there are ~15,500 genes in the *Drosophila* genome in total, with ~1000 genes predicted to encode CSMs (Kurusu et al., 2008).

CSMs initiate cell-cell interactions

Genes that regulate synapse specificity can theoretically belong to any class of genes, but CSMs have been a major research focus due to their subcellular position at the cell membrane, which is a prime position for cell recognition events. There are many classes of CSMs, including enzymes, receptors, channels, and adhesion molecules, that enable the cell to interact with its environment. Adhesion molecules contain a transmembrane domain or a glycosylphosphatidylinositol domain, that anchors them to the plasma membrane. Their extracellular domain can either bind homophilically with itself on adjacent cell membranes, or heterophilically either with another CSM, or with the extracellular matrix. Adhesion molecules have intracellular domains, which vary in size and function, where some of them have protein binding sites and some have kinase functionality, both of which can lead to downstream signaling cascades. Their position at the surface of the cell makes CSMs good candidates for cell recognition events because they can bind CSMs on other cells, then pass on that signal to other parts of the cell (Özkan et al., 2013).

In the context of the nervous system, many have hypothesized the importance of cell recognition events in the establishment of synapse specificity, including Roger

Sperry in the mid-1900s. Sperry hypothesized that synapse specificity arose from a 'lock and key' mechanism, where neurons destined to become synaptic partners express a complementary set of cell adhesion molecules. In a simple example, a neuron A expresses a cell adhesion molecule and its synaptic partner, neuron B, expresses the binding adhesion molecule. When these two neurons interact with each other, they will then stick to each other due to the complementary expression of cell adhesion molecules. Recent work in culture and other model organisms showed that this cell-cell adhesion leads to the recruitment of synaptic machinery to that site of membrane contact (Washbourne, 2015). If this model is correct, in its simplest form, one would predict that synaptic partners express binding cell adhesion molecules, and non-synaptically coupled neurons would not express binding cell adhesion molecules.

Towards the identification of CSMs that regulate synapse formation in *Drosophila*

Valiant efforts have been made to identify CSMs in *Drosophila* that bind to each other, with the aim to determine which might act as 'locks and keys'. In 2013, Ozkan and colleagues developed a novel in vitro binding assay to define the full repertoire of *Drosophila* cell adhesion molecule binding interactions, or 'interactome'. They tested 203 adhesion molecules in the leucine rich repeat, immunoglobulin superfamily, and fibronectin type III families. Of the 20,503 unique cell adhesion molecule pairs, they identified 106 detectible binding interactions (Özkan et al., 2013). These binding cell adhesion molecules, if expressed complimentarily in potential synaptic partners, are good candidates for regulating synapse specificity.

To identify potential cell adhesion molecules that regulate synapse specificity in my model system, I aimed to identify the binding molecules expressed in the synaptically coupled neuron pair, dbd and A08a, using single cell RNA sequencing (scRNAseq). Using this method, one could theoretically identify all of the cell adhesion molecules in these neurons, then cross reference the in vitro binding assay by Ozkan et al. to determine which cell adhesion molecules have binding interactions, and then test their function in synapse formation. One caveat with this technique is that scRNAseq is technically challenging, as a very small population of cells of interest would have to be isolated, and furthermore, isolating cell bodies would miss transcripts that are not present in the cell

body. One advantage to this strategy is that many transcripts would be identified, including cell adhesion molecules, but also molecules in any gene family, including genes that may participate in upstream or downstream of cell adhesion events, which could enable the identification of complete cellular signaling pathways.

One approach to identify RNA transcripts in single cells is to gather cells using fluorescence activated cell sorting (FACS), then sequence the transcripts. The model neurons dbd and A08a are such a rare population, with only one neuron per hemisegment in the larval ventral nerve cord (~14-20 neurons), this pipeline was not a feasible technique to obtain transcripts due to low signal to noise. The second approach to identify transcripts in single cells, dbd and A08a, was to manually isolate the cells, group them into a larger population, then amplify and sequence the transcripts. First, we labeled the neurons with very bright fluorescence membrane labels in the first instar larvae using the Gal4-UAS system, then we collaborated with an expert in micromanipulation, Torsten Bossing at the University of Plymouth, to manually collect A08a cell bodies using a micropipette. The dbd cell body was unamendable to manual cell collection and RNA sequencing due to the physical interference of the thick body wall making it impossible to collect the cell, and because the dbd cell body and dendrites are completely encased by supporting glia, which would also potentially contaminate the dbd transcripts. Contrasting, the A08a cell body is positioned on the outer surface of the ventral nerve cord, and upon protease application to untether the cell body from cortex glia, the A08a cell body is much more accessible for capture. Using this strategy, Bossing collected 5-10 A08a cell bodies in a tube, amplified the transcripts, and sent them back to us for sequencing analyses. Upon analyses, we still did not have enough signal to noise to reliably detect transcripts in this small population of cells (data not shown). Ultimately, neither FACS nor manually picking cells were not successful at determining cell adhesion molecule expression in dbd or A08a.

A candidate gene approach: The Dpr and DIP families of cell adhesion molecules

Next, I took a candidate gene approach to identify regulators of synapse specificity between dbd and A08a. The extracellular interactome of cell adhesion molecules provided a good candidate list of potential ‘lock and keys’ that might be

utilized by the developing nervous system. If these molecules regulated synapse specificity, one would expect them to be expressed in synaptic partners, where a presynaptic neuron expresses a cell adhesion molecule, and a postsynaptic neuron expresses the binding, or complementary, adhesion molecule. To this end, I started investigating the Dpr and DIP families of genes, by first characterizing their expression pattern in dbd and A08a neurons, and then testing their role in dbd-A08a synapse formation.

Dpr and DIP gene families are promising candidates for regulating synapse specificity due to their protein structure, binding interactions, expression in the nervous system, and role in synapse formation. Dpr and DIP genes are in the immunoglobulin superfamily and contain two or three extracellular immunoglobulin domains respectively. Researchers have characterized the adhesive properties of Dpr and DIP proteins both in terms of their dissociation constants (K_d) and their binding interactions (Figure 3.1) (Carrillo et al., 2015; Cosmanescu et al., 2018; Özkan et al., 2013).

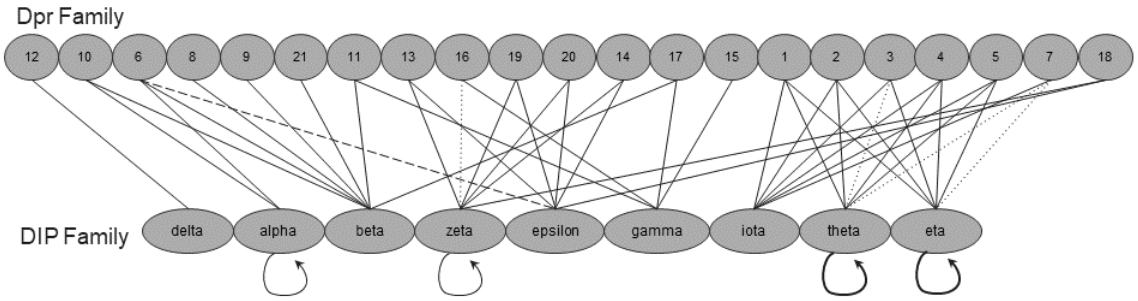

Figure 3.1. In vitro binding interactions of the Dpr and DIP cell adhesion molecules. The Dpr proteins (Dpr-1 through Dpr-21, top row, circles) have unique binding interactions with the DIP proteins (DIP-alpha through DIP-iota, bottom row, ovals). Lines between proteins indicate binding interactions. Dotted lines indicate week interactions and bold lines indicate strong interactions. Some DIP proteins bind homophilically, arced arrows. A subset of Dpr and DIP proteins interact with cDIP (not shown here), a secreted leucine rich repeat protein. Figure adapted from Carrillo et al., 2015; Cosmanescu et al., 2018; Özkan et al., 2013.

The outermost, N-terminal immunoglobulin domain on DIP-alpha, termed the D1 domain, binds to the D1 domain of the binding molecule dpr-6 at a 130^0 angle (Cheng et al., 2019). This binding interaction resembles other well-known Ig-type interactions, including the JAML-CAR complex, an immune system signaling complex, the SYG-1-

SYG-2 complex, a complex reported to initiate synapse formation, and Nectin complexes. While most of these binding interactions rely upon charge complementary salt-bridges, Dpr-DIP binding relies on hydrophobic interactions and shape complimentarily (Carrillo et al., 2015).

Although the Dpr and DIP genes have no clear mammalian homolog, the Dpr-DIP interactions structurally resemble Necl-Nectin interactions, the closest vertebrate homologs are the IgLON family. IgLON family members mediate many aspects of neural development, including dendritogenesis, neurite outgrowth, and synapse formation (reviewed in Kubick et al., 2018) While these proteins have intracellular domains that lead to downstream signaling cascades, Dpr and DIP proteins contain very small intracellular domains with no predicted protein binding sites or phosphorylation abilities (personal communication). It is alternatively possible Dpr-DIP proteins purely participate in adhesive activities, or they could potentially interact with other proteins, including non-CSMs, that do have signaling capabilities. Many dpr and DIP proteins bind to common DIP, or cDIP, a secreted leucine rich repeat protein with unknown function.

The *dpr* family was first described by Nakamura and colleagues, who showed that *dpr-1* is required for salt aversion in a proboscis extension response assay (Nakamura et al., 2002). First, they showed that loss of *dpr-1* function resulted in defective salt, but not sugar, gustatory response in adult flies. Furthermore, expression of a *dpr-1* reporter gene was localized to chemosensory sensilla in the adult wing, legs, and the taste organs on the distal end of the proboscis, while all mechanosensory sensilla were absent of reporter staining. Staining was also observed in other sensory neurons, including R8 photoreceptors and olfactory cells, and non-sensory neurons, including subsets of neurons in the central nervous system (Nakamura et al., 2002). While they showed that *dpr-1* is required for a gustatory response to salt, the specific roles of Dpr-1 adhesion in gustation or sensory information processing, have yet to be elucidated.

More recent work in *Drosophila* has started to characterize Dpr and DIP function in neural development. Dpr and DIP proteins have been confirmed to interact in live embryonic neurons (Özkan et al., 2013). In the adult peripheral nervous system (PNS), DIP-alpha and Dpr-10 binding mediate terminal axon branching of leg motor neurons (Venkatasubramanian et al., 2019), while in the larval PNS, DIP-alpha and Dpr-10

mediate motor neuron targeting specificity (Ashley et al., 2019). In the central nervous system, several Dpr and DIP members are expressed in layers of the medulla, and loss of gene function affects the targeting of neurons to specific layers and cell survival (Carrillo et al., 2015; Tan et al., 2015)

Taken together, the *dpr* and *DIP* genes are good candidates to mediate synaptic specificity due to their binding interactions (possible 'locks and keys') and their known roles in laminar neural circuit assembly (layer specificity) and motor neuron targeting (muscle targeting). Here, I aimed to test their role in synapse formation in a different neural circuit architecture, the larval ventral nerve cord, and began by investigating their expression pattern and function in dbd and A08a neurons.

Determining the expression of Dpr and DIP proteins in dbd and A08a neurons

In order to identify which Dpr and DIP binding interactions may regulate synapse specificity, I needed to identify which Dpr and DIP family members are expressed by synaptic partners, dbd and A08a. I hypothesized, that if Dpr and DIP binding interactions are necessary for synaptic partner choice, then dbd and A08a 1) will express known binding Dpr and DIP proteins and 2) that Dpr-DIP binding will be necessary for dbd-A08a synapse formation. In order to determine which Dpr and DIP molecules were expressed by these neurons, I utilized the MiMIC genetic toolkit to visualize expression patterns of these molecules (Li-Kroeger et al., 2018; Venken et al., 2011). The MiMIC toolkit is a large collection of fly lines that contain insertions into genes, in both exon and intron locations, that contain various genetic constructs.

The MiMIC-GFP lines contain a green fluorescent protein reporter construct, which allows for the visualization of gene expression or nearby enhancer activity. Some MiMIC-GFP insertions are in exons, resulting in expression of a truncated protein tagged with GFP, while some insertions are in introns, resulting in GFP sandwiched in the middle of the protein. First, I combined the various types of MiMIC-GFP lines for the *dpr* and *DIP* genes in with the dbd- and A08a-Gal4 lines, which I used to drive expression of membrane bound reporters to identify and visualize the neurons. Then, I utilized immunohistochemistry to amplify both the MiMIC-GFP and neuron signals, then looked for colocalization of these two reporters in the cell body to determine which *dpr*

and *DIP* genes where expressed in dbd and A08a neurons. One limitation to this approach is that Dpr or DIP GFP expression might be localized to the neuron processes, as opposed to the neuron cell body, making expression difficult to assess due to the close apposition to other neurons in the dense neuropil. Despite amplification of the signal with antibodies, many Dpr::GFP and DIP::GFP constructs were faint and difficult to visualize. Next, I switched to using MiMIC-Gal4 lines to more robustly amplify the signal.

The MiMIC-Gal4 lines contain insertions of Gal4 within my gene of interest, rather than GFP, and can be used with the UAS system to drive expression of membrane bound reporters. Some insertions contain T2A constructs, a bicistronic component, to separate the endogenous gene product from the inserted Gal4, resulting in normal protein production and expression of a detached Gal4 that can enter the nucleus. I then used the dbd- and A08a-LexA lines in combination with a different membrane reporter to label the dbd and A08a neurons. This genetic approach resulted in much brighter expression of Dpr and DIP MiMIC lines. I found that dbd expressed dpr-1 (Figure 3.2A-A'') and DIP-eta (data not shown, summarized in Figure 3.3), while A08a neuron expressed dpr-8 (Figure 3.2B-B'), DIP-gamma, and DIP-delta (data not shown, summarized in Figure 3.4).

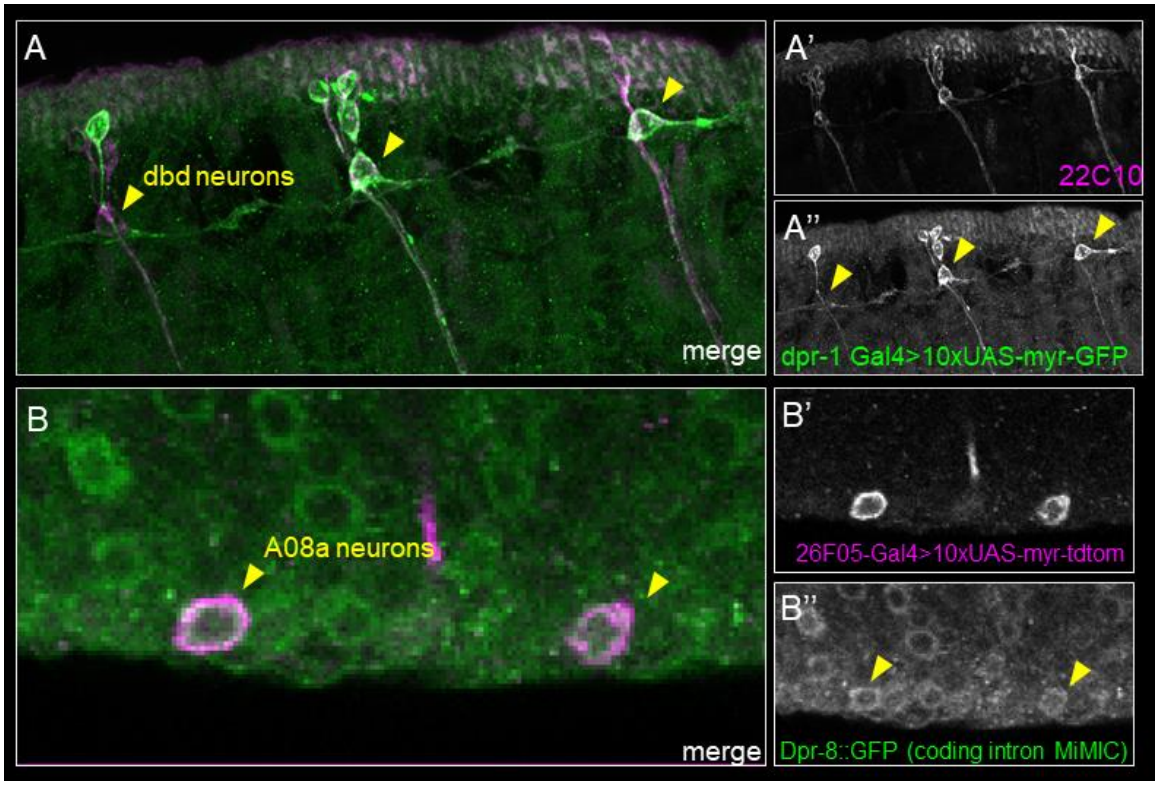

Figure 3.2. Expression of Dpr and DIP MiMIC lines in dbd and A08a neurons. A) Embryonic dbd neurons (yellow arrowheads) express dpr-1 Gal4 (merge). A') 22C10 labels sensory neurons, including dbd, in the body wall. A'') dpr-1 Gal4 drives expression of 10xUAS-myristolated-green fluorescent protein (GFP) reporter in most dbd neurons. B) Larval A08a neurons (yellow arrowheads) express Dpr-8::GFP (merge). B') The 26F05-Gal4 drives expression of a 10xUAS-myristolated-tandom tomato reporter in A08a neurons. B'') Dpr8::GFP labels many cells in the ventral nerve cord, including A08a (yellow arrowheads).

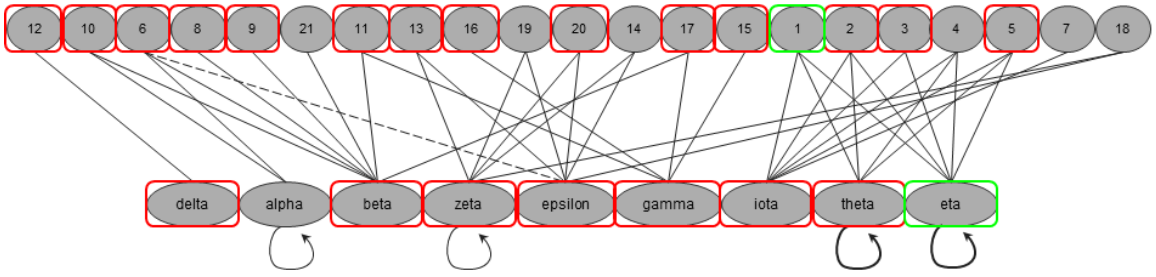

Figure 3.3. Expression summary of Dpr- and DIP-Gal4 lines in embryonic dbd neurons. dbd neurons express Dpr-1 Gal4 and DIP-eta Gal4 lines. Figure adapted from Carrillo et al., 2015; Cosmanescu et al., 2018; Özkan et al., 2013.

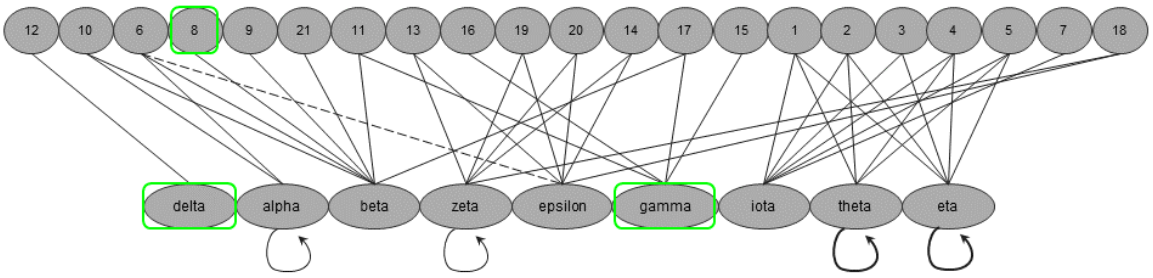

Figure 3.4. Expression summary of Dpr:: and DIP::GFP lines in larval A08a neurons. A08a neurons express DIP-delta::GFP, DIP-gamma::GFP, and dpr-8::GFP. Figure adapted from Carrillo et al., 2015; Cosmanescu et al., 2018; Özkan et al., 2013.

While I hypothesized the synaptic partners dbd and A08a would express binding dpr and DIP molecules, I did not observe that expression pattern with the reporters I tested. It is possible, however, that dbd and A08a do express complementary dpr and DIP genes, but the reporter lines used here were either too weak for visualization. I was also not able to prioritize testing all of the Dpr and DIP reporter lines and some lines are not available due to a lack of MiMIC insertion in that gene region. Regardless, I proceeded to test if Dpr-1 or DIP-eta was necessary for dbd-A08a synapse formation.

Determining if Dpr-1 or DIP-eta expression in dbd is necessary for dbd-A08a synapse formation

In order to determine if Dpr-1 or DIP-eta expression in dbd is required for dbd-A08a synapse formation, I used the model system described above to drive expression of the respective RNAi constructs in dbd. Then I looked to see if there were still synapse voxels present between dbd and A08a in larval stages. I found that knockdown of Dpr-1 or DIP-eta via RNAi expression did not result in a complete loss of putative synaptic contacts, suggesting they are not required for dbd-A08a synapse formation (Figure 3.5).

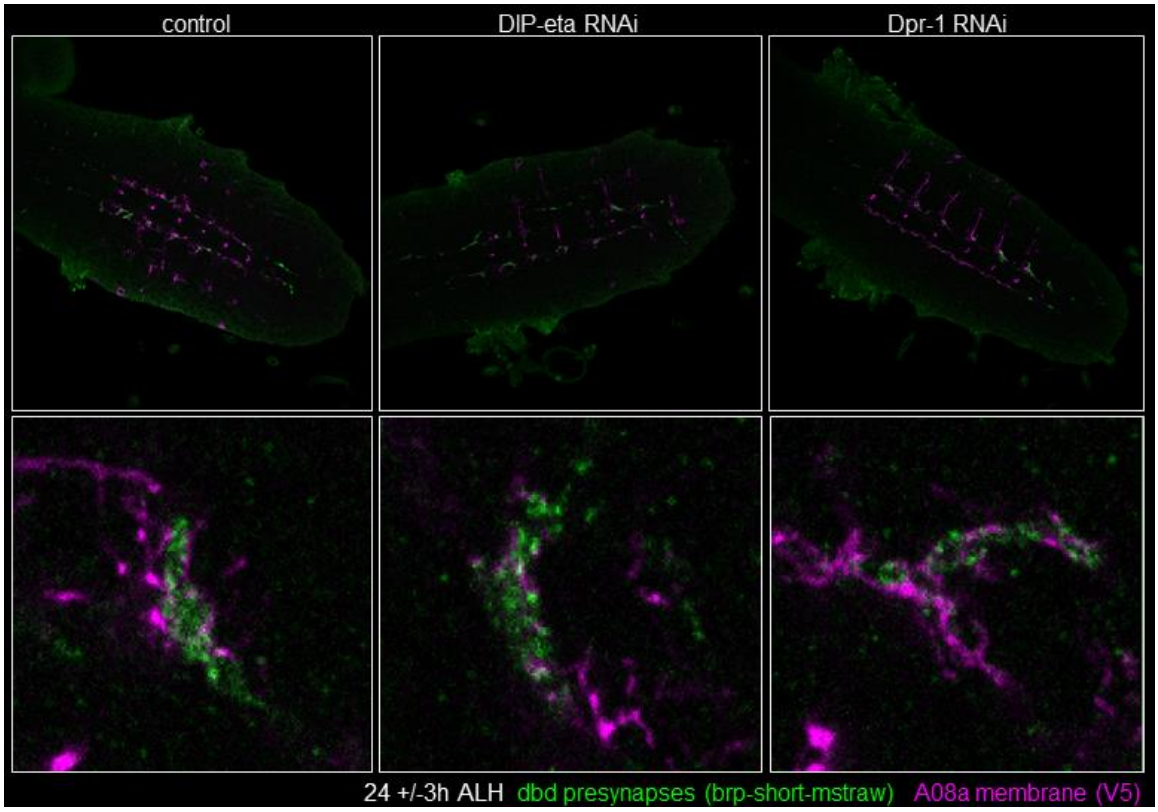

Figure 3.5. Expression of Dpr-1 RNAi or DIP-eta RNAi does not eliminate dbd-A08a putative synaptic contacts. Top panels show single z-slice through ventral nerve cord in control, DIP-eta RNAi, and Dpr-1 RNAi experimental conditions. A08a membrane (magenta) is labeled by a V5 tag. dbd pre-synapses (green) are labeled by mcherry (brp-short-mstraw). Lower panels show enlarged regions where dbd pre-synapses (brp-short-mstraw, green) are in close proximity to A08a membrane (V5, magenta).

In future experiments it will be important to determine the effectiveness of gene knockdown and characterize the timing of the knockdown relative to neuron development, as incomplete penetrance or expressivity could alternatively explain my RNAi results. One additional possibility for not observing synapse loss upon Dpr-1 and DIP-eta RNAi expression, is if DIP-eta and Dpr-1 are acting redundantly. Combined expression of both RNAi constructs in dbd would potentially reveal a function for DIP-eta and Dpr-1 in synapse formation. It is also a possibility that dbd-A08a synapses were compromised (ie. disorganized T-bars) upon Dpr-1 or DIP-eta knockdown, but the model system was unable to detect these changes. Future studies might benefit from synapse analyses at the electron microscopy level, which would allow for ultrastructural analyses of the synapse, but also more details regarding synapse number changes upon gene

knockdown. Another possibility is that DIP-eta and Dpr-1 do not regulate synapse specificity between dbd and A08a neurons, but rather function in a different aspect of dbd cell biology, such as participating in a different cell-cell interaction.

On the expression and putative function of DIP-eta in dbd neurons

I determined the expression of DIP-eta in dbd by driving expression of a membrane reporter under the control of the DIP-eta MiMIC-Gal4. This technique allowed me to see if the dbd neuron expressed the *DIP-eta* gene but did not allow me to visualize the subcellular location of DIP-eta protein expression (Figure 3.2). One reason I may not have observed a role for DIP-eta in dbd-A08a synapse formation, is that DIP-eta might not function in the dbd axon, where it synapses with A08a, but rather, might be important for different subcellular structures, such as the dendritic domain of dbd. Towards this end, I wanted to determine the subcellular location of DIP-eta proteins in dbd neurons. First, I labeled the dbd cell body with a pan-sensory neuron marker, the 22C10 antibody, then labeled DIP-eta expression with a custom antibody. While I found expression of DIP-eta along the dendrites of dbd, I did not observe strong DIP-eta expression in the axons of dbd (Figures 3.6 – 3.8). This expression pattern suggests DIP-eta may have a dendritic function.

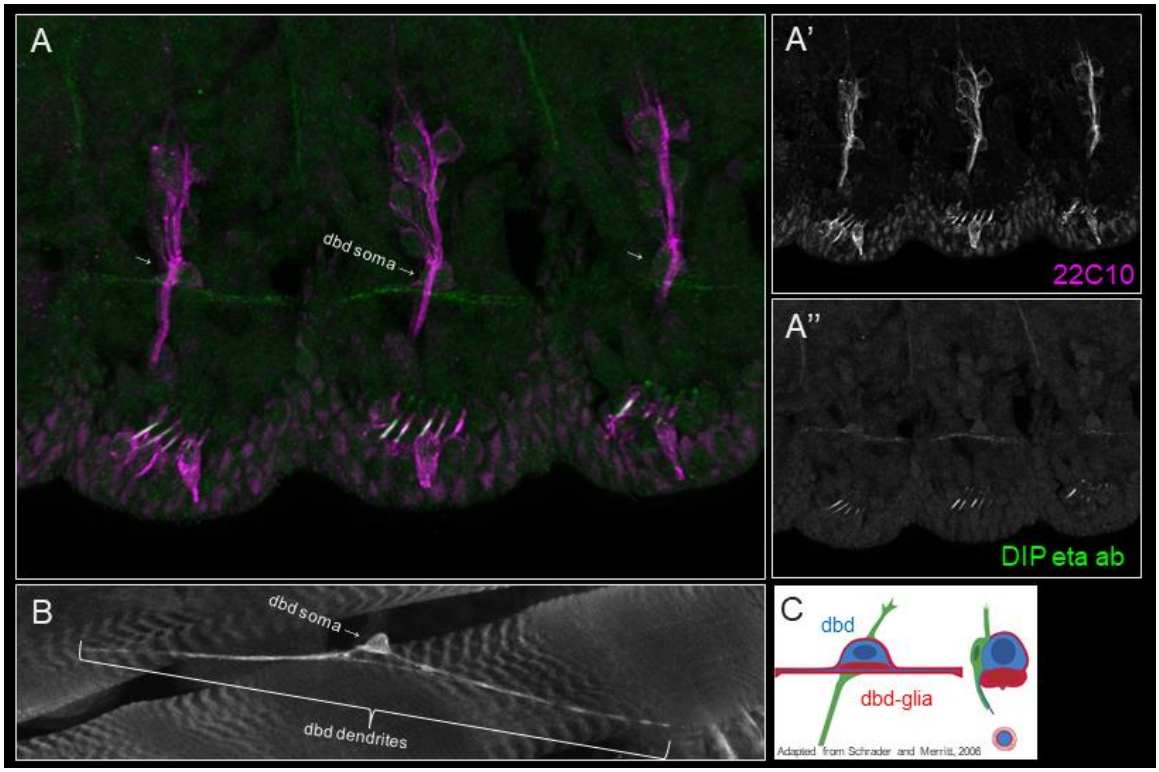

Figure 3.6. DIP-eta antibody is localized to the dendrites of dbd. A-A'') Micrograph of embryonic body wall showing dbd (white arrows) labeled by 22C10 (magenta). The DIP-eta antibody (green) localizes to the dendrites of dbd (not labeled by 22C10 antibody). B) Micrograph of larval dbd neurons labeled by the *165-Gal4* line in a fillet preparation shows the anatomy of dbd neurons. dbd extends two dendrites, one anteriorly and one posteriorly. C) Figure adapted from Schrader and Merritt, 2006. The dbd dendrites are wrapped completely by the dbd-glial cell.

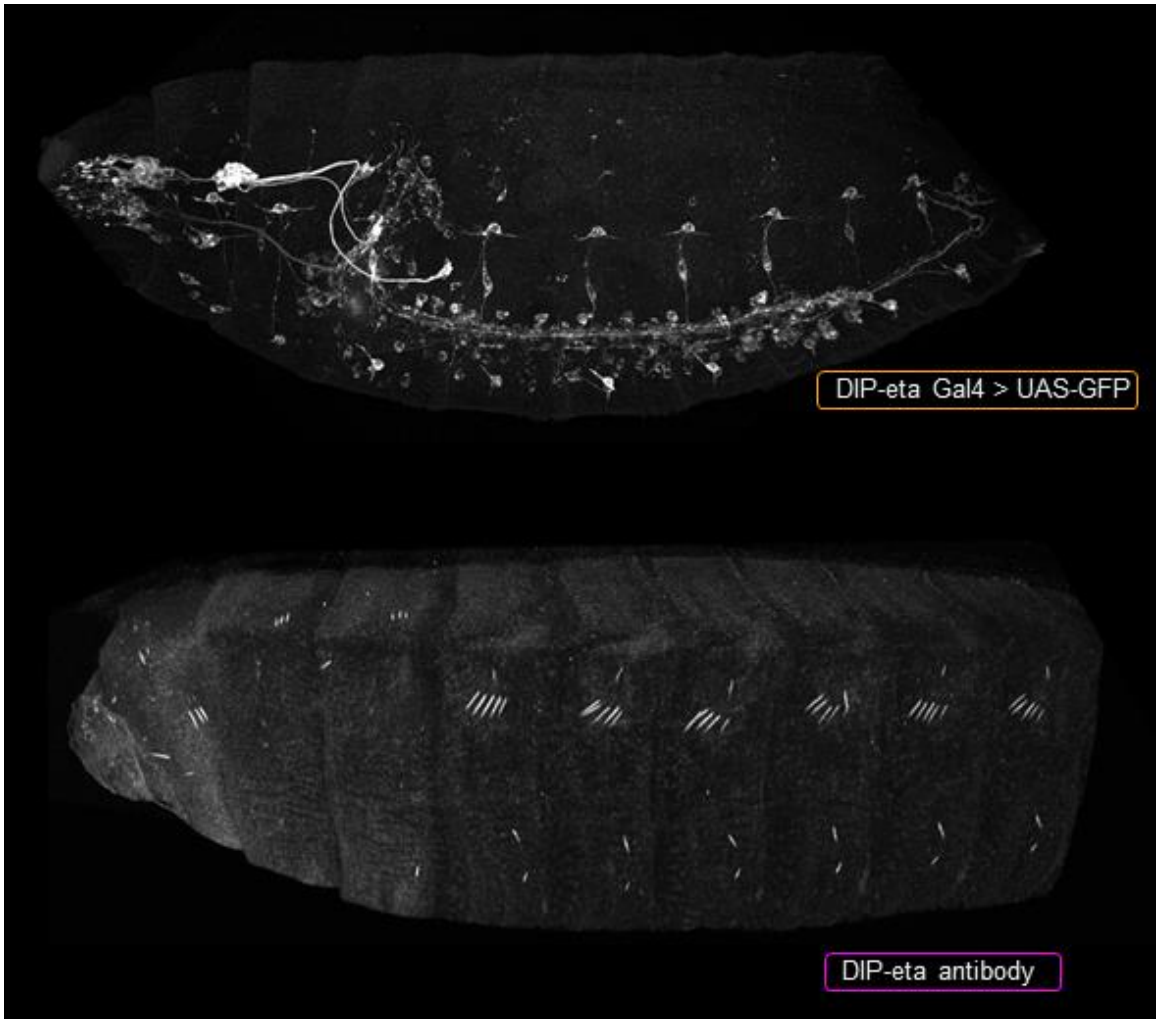

Figure 3.7. Comparison of DIP-eta-Gal4 and DIP-eta antibody in *Drosophila* embryos. Top panel shows DIP-eta Gal4 driving expression of UAS-GFP. Bottom panel shows DIP-eta antibody labeling.

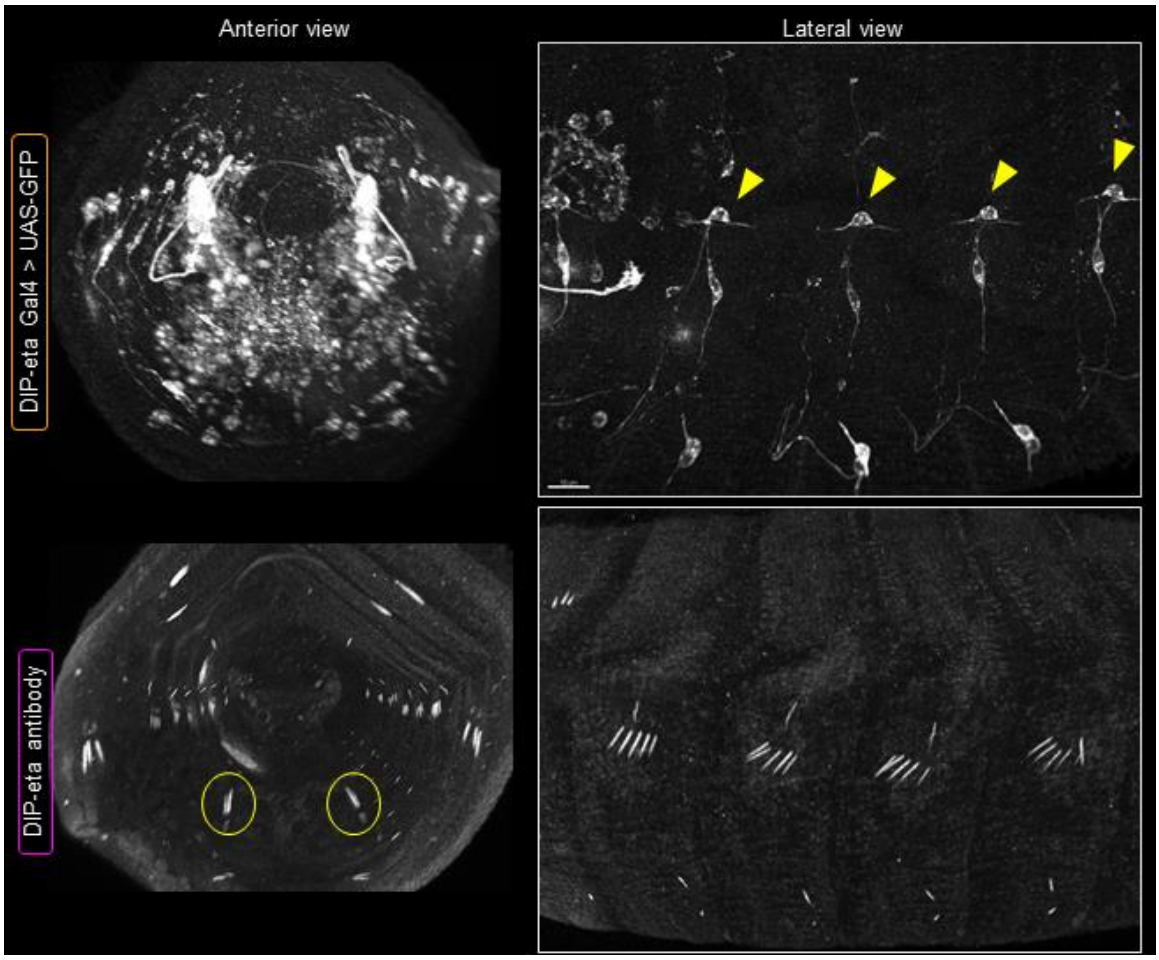

Figure 3.8. Comparison of DIP-eta-Gal4 and DIP-eta antibody in *Drosophila* embryos II. DIP-eta Gal4 expression (top panel) can be visualized in many neurons, including dbd (yellow arrowheads). The DIP-eta antibody (bottom panel) strongly labels the dendrites of chordotonal neurons on the body wall and also labels unidentified cells in the embryonic head (bottom left panel, yellow circles).

The dbd neurons are proprioceptive neurons that respond to changes in body wall stretching (Suslak et al., 2015). Each dbd neuron has two dendrites that span the body wall segment, one extends anteriorly, and one extends posteriorly. dbd is ensheathed by two glial cells: the dbd glia, a sibling cell to dbd, which encircles the dendrites of dbd, and the pg3 glia, which is adjacent to the dbd cell body (Schrader & Merritt, 2000). dbd itself does not contact the body wall, but rather is indirectly tethered to the body wall folds through the its glial sheath, which contacts the epidermis. Together, these three cells make up a very small stretch receptor organ, termed the longitudinal stretch receptor (Schrader & Merritt, 2000; Suslak & Jarman, 2016). Due to this anatomy, I hypothesized

that DIP-eta may function to adhere the dbd dendrites to the dbd glial cell. Furthermore, disrupting dbd-dbd glia cell adhesion may prevent dbd from attaching to the body wall and adopting its bipolar dendritic morphology. Towards this end, I wanted to determine if DIP-eta is necessary for dbd dendritic morphology.

Using the Gal4 driver that is expressed in dbd neurons before axon extension, I drove expression of DIP-eta-RNAi, then qualitatively assayed dendritic morphology at larval stages in a fillet preparation. I found that DIP-eta-RNAi expression resulted in some morphological changes, including the presence of filopodia-like protrusions from the dendrites, and a less orderly dendritic domain (Figures 3.9 - 3.10). Notably, the region where dbd-glia resides, a pocket in between the dbd soma and dbd dendrites, was variably reduced. Some neurons showed a regular sized pocket, and some completely lacked the pocket. The bipolar nature of dbd dendrites remained upon expression of DIP-eta-RNAi, suggesting the contact between dbd and the dbd-glia was still strong enough for the dbd-glia to tether the dendrites of dbd to the epidermis. I did observe one severely disrupted dbd, which had the axonal terminal adjacent to one dendritic terminal (Figure 3.10, bottom panel). Further experiments with more sample numbers and careful analyses of DIP-eta knockdown would be necessary to confirm the role of DIP-eta in dbd dendritic morphology.

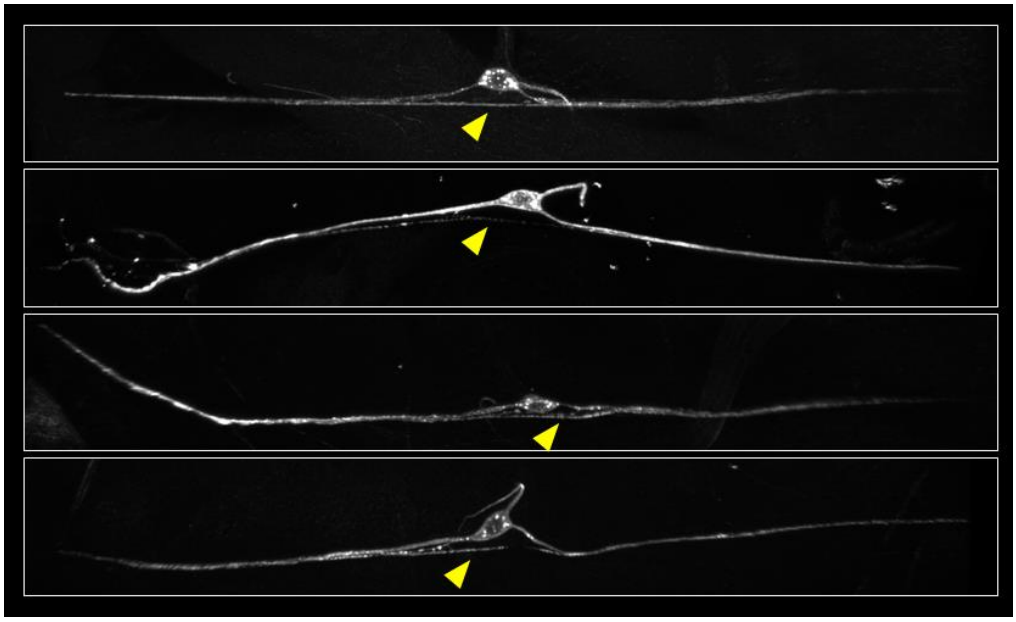

Figure 3.9. Larval dbd neurons expressing control RNAi (empty vector) in a fillet preparation. The dendrites of dbd are connected by cell membrane (yellow arrow) to house the dbd-glia soma (not shown).

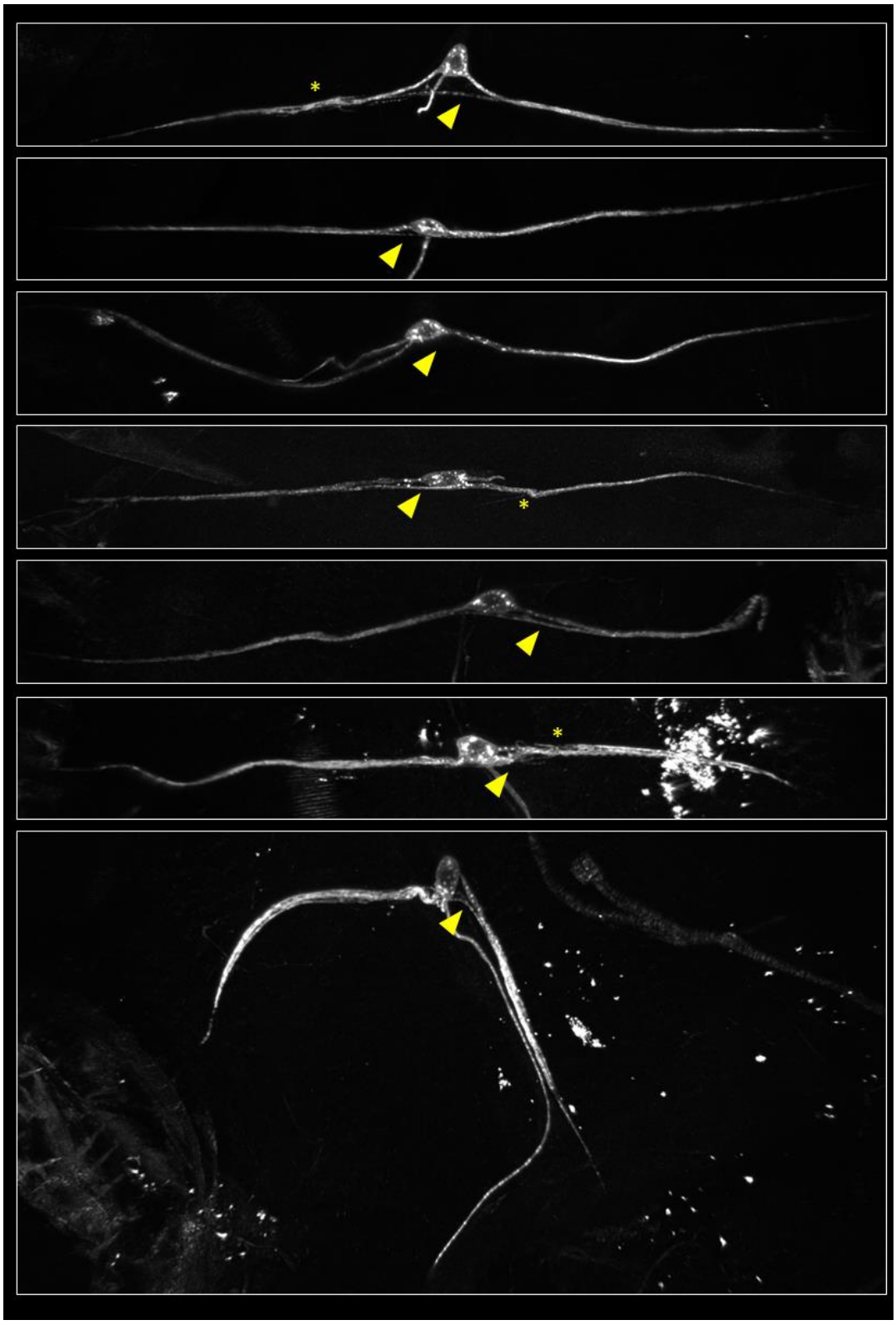

Figure 3.10. Larval dbd neurons expressing DIP-eta RNAi in a fillet preparation. Some dbd neurons retain the membrane connecting the dendrites of dbd (yellow arrows, top panel), while other neurons have a smaller membrane connection, or no connection at all. Some dendritic domains also show filopodia like

extensions (yellow asterisks). One severe instance shows a mistargeting of dbd dendrites towards the dbd axonal domain (lower panel).

On the expression of DIP-eta in other sensory neurons

Upon further analyses of DIP-eta expression, I noticed that other sensory neurons with proprioceptive function also express DIP-eta, such as a subset of ciliated stretch receptors called chordotonal neurons (Figure 3.8). The dendrites of chordotonal neurons are partially ensheathed by scolopale cells and are held in tension between the cuticle by a ligament and a cap cell. The tension of chordotonal neurons is necessary for their mechanotransduction properties (Prahlad et al., 2017). Cell adhesion molecules, such as DIP-eta shown here, are well positioned to mediate the chordotonal-cap cell interaction and generate this tension. Surprisingly, not all chordotonal neurons expressed DIP-eta (summarized in Figure 3.11), suggesting heterogeneity within the chordotonal neuron population in the larval body wall. I also observed strong DIP-eta labeling in a few cells in the central embryonic head, possibly located in the internal taste organs of the pharynx (ventral pharyngeal sense organ), and labeling of subsets of cells in the external chemosensory organs on the anterior tip of the head (Figure 3.8, bottom left panel). The expression of DIP-eta, a binding partner to Dpr-1, in gustatory receptor neurons, suggests Dpr-1/DIP-eta binding may be necessary for salt aversion in adults, and that DIP-eta mutants may phenocopy dpr-1 mutants in the proboscis extension response assay (Nakamura et al., 2002).

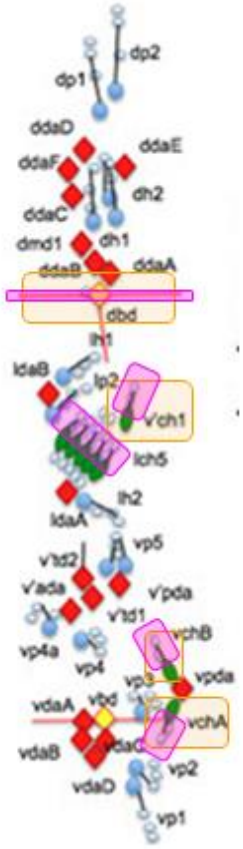

Figure 3.11. Summary of DIP-eta-Gal4 and DIP-eta antibody expression in embryonic sensory neurons. The DIP-eta Gal4 driver (yellow) is expressed in dbd neurons, ch1 neurons, and vchA neurons. The DIP-eta antibody (magenta) is localized to the dendrites of dbd neurons, ch1 neurons, ich5 neurons, vchA neurons, and vchB neurons. Figure adapted from Suslak and Jarman, 2015.

Expression of DIP-eta in several types of sensory neurons, such as dbd, chordotonal, and gustatory receptor neurons, suggests that DIP-eta may regulate important aspects of chemo- and mechano-transduction. I did observe differences in DIP-eta MiMIC Gal4 expression and DIP-eta antibody localization, suggesting that post-transcriptional regulatory mechanisms may further refine DIP-eta expression patterns in *Drosophila* sensory neurons. Further characterization of the DIP-eta expression patterns and function in these neurons may provide insight into how these neurons sense stretch and how other ciliated sensory neurons, such as the inner hair cell of vertebrates, function in wild-type and diseased states.

Determining the role of Dpr and DIP function in A08a neurons

While the expression pattern of Dpr and DIP proteins in synaptic partners dbd and A08a were not suggestive of a requirement for these proteins in dbd-A08a synapse specificity, it is possible that the *dpr* and *DIP* genes expressed by A08a may play a role in synapse specificity between A08a and its downstream synaptic partners. Towards this end, I wanted to test the role of DIP-gamma, DIP-delta, and Dpr-8 in A08a axonal morphology and pre-synapse amount. I expressed RNAi constructs for each of these genes, and cDIP-RNAi, using the A08a-Gal4 driver, which turns on at larval hatching and assayed for A08a neuron morphology and presence of presynaptic sites in later larval stages. I found that expression of these RNAi constructs qualitatively does not result in aberrant axonal morphology, presynapse number, or position (Figure 3.12). All major subcellular domains, including the dendritic domain, maintained its wildtype morphological features. Although, I was unable to test for RNAi effectiveness, these results suggest that these Dpr and DIP genes do not regulate synapse specificity in my model neurons. It is possible that these Dpr and DIP genes function at earlier stages when the A08a-Gal4 driver is not expressed. Further investigations that measure synapse number and synaptic partner choice upon manipulation of Dpr and DIP genes across developmental stages would be needed to fully characterize the role of these genes in A08a synapse specificity.

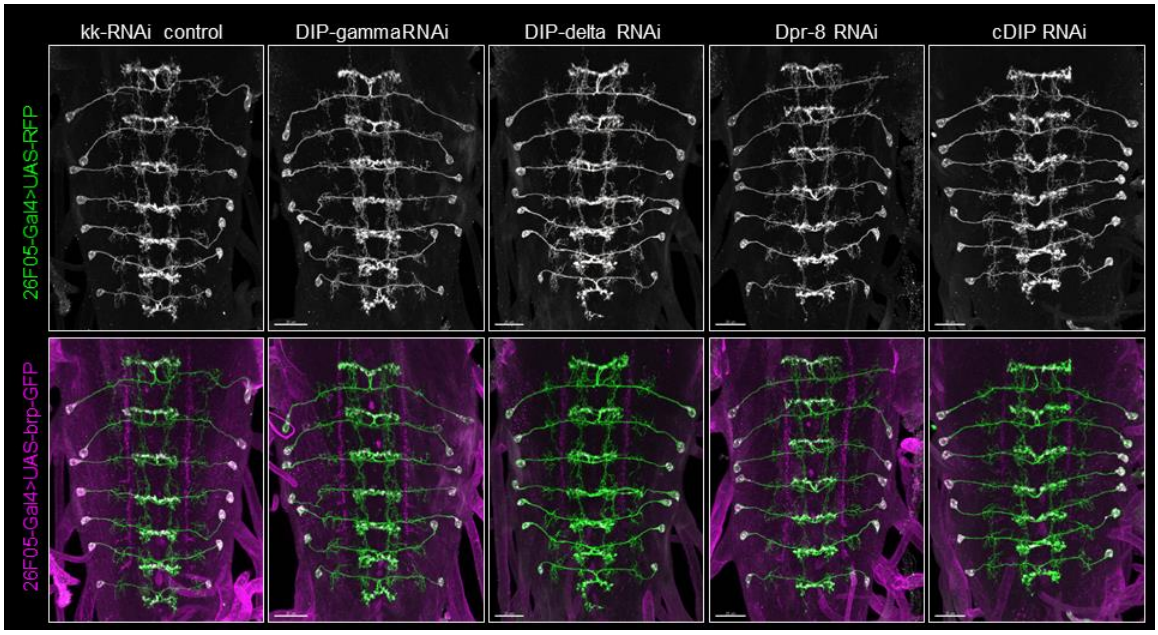

Figure 3.12. Expression of Dpr- or DIP-RNAi constructs does not disrupt A08a morphology or subcellular position of pre-synaptic sites. A08a neurons are labeled by the 26F05-Gal4 driver (white in top panel, green in bottom panel). Presynaptic sites are labeled by UAS-brp-short-GFP (magenta, bottom panel).

Regulating the expression of Dpr and DIP genes in different neurons across development

I found that *dpr* and *DIP* expression is tightly regulated across development, with some genes showing expression in small subsets of neurons at early stages (eg. DIP-eta expressing in some motor neurons at early stage 16) and large subsets of neurons expressing at late larval stages (eg. DIP-eta expressing in many motor neurons, interneurons, and sensory neurons at ~72 hours after larval hatching) (Figure 3.13). The functional relevance of this expression pattern is not characterized. For example, do neurons that first express Dpr and DIP genes act as "pioneer neurons" to establish specific fasciculation patterns? Do these fasciculation patterns influence the organization of functional domains within the larval ventral nerve cord neuropil? Furthermore, do neurons that express a particular set of Dpr and DIP genes process a particular type of neural information, such as proprioception in the body wall? Do neural stem cells regulate expression of Dpr and DIP genes in their progeny? Further analyses of *Dpr* and *DIP* genes in individual neurons in the context of developmental stages and neural circuit establishment will help define their role in neural circuit function.

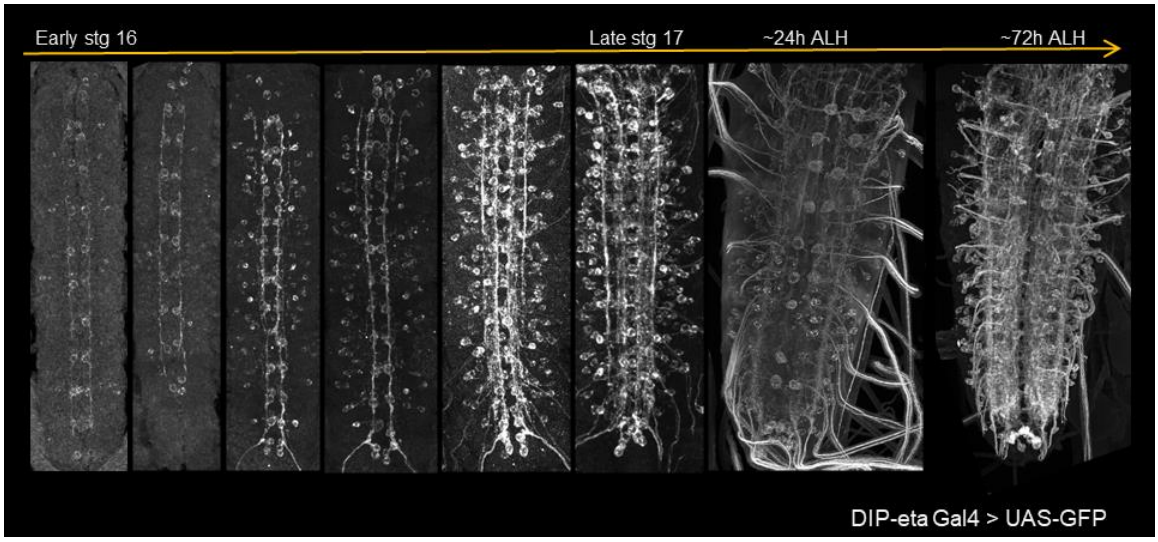

Figure 3.13. DIP-eta-Gal4 expression in the ventral nerve cord expands during development. Early stage 16 embryonic ventral nerve cords show DIP-eta-Gal4 expression in small subsets of neurons, including motor neurons (left, anterior up). Stage ~72 hours after larval hatching ventral nerve cords show DIP-eta-Gal4 expression in a larger subset of neurons (right).

Summary

In order to identify genes that regulate synapse specificity, I focused on testing the role of CSMs in the model neurons dbd and A08a. The first approach I took to identify relevant CSMs was to first perform scRNAseq to characterize all CSM transcripts expressed by dbd and A08a, then use biochemical interaction data to identify which of these CSMs bind each other and could potentially participate in cell-cell interactions. Since scRNAseq turned out to be technically infeasible, and a whole genome RNAi screen would be resource intensive, I decided to take a candidate gene approach focusing on the Dpr and DIP proteins.

The Dpr and DIP proteins are prime candidates to regulate synapse specificity in *Drosophila* based on their expression patterns in the nervous system and their potential role as CSMs to initiate cell-cell contact and recognition. I tested the role of DIP-eta and Dpr-1 in the context of dbd-A08a synapse formation. While further investigations will be necessary to elucidate their synaptic role, I preliminarily conclude that these genes do not regulate synapse specificity between dbd and A08a neurons. DIP-eta however does localize to dbd dendrites and may play a role establishing dbd-dbd glial cell contact and therefore dbd dendritic morphology. DIP-eta expression in the dendrites of other

proprioceptive and gustatory neurons may suggest a common function of this cell adhesion molecule in the transduction of sensory information.

Further experiments can utilize the model system I developed to identify genes that are either necessary or sufficient for synapse formation. For example, one can perform an RNAi screen targeting CSMs in synaptically coupled neurons, dbd and A08a, to determine which genes are necessary for synapse formation. On the contrary, one could utilize non-synaptically coupled neurons to perform an overexpression screen and identify genes that may be sufficient for synapse formation. Future studies may benefit from knocking down or misexpressing several different genes simultaneously in these neurons to overcome redundancy of large gene families and identify gene function. The further development of a Gal4/UAS controlled Crispr-cas9 systems would be well positioned to simultaneously knockdown entire gene families with cellular and temporal control. Finally, with the better characterization of synaptic connectivity through electron microscopy studies and the development and characterization of additional neuron-specific Gal4 and LexA driver lines, the role of synapse specificity genes can be tested in additional neurons, with varying developmental origins, morphologies, and circuit functions to create a more comprehensive understanding of the genetic control of synapse specificity.

CHAPTER IV

REGULATION OF SUBCELLULAR DENDRITIC SYNAPSE SPECIFICITY BY AXON GUIDANCE CUES

From Sales, E. C., Heckman, E. L., Warren, T. L., Doe, C. Q. 2019. Regulation of subcellular dendritic synapse specificity by axon guidance cues. *eLife* 2019;8:e43478 DOI: 10.7554/eLife.43478

Abstract

Neural circuit assembly occurs with subcellular precision, yet the mechanisms underlying this precision remain largely unknown. Subcellular synaptic specificity could be achieved by molecularly distinct subcellular domains that locally regulate synapse formation, or by axon guidance cues restricting access to one of several acceptable targets. We address these models using two *Drosophila* neurons: the dbd sensory neuron and the A08a interneuron. In wild-type larvae, dbd synapses with the A08a medial dendrite but not the A08a lateral dendrite. dbd-specific overexpression of the guidance receptors Unc-5 or Robo-2 results in lateralization of the dbd axon, which forms anatomical and functional monosynaptic connections with the A08a lateral dendrite. In addition, dbd lateralization results in a corresponding lateral shift in A08a dendritic membrane, indicating that dbd can induce or stabilize dendrites. We conclude that axon guidance cues, not molecularly distinct dendritic arbors, are a major determinant of dbd-A08a subcellular synapse specificity.

Introduction

Nervous system function is determined by the precise connectivity of neurons. From the *Drosophila* larva with 10,000 neurons to the human with 80 billion neurons, all neurons are faced with the challenge of identifying the correct subset of synaptic partners among many potential target neurons. In addition to specificity at a cellular level, neural circuits also exhibit synaptic specificity at the subcellular level (reviewed in Yogev & Shen, 2014). In *Drosophila*, the giant fiber descending neuron targets a specific dendritic domain of the tergotrochanteral motor neuron in a fast jump escape circuit

(Godenschwege et al., 2002; Godenschwege & Murphey, 2009). In mammals, cortical pyramidal neurons receive input from martinotti neurons on their distal dendrites and basket neurons on their proximal dendrites (Huang et al., 2007) (Figure 4.1A). The precise targeting of inhibitory neurons to distinct subcellular domains of their target neurons has profound effects on neural processing and circuit function by gating action potential initiation, providing a substrate for plasticity, altering mEPSP amplitude, and modulating dendritic integration (Bloss et al., 2016; Hao et al., 2009; Miles et al., 1996; Pouille et al., 2013; Tobin et al., 2017). Although the precise subcellular positioning of synapses is important for proper circuit function, the mechanisms necessary to achieve such specificity are just starting to be explored (Telley et al., 2016).

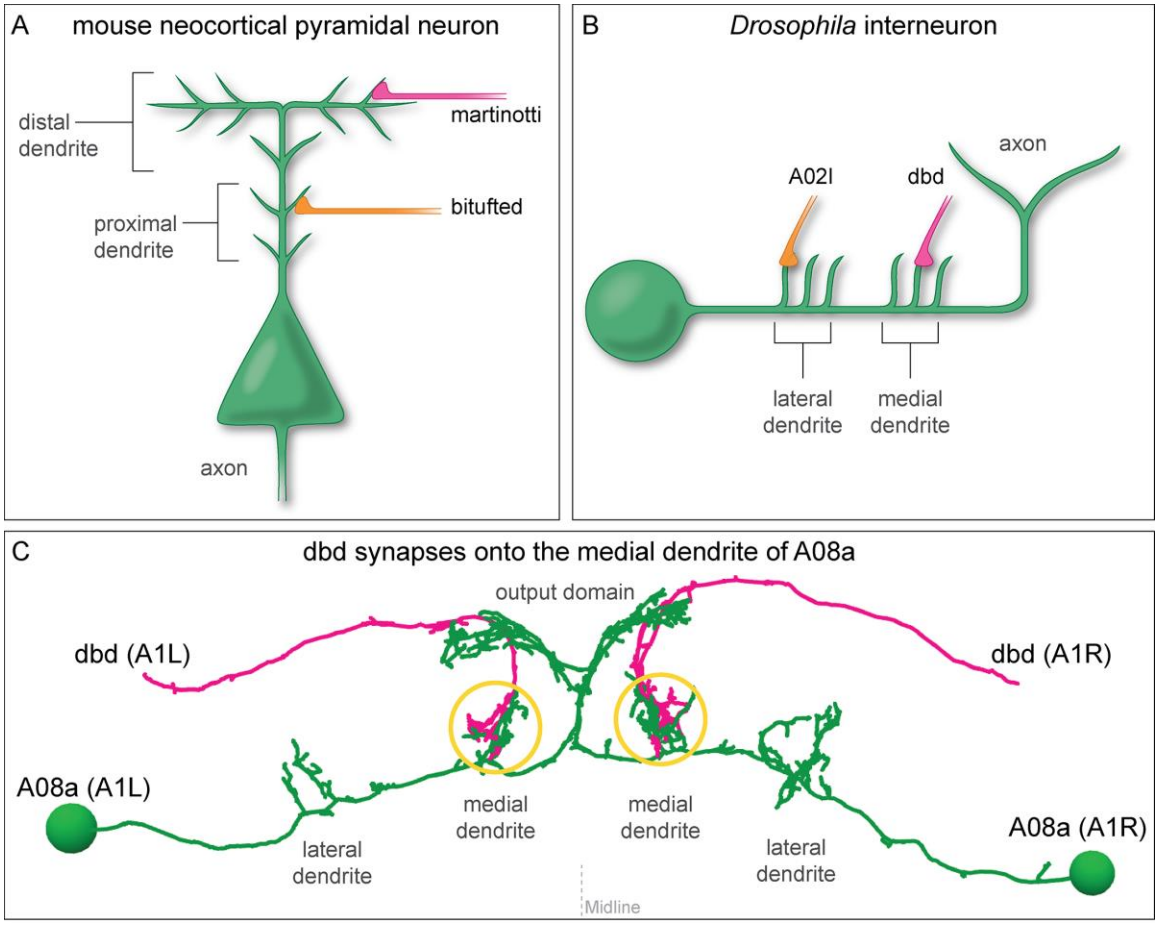

Figure 4.1. Mammalian and insect neurons display subcellular synaptic specificity.
(A) Schematic of mouse neocortical pyramidal neuron (green) with a martinotti neuron (magenta) forming synapses onto the distal dendrite and the bitufted neuron (orange) forming synapses onto the proximal dendrite.
(B) Schematic of fly A08a neuron (green) with a dbd neuron (magenta) forming synapses onto the medial dendrite and an A02l neuron (orange) forming synapses onto the lateral dendrite.

(C) Electron microscopy reconstruction of dbd neurons (magenta) and A08a neurons (green) morphologies in one abdominal (A) segment (A1 left and A1 right) of the *Drosophila* ventral nerve cord (posterior view). dbd forms synapses specifically with the medial dendritic domain, and does not synapse with the lateral dendritic domain or the output domain.

Two distinct developmental models could explain subcellular synaptic specificity. The first model relies on molecular differences between two subcellular domains to restrict synapse formation to one domain (the 'labeled arbor' model). This model is supported by evidence in mouse and *C. elegans* whereby local clustering of CSMs on a postsynaptic neuron dictates synapse position (Ango et al., 2004; Colon-Ramos, Margeta, & Shen, 2007; Klassen & Shen, 2007; Mizumoto & Shen, 2013). An alternative mechanism relies on axon guidance cues to restrict pre-synaptic access to one of several acceptable postsynaptic targets (the 'guidance cue' model). Guidance cues have a well-characterized role in axon and dendrite guidance (Chisholm et al., 2016; Dickson, 2002; Keleman & Dickson, 2001; Tessier-Lavigne & Goodman, 1996; Zlatic et al., 2009), but their role in regulating the subcellular position of synapses has yet to be tested.

We sought to test which of these two models generate dendritic subcellular synaptic specificity using a pair of synaptically coupled neurons in the *Drosophila* larval ventral nerve cord (VNC): the dbd sensory neuron and A08a interneuron (Itakura et al., 2015; Schneider-Mizell et al., 2016). A08a has two spatially distinct dendritic arbors, one medial and one lateral, and dbd synapses specifically with the medial dendritic arbor (Figure 4.1B,C). Is this subcellular target choice due to molecular differences between the medial and lateral A08a dendritic arbors? Or are both dendritic arbors competent to accept dbd synaptic input, but axon guidance cues restrict dbd targeting to the medial arbor? Our results support the guidance cue model: we find that when the when the dbd axon is lateralized in the neuropil by misexpression of the axon guidance receptor Unc-5, it forms functional synapses with the A08a lateral dendritic arbor. Changes in dbd-A08a subcellular targeting are accompanied by changes in the distribution of A08a dendritic membrane, suggesting that the dbd axon terminal can induce or stabilize dendrite outgrowth. Taken together, our data suggest that axon guidance cues establish subcellular synaptic targeting and

that there are no molecular differences in the A08a medial and lateral dendritic arbors that restrict dbd synapse formation.

Results

A08a interneuron has two dendritic arbors that receive distinct synaptic input

To determine which of our proposed developmental mechanisms regulates subcellular synaptic specificity, we focused on the A08a interneuron as a model system. A08a has spatially distinct medial and lateral dendrites, and receives distinct input to each of these dendrites (Figure 4.2). A08a interneurons can be visualized by light microscopy using the *R26F05(A08a)-LexA* line in larvae (24 ± 4 hours after larval hatching; ALH) in abdominal segments (A) 1-7 (Figure 4.2A-A',B). By expressing molecular markers, we determined that A08a has a distinct distal axonal (output) domain (mixed pre- and post-synapses) and a more proximal dendritic domain (predominantly post-synapses). A08a targets the dendritic marker DenMark::mCherry (Nicolaï et al., 2010) to the dendritic domain which includes two spatially distinct medial and lateral arbors. The A08a output domain forms a characteristic V-shaped projection at the midline, which is specifically labeled by the pre-synaptic marker Synaptotagmin::GFP (Wang et al., 2007) (Figure 4.2C-C'').

A08a can also be visualized by electron microscopy (EM) in first instar larvae (~5 hours ALH, Figure 4.2D-D') (Gerhard et al., 2017; Itakura et al., 2015; Schneider-Mizell et al., 2016). The EM reconstruction of A08a has been completed in four hemisegments (A1 left/right, A2 left/right) and in all cases the A08a neuron has the same arbors as seen in light microscopy: two spatially distinct dendritic arbors that contain only post-synapses, and a V-shaped output domain that contains both pre- and post-synapses (Figure 4.2E). Moreover, the same output and dendritic subcellular compartments as seen with DenMark::mCherry and Synaptotagmin::GFP can also be detected in the EM reconstructed A08a neuron using the synapse flow centrality algorithm (Schneider-Mizell et al., 2016), which considers path directionality between synaptic input and output locations in the A08a neuron (Figure 4.2F).

Next, we used the EM reconstruction to identify neurons with the most inputs onto A08a. We characterized the four neurons with the most synapses onto A08a dendrites (Table 4.1), and observed that dbd and A02d selectively synapse onto the A08a medial dendrite, whereas A02l and A31x selectively synapse onto the A08a lateral dendrite (Figure 4.2G; Table 4.1). A08a also receives synaptic input from additional neurons at its medial and lateral dendritic arbors, and these neurons also show a preference for either the medial or lateral dendritic arbor; a different set of neurons has synaptic input on the V-shaped output domain (data not shown). We conclude that the A08a neuron is an ideal model system to investigate the mechanisms generating subcellular synaptic specificity due to (a) Gal4 and LexA lines specifically expressed in A08a, (b) spatially distinct dendritic arbors with highly specific neuronal inputs onto each arbor, and (c) our ability to visualize A08a morphology by both light and electron microscopies. In addition, we have highly specific Gal4 and LexA lines for the dbd sensory neuron, which has specific synaptic input onto the A08a medial arbor (see below).

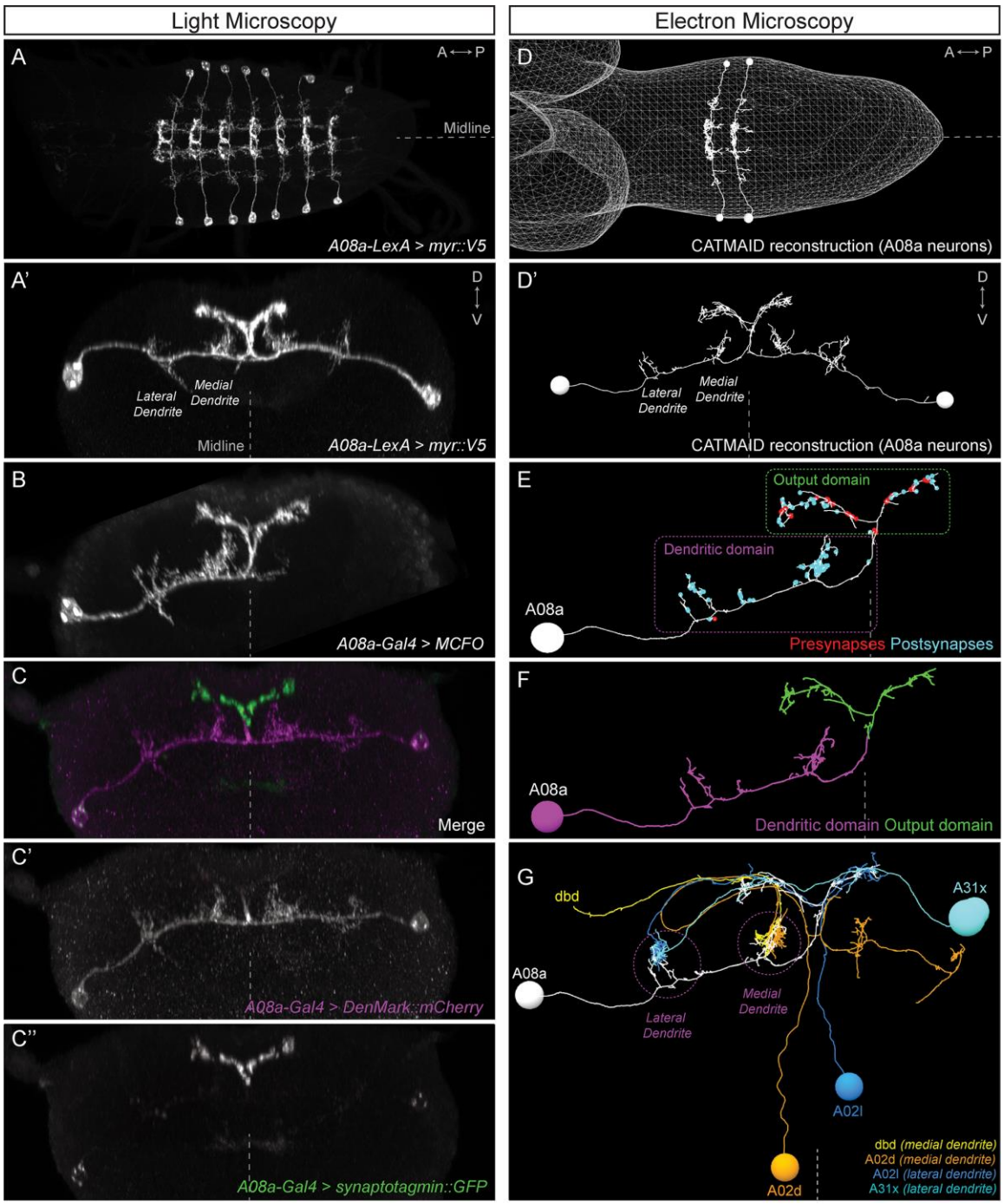

Figure 4.2. The A08a neuron receives arbor-specific synaptic inputs.
(A-C'') Light microscopy (point scanning confocal) imaging of A08a neurons.
(A) Dorsal view of the light micrograph (LM) 3D reconstruction of A08a neurons in the larval ventral nerve cord segmentsA1-7. The A08a neurons are visualized by *26F05*(*A08a)-LexA > LexAop-myr::smGdP::V5*. Midline, dashed line in all panels.
(A') Posterior view of the LM 3D reconstruction of paired A08a neurons in segment A1 left/right.
(B) Posterior view of a single A08a labeled by MultiColor FlpOut (MCFO), visualized by *A08a-Gal4 > UAS-MCFO*.

(C-C'') *A08a-Gal4* drives expression of *UAS-DenMark::mCherry* (dendrite marker) and *UAS-synaptotagmin::GFP* (presynaptic marker). Note the complementary expression in the dendritic and output domains.
(D-G) Electron microscopy (EM) reconstruction of A08a and four synaptic partner neurons.
(D) Dorsal view of A08a neurons in segments A1-2.
(D') Posterior view of A08a neurons in segment A1.
(E) A single A08a with presynaptic and postsynaptic sites labeled in red and blue respectively highlight a distinct dendritic domain and a mixed pre- and post-synaptic output domain.
(F) Synapse flow centrality analyses (Schneider-Mizell et al., 2016) shows that A08a has distinct mixed axonal (output) and dendritic compartments.
(G) A08a receives dendritic arbor-specific input: dbd (yellow) and A02d (orange) synapse specifically on the medial dendrite, whereas A02l (blue) and A31x (cyan) synapse specifically on the lateral dendrite.

A08a inputs (hemisegment)	**Pre-synapse number**		**A08a arbor targeted**
	Total	with A08a	
dbd (A1L)	79	10	medial only
dbd (A1R)	78	13	medial only
A02d (A1L)	66	22	medial only
A02d (A1R)	63	8	medial only
A02l (A1L)	38	12	lateral only
A02l (A1R)	31	4	lateral only
A31x (A1L)	19	3	lateral only
A31x (A1R)	26	9	lateral only

Table 4.1. Summary of inputs to A08a medial and lateral dendritic arbors from the first instar larval EM reconstruction. Neurons with the most synapses to A08a medial and lateral arbors shown. Neurons with fewer synapses also show specificity for medial or lateral dendritic arbors.

Quantifying dbd-A08a synapse voxel position by light microscopy

The EM reconstruction allows precise quantification of synapse number and position between dbd and A08a, but EM is not a high-throughput method for experimental analysis of synaptic contacts. Thus, we developed a light microscopy method for quantifying the position of dbd-A08a putative synapse contacts. We used the genetics described above to label A08a, and additionally used the *165(dbd)-Gal4* line (Gohl et al., 2011) to label the dbd sensory neuron in 24 ± 4 hours ALH larvae. We conclude that dbd and A08a morphology seen in light microscopy precisely matches dbd and A08a morphology seen in the EM reconstruction (Figure 4.3A-B'', Video 1).

We next quantified the position of dbd pre-synaptic contacts along the medio-lateral axis of the A08a dendrite. We used *dbd-Gal4* to express the active zone marker Bruchpilot-Short::mStrawberry (Brp-Short-mStraw, Owald et al., 2010) in the

dbd neuron; the truncated Brp protein localizes to presynaptic sites but is not functional for inducing synapse formation, making it an excellent reporter for pre-synapses (Fouquet et al., 2009). In the same larvae we used the *26F05(A08a)-LexA* line to label the A08a interneuron to express a myristoylated::V5 epitope. The dbd neuron forms synapses with many neurons in addition to A08a, so we considered only the Brp signal in close proximity (<90nm) to the A08a membrane to define the position of dbd-A08a "synapse voxels" (Figure 4.3C-C'''). Note that this is not designed to count individual synapse numbers, which are below the resolution limit of standard light microscopy, but rather to measure the position of putative synapses along the medio-lateral axis of the A08a dendrite. Quantifying synapse voxels across the medial-lateral axis of A08a dendrites in wild-type larvae (Figure 4.3D, n=27 hemisegments, N=18 animals) mirrors the position of synapses seen by EM (Figure 4.3F). In contrast, we do not observe synapse voxels between the dbd and the A08a output domain, consistent with lack of dbd synapses on the A08a output domain in the EM reconstruction (data not shown). Thus, we have established a light microscopy method for imaging and quantifying the position of dbd pre-synapses along the A08a dendritic membrane, which is a necessary prerequisite for investigating the mechanisms regulating dbd-A08a subcellular synaptic specificity.

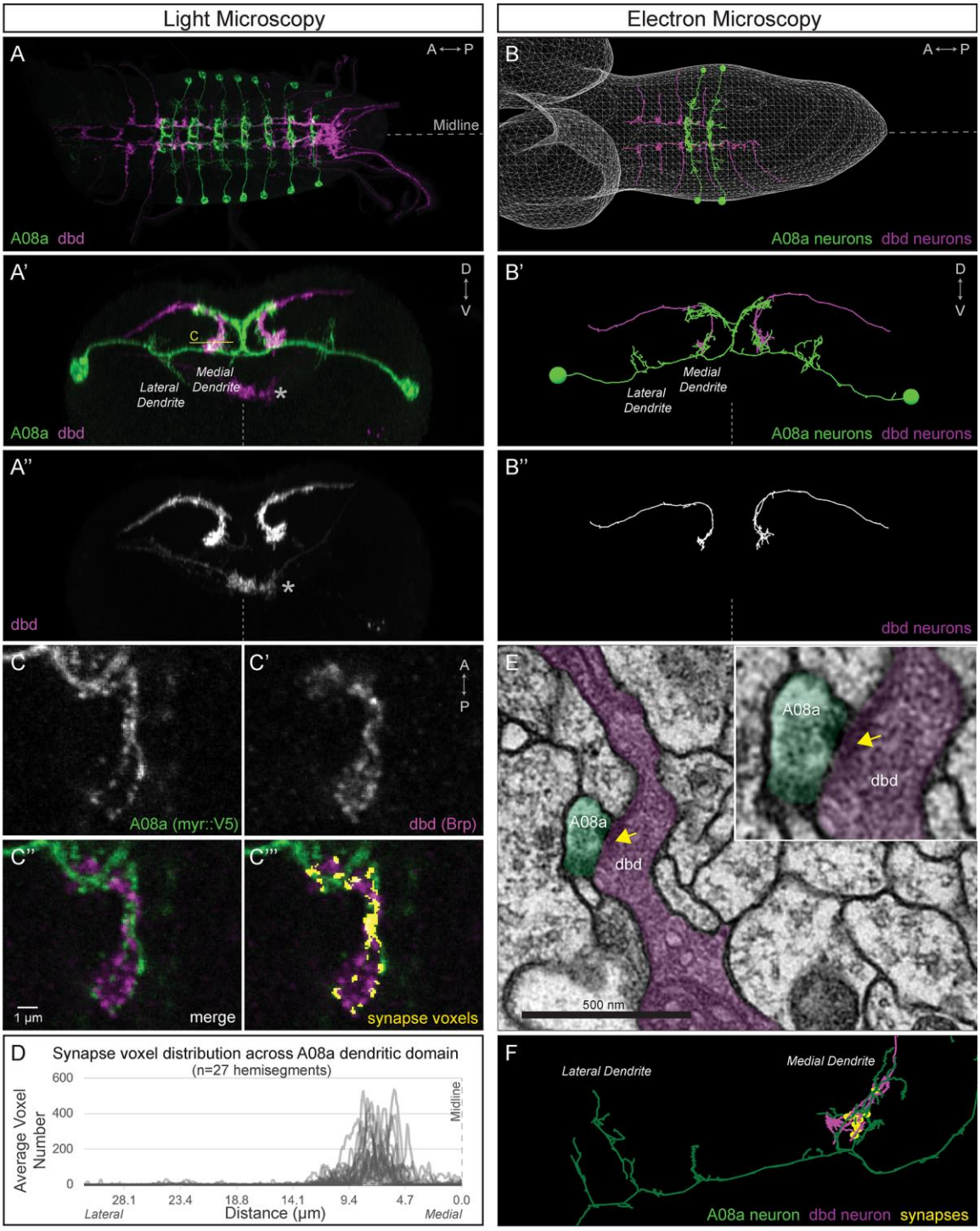

Figure 4.3. dbd and A08a neurons are synaptic partners by light and electron microscopy analyses.
(A) Dorsal view, light microscopy 3D reconstruction showing dbd (magenta) and A08a (green) neurons. A08a is visualized with *A08a-LexA > LexAop-myr::smGdP::V5*. dbd is visualized with *dbd-Gal4 > UAS-myr::smGdP::HA*. Anterior to left; midline, dashed line in all panels.
(A'-A'') Posterior view, light microscopy 3D reconstruction showing dbd and A08a neurons. dbd projects to the A08a medial dendritic arbor but not the A08a lateral dendritic arbor. Apparent

colocalization of dbd with the A08a output domain is an artifact of the 3D projection. Asterisk, ventral off target expression of *dbd-Gal4*. C, focal plane shown in panel C, below.
(B-B'') EM reconstruction of dbd and A08a neurons; B, dorsal view, (A1-A2); B'-B'', posterior view, (A1).
(C-C''') Single optical section showing a subset of dbd pre-synapses (magenta, labeled with *dbd-Gal4 > UAS-brp-short-mstraw*) positioned in close proximity to the A08a membrane (green, labeled with *A08a-LexA > LexAop-myr::smGdP::V5*). Voxels containing A08a membrane within 90nm of voxels containing Brp-mstraw are defined as "synapse voxels" (C''', yellow).
(D) Quantification of synapse voxel position across A08a dendritic domain shows enrichment on the A08a medial dendritic arbor.
(E) Representative chemical synapse between dbd and A08a (arrowhead) in the EM volume.
(F) EM reconstruction showing that the dbd neuron (magenta) synapses specifically with the A08a medial but not lateral dendritic arbor (green); synapses, yellow circles.

Lateralized dbd has Brp+ synapse voxels at the A08a lateral dendritic arbor

To determine if the lateral dendritic arbor of A08a is competent to receive input from the dbd neuron, we needed a way to re-direct dbd to a lateral location, giving it the opportunity to interact with the lateral dendrite of A08a. In *Drosophila*, neurons expressing the Netrin receptor Unc-5 or the Slit receptor Robo-2 have a repulsive response to midline-secreted Netrin and Slit ligands, respectively (Keleman & Dickson, 2001; Simpson et al., 2000a; Simpson et al., 2000b; Wang et al., 2007; Zlatic et al., 2003). Here we used *dbd-Gal4* to express either Unc-5 or Robo-2 and found that both receptors could lateralize the dbd axon terminal to varying degrees, with Unc-5 being most effective and Robo-2 having a milder effect (Figure 4.4 – Supplement 1).

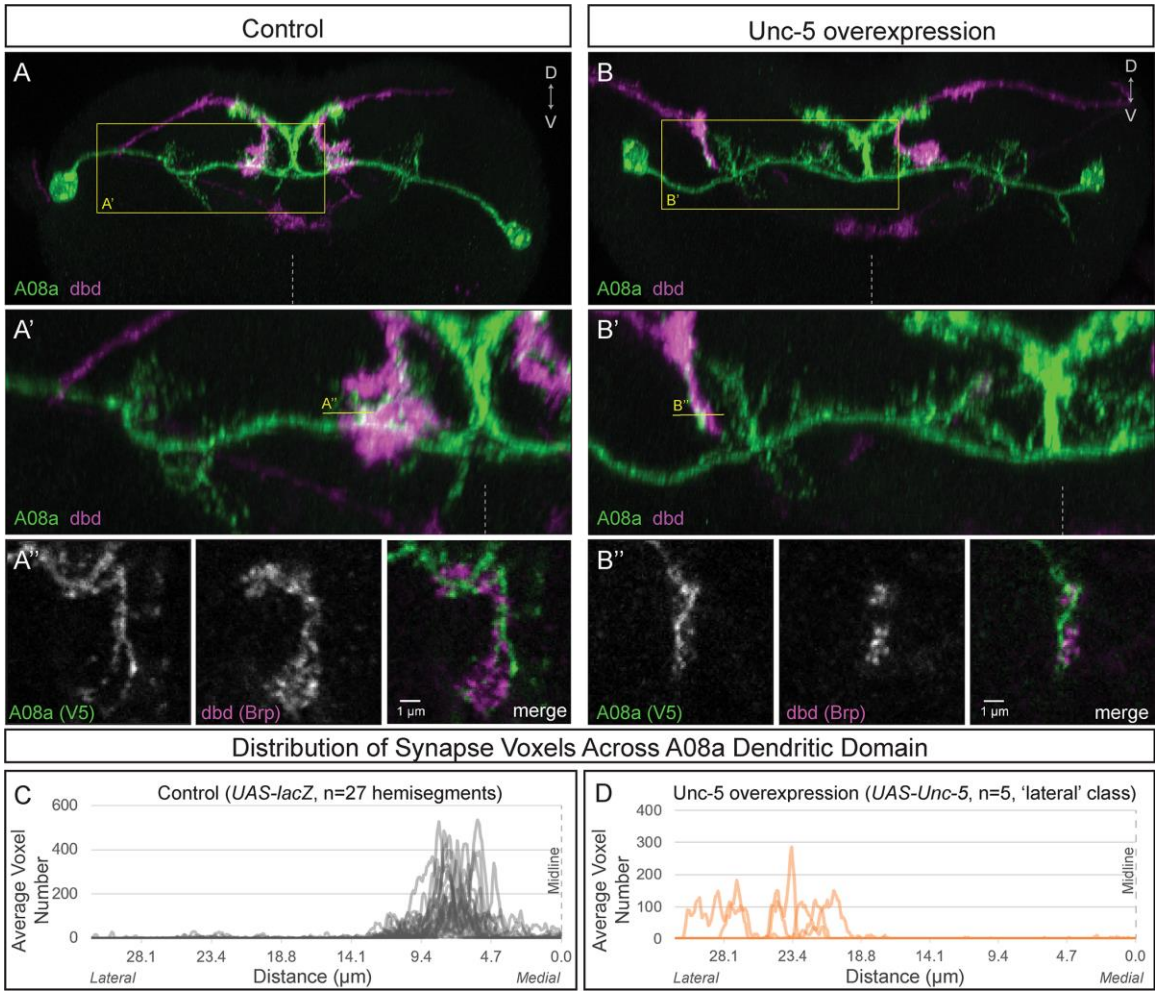

Figure 4.4. Lateralizing dbd results in Brp+ putative synapses at the A08a lateral dendritic arbor.

(A-A') In control animals, dbd membrane (magenta, labeled with *dbd-Gal4 > UAS-smGdP::myr::HA*) are positioned in close proximity to the A08a medial dendritic arbor membrane (green, labeled with *A08a-LexA > LexAop-myr::smGdP::V5*). (A) Posterior view of one segment; midline, dashed line in all panels; box, area enlarged in A'. (A') Posterior view of the dbd and the A08a medial dendritic arbor; A'' line, optical section shown in A''.

(A'') Single z-slice shows a subset of dbd pre-synapses (magenta, labeled with *dbd-Gal4 > UAS-brp-short::mstraw* in close proximity to the A08a medial dendritic arbor membrane.

(B-B') Overexpression of Unc-5 in dbd can lateralize the axon terminal of dbd. B'' line, position of optical section shown in B'' below. See Figure 4.4 – Supplement 1E for quantification of lateralization classes.

(B'') Single z-slice shows a subset of dbd pre-synapses (magenta, labeled with *dbd-Gal4 > UAS-brp-short::mstraw*) positioned in close proximity to A08a membrane (green, labeled with A08a-LexA > LexAop-myr::smGdP::V5).

(C-D) Quantification of synapse voxel position across the dendritic domain of A08a. (C) In control animals, dbd forms synapse voxels on the medial dendritic arbor of A08a; n = 27 hemisegments from 18 animals. Data reproduced from Figure 3D. (D) In hemisegments with full lateralization of dbd (as shown in B'), dbd forms synapse voxels on the lateral dendritic arbor of A08a; n = 5 hemisegments from 5 animals. See Figure 4.4 – Supplement 1E for quantification of lateralization classes.

Wild-type dbd forms synapse voxels with the A08a medial dendritic arbor (Figure 4.4A-A'',C; Figure 4.4 – Supplement 1B,E). In contrast, overexpression of Unc-5 in dbd can lateralize the dbd axon terminal, positioning dbd adjacent to the A08a lateral dendritic arbor (Figure 4.4B-B'; Figure 4.4 – Supplement 1D,E). These lateralized dbd terminals formed synapse voxels with the lateral dendritic arbor of A08a (Figure 4.4B''). Similarly, overexpression of Robo-2 in dbd resulted in lateralization of the dbd axon terminal; the majority of dbd terminals formed synapse voxels in the intermediate zone between the medial and lateral dendrites (Figure 4.4 – Supplement 1C,E). The close apposition of dbd presynaptic Brp to the A08a dendritic membrane is consistent with, but does not prove, that there is functional connectivity between dbd and A08a at this arbor. Taken together, these results suggest that dbd can form Brp+ putative synapses throughout the entire A08a dendritic domain, which is more consistent with the "guidance cue" model and less consistent with the "labeled arbor" model.

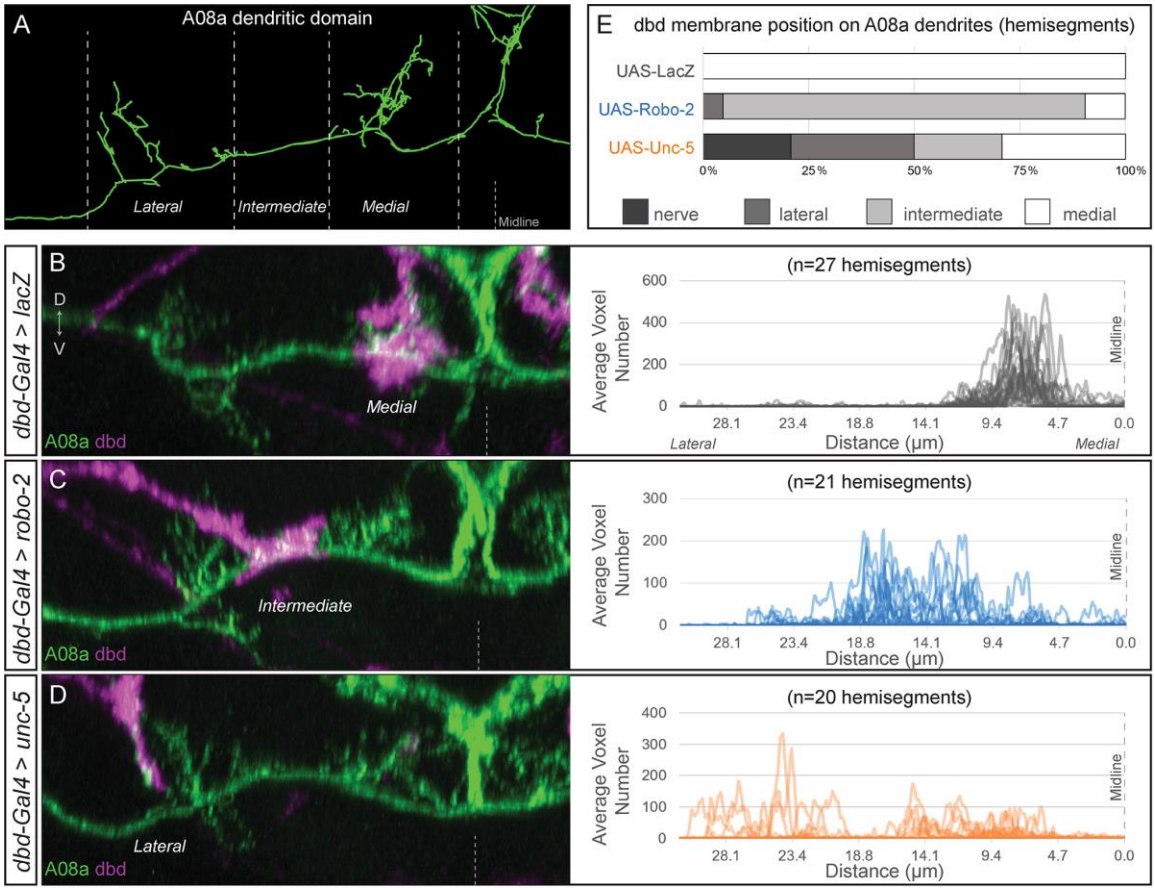

Figure 4.4 – Supplement 1. dbd axons can be variably lateralized by expression of axon guidance receptors Unc-5 and Robo-2.
(A) The A08a neuron in the EM reconstruction can be divided into medial, intermediate, and lateral dendritic domains.
(B-D) The dbd neuron membrane (magenta) can target different subcellular domains of A08a (green), posterior view of one hemisegment. (B) Control: dbd contacts the A08a medial dendritic arbor (*dbd-Gal4 > UAS-lacZ*). Data reproduced from Figure 3D. (C) Partial lateralization example: dbd contacts the intermediate dendrite domain (*dbd-Gal4 > UAS-robo-2*). (D) Full lateralization example: dbd contacts that lateral A08a dendritic arbor (*dbd-Gal4 > UAS-unc-5*). Data reproduced from Figure 4B',D. Right panels show the distribution of synapse voxels for each genotype. Control, *UAS-lacZ*, n=27 hemisegments from 18 animals; *UAS-robo-2*, n=21 hemisegments from 15 animals; *UAS-unc-5*, n=20 hemisegments from 17 animals.
(E) Frequency of dbd membrane lateralization by genotype. dbd will either target mostly the medial, intermediate, or lateral dendritic domains, or not enter the neuropil ('nerve' category). See methods for full genotypes.

Lateralization of dbd results in a lateral shift of A08a dendritic membrane

In wild-type A08a neurons, there is little or no arborization present in the intermediate domain of the main dendritic process (Figure 4.2C',F; Figure 4.4 – supplement 1A,B). In contrast, when the dbd axon terminal was lateralized to be

adjacent to the intermediate domain, dendritic arbors present in the intermediate domain and were intimately associated with the dbd axon terminal (Figure 4.4 – supplement 1B,C). This raised the question of whether the dbd axon terminal might induce or stabilize dendritic arbors. Therefore, we quantified the position of A08a dendritic membrane across the medial-lateral axis in control larvae, where dbd targeted the A08a medial dendritic domain (Figure 4.5A,D), and in larvae overexpressing Robo-2 or Unc-5 in dbd, where dbd was positioned at the intermediate or lateral domain respectively (Figure 4.5B-D). When dbd was shifted to the A08a intermediate domain by Robo-2 overexpression, the A08a arbors were reduced medially and increased in the intermediate domain, where there is usually little or no arbor material; in addition, the new intermediate arbor was closely associated with the dbd axon terminal (Figure 4.5B,D). When dbd was shifted to the A08a lateral domain by Unc-5 overexpression, the A08a arbors were reduced medially and increased laterally, again showing close association with the lateralized dbd axon terminal (Figure 4.5C,D). Analyzing dendritic arbor position by weighted mean analysis confirms the lateral shift in arbor material following Robo-2 or Unc-5 overexpression (Figure 4.5E). These changes in A08a dendrite distribution suggest that axon guidance cues position the dbd axon terminal at a particular neuropil domain, where it may induce or stabilize dendrites at the appropriate subcellular domain of its synaptic partner, A08a.

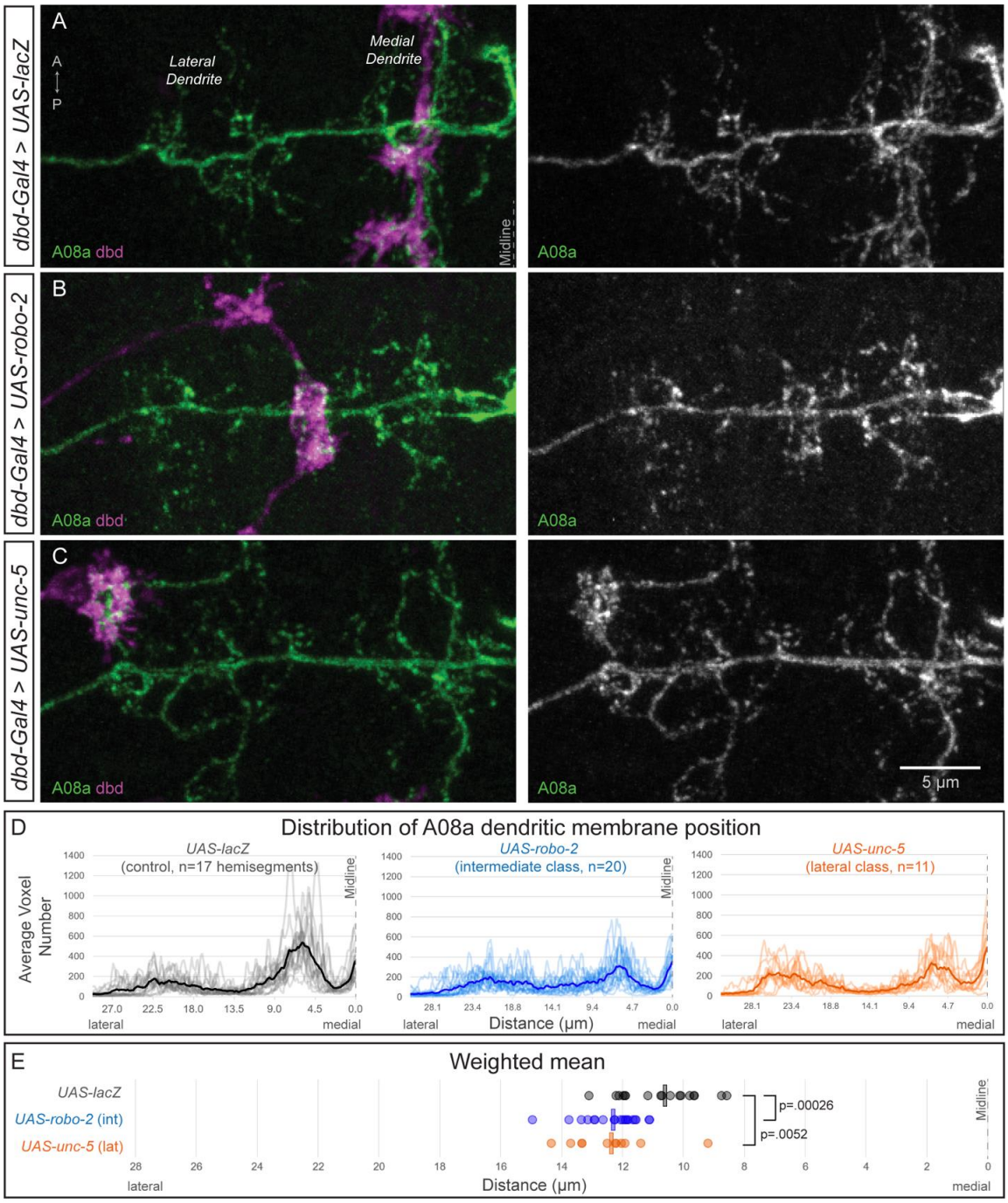

Figure 4.5. Lateralization of the dbd axon terminal results in lateralization of A08a dendrites.
(A-C) Confocal maximum intensity projection of the dbd axon terminal (magenta) and the A08a dendritic domain (green) in one hemisegment; lateral to the left, midline on the right (dorsal view). (A) In wild type, dbd targets the A08a medial arbor. (B) In *UAS-robo-2*, dbd often contacts the A08a intermediate domain; (C) In *UAS-unc-5*, dbd often contacts the A08a lateral arbor. Control, n=17 hemisegments from 11 animals; *UAS-robo-2*, intermediate class only, n=20 hemisegments from 10 animals; *UAS-unc-5*, lateral class only, n=11 hemisegments from 10 animals.

(D) Quantification of the distribution of A08a dendrite position in the context of medial, intermediate, and lateral innervating dbd neurons. Each transparent line represents one hemisegment and each solid line represents the average for the cohort.
(E) Weighted mean of the dendrite distributions shown in D. Each circle represents the weighted mean for each hemisegment and the bar represents the average weighted mean for each cohort. Average weighted mean: *UAS-lacZ:* 10.63 µm; *UAS-robo-2*, intermediate: 12.33 µm; *UAS-unc-5*, lateral: 12.38 µm. P-values were obtained using an unpaired t-test.

Lateralized dbd forms functional synapses with the A08a lateral dendritic arbor

Our finding that the lateralized dbd axon terminal localizes Brp+ puncta in close apposition to the lateral A08a dendritic arbor suggests that these two neurons are synaptically connected, but falls short of proving functional connectivity. To test for functional connectivity between the lateralized dbd and A08a, we took an optogenetics approach. We used the Gal4/UAS and LexA/LexAop binary expression systems (Brand & Perrimon, 1993; Lai & Lee, 2006) to express the light-gated cation channel CsChrimson (Chrimson) in dbd, and the calcium indicator GCaMP6m in A08a. For technical feasibility, all optogenetic experiments were done at the third instar larval stage (72 ± 4 hours ALH). Note that the A08a neuron at this stage retains its morphological features, including medial and lateral dendritic arbors plus a V-shaped output domain (Figure 4.6 – Supplement 1).

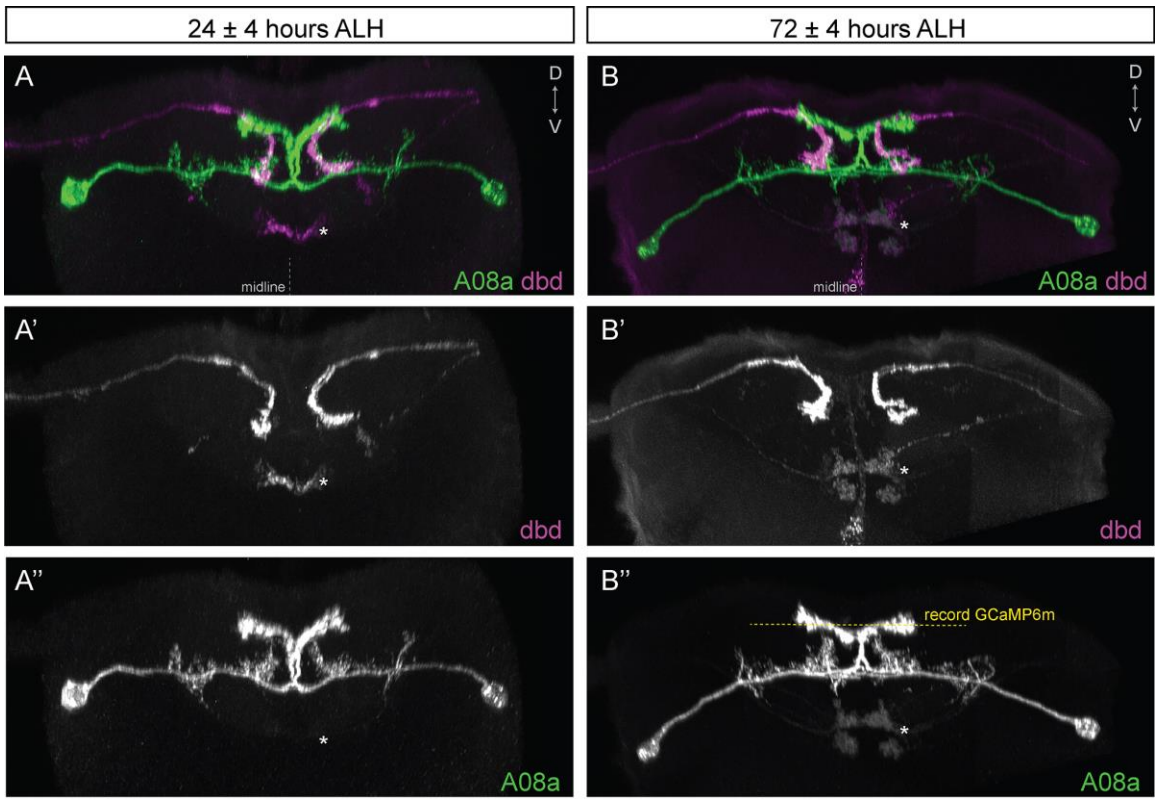

Figure 4.6 – Supplement 1. dbd and A08a neuronal morphology is similar at 24 hours and 72 hours after larval hatching (ALH).
(A-A'') Posterior view of a 3D light microscopy reconstruction in Imaris showing dbd (magenta) and A08a (green) neurons at 24 ± 4 hours ALH. Midline, dashed line in all panels. Asterisk, ventral off-target neurons.
(A') The dbd neurons are visualized by *165(dbd)-Gal4 > UAS-myr::smGdP::HA*.
(A'') The A08a neurons are visualized by *26F05(A08a)-LexA > LexAop-myr::smGdP::V5*.
(B-B'') Posterior view of a 3D light microscopy reconstruction in Imaris showing dbd (magenta) and A08a (green) neurons at 72 ± 4 hours ALH. Yellow dashed line indicates the imaging focal plane used to record GCaMP6m fluorescence changes in A08a neurons. Asterisk, position of ventral off-target neurons.
(B') The dbd neurons are visualized by *165(dbd)-Gal4 > UAS-myr::smGdP::HA*.
(B'') The A08a neurons are visualized by *26F05(A08a)-LexA > LexAop-myr::smGdP::V5*.

We first tested for functional connectivity between the wild-type dbd and A08a, which had not yet been documented. In wild-type, Chrimson-induced activation of dbd resulted in a significant increase in GCaMP6m fluorescence in A08a, but not in the absence of the Chrimson co-factor all-*trans* retinal (ATR) (Figure 4.6A, quantified in D; Video 2), or in the absence of the *dbd-Gal4* transgene (Figure 4.6E; quantified in F). We measured GCaMP6m levels in the output domain of A08a, which emitted a larger fluorescence signal compared to the

arborizations in the dendritic domain (Figure 4.6C). This is the first experiment showing functional, excitatory connectivity between dbd and A08a. Next, we sought to determine whether the putative synapses between the lateralized dbd and the A08a lateral dendritic arbor are also functional. Using the same paradigm as in wild-type controls, we find that Chrimson activation of lateralized dbd resulted in an increase in GCaMP6m fluorescence in A08a that is statistically indistinguishable from wild-type controls (Figure 4.6B, quantified in D; Video 3). These data are consistent with dbd activating A08a equally well using medial arbor connectivity (control) or lateral arbor connectivity (following Unc-5 expression).

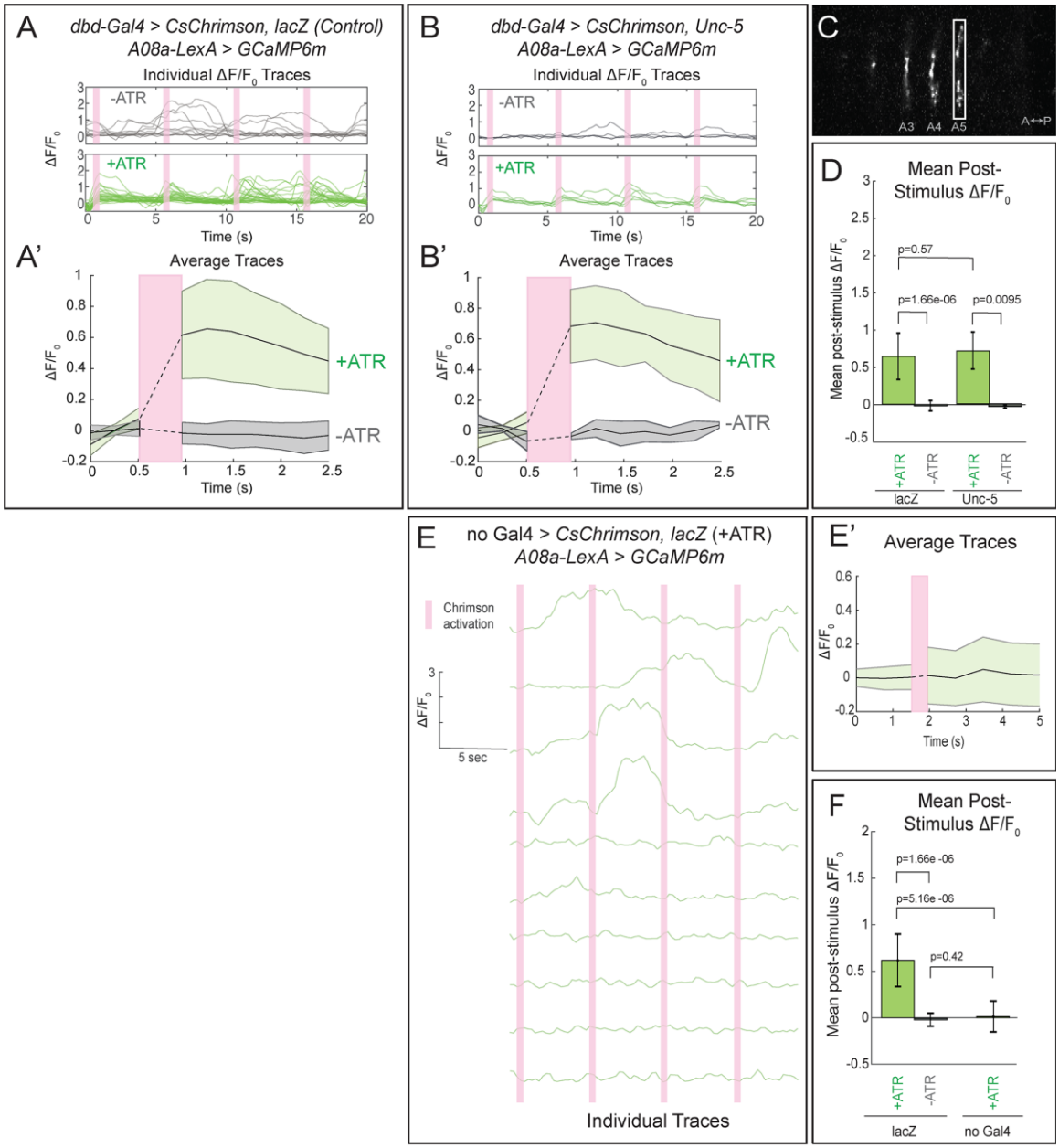

Figure 4.6. Confocal activation of Chrimson in control and lateralized dbd increases A08a GCaMP6m fluorescence.

(A-A') In wild-type animals, Chrimson activation of dbd neurons results in increased GCaMP6m fluorescence in the A08a output domain. For all figures, +ATR is shown in green, -ATR is shown in gray, and timing of Chrimson activation is represented with a pink bar.

(A) A08a GCaMP6m $\Delta F/F_0$ traces from individual A08a pairs resulting from wild-type dbd activation. Non-evoked spontaneous activity is present in -ATR control.

(A') Average A08a GCaMP6m $\Delta F/F_0$ traces, before and after Chrimson activation of dbd neurons. Solid black lines represent the mean $\Delta F/F_0$. Shaded regions represent the standard deviation from the mean. +ATR, n=28 A08a pairs, from 10 animals; -ATR, n=11 A08a pairs, from 5 animals.

(B-B') In animals with fully lateralized dbd, Chrimson activation of dbd results in increased GCaMP6m fluorescence in A08a axon terminals.

(B) A08a GCaMP6m $\Delta F/F_0$ traces from individual A08a pairs resulting from activation of lateralized dbd.

(B') Average A08a GCaMP6m $\Delta F/F_0$ traces, before and after Chrimson activation of dbd neurons. Solid black lines represent the mean $\Delta F/F_0$. Shaded regions represent the standard deviation from the mean. +ATR, n=6 A08a pairs, from 5 animals; -ATR, n=4 A08a pairs, from 3 animals.
(C) Example ROI used for quantification drawn around A08a axon terminals in segment A5.
(D) Quantification of the mean post-stimulus $\Delta F/F_0$ for *lacZ* control and *unc-5*. Error bars represent the standard deviation from the mean. Mean post-stimulus $\Delta F/F_0$: *lacZ* Control +ATR, 0.62 ± 0.28, n=28 A08a pairs, from 10 animals; *lacZ* Control -ATR, -0.0172 ± 0.07, n=11 A08a pairs, from 5 animals; *unc-5* +ATR, 0.68 ± 0.24, n=6 A08a pairs, from 5 animals; *unc-5* -ATR, -0.035 ± 0.02, n=4 A08a pairs, from 3 animals.
(E-E') *dbd-Gal4* is required to produce Chrimson-evoked responses in A08a. A08a expresses GCaMP6m in a genetic background containing *UAS-lacZ* and *20XUAS-CsChrimson.*
(E) A08a GCaMP6m $\Delta F/F_0$ traces from individual A08a pairs.
(E') Average A08a GCaMP6m $\Delta F/F_0$ traces before and after light stimulus (pink bar). Solid black line represents the mean $\Delta F/F_0$. Shaded region represents the standard deviation from the mean. +ATR is represented in green (n=10 A08a pairs).
(F) Quantification of the mean post-stimulus $\Delta F/F_0$ for *lacZ* control +ATR, *lacZ* control -ATR, and no dbd-*gal4* control. Error bars represent the standard deviation from the mean. Mean post-stimulus $\Delta F/F_0$: *lacZ* Control +ATR, 0.62 ± 0.28, n=28 A08a pairs, from 10 animals (Data reproduced from Figure 6D); *lacZ* control -ATR, -0.0172 ± 0.07, n=11 A08a pairs, from 5 animals (Data reproduced from Figure 6D); No *dbd-gal4*Control +ATR, 0.013 ± 0.17, n=10 A08a pairs, from 5 animals. Significance between two groups was determined using a Mann-Whitney test.

We observed that the Gal4 line used to express Chrimson in dbd also has expression in a subset of ventral neurons (Figure 4.3; Figure 4.6 – Supplement 1), which may provide indirect activation of A08a. Thus, we used two-photon microscopy (Figure 4.7A,B) to specifically activate dbd or the ventral off-target neurons by selecting regions of interest (ROIs) that were specific for each without overlapping in the xy-axis (Figure 4.7C). We sequentially activated the dbd and off-target neurons within the same larva, and found that A08a had significantly larger GCaMP6m responses following Chrimson activation of dbd compared to the off-target neurons (Figure 4.7E, quantified in F). Similar results were observed for larvae where Unc-5 misexpression was used to lateralize the dbd axon (Figure 4.7G, I; quantified in J). We conclude that Chrimson activation of dbd neurons is able to increase GCaMP6m fluorescence in A08a neurons in both wild-type and Unc-5 misexpression genotypes.

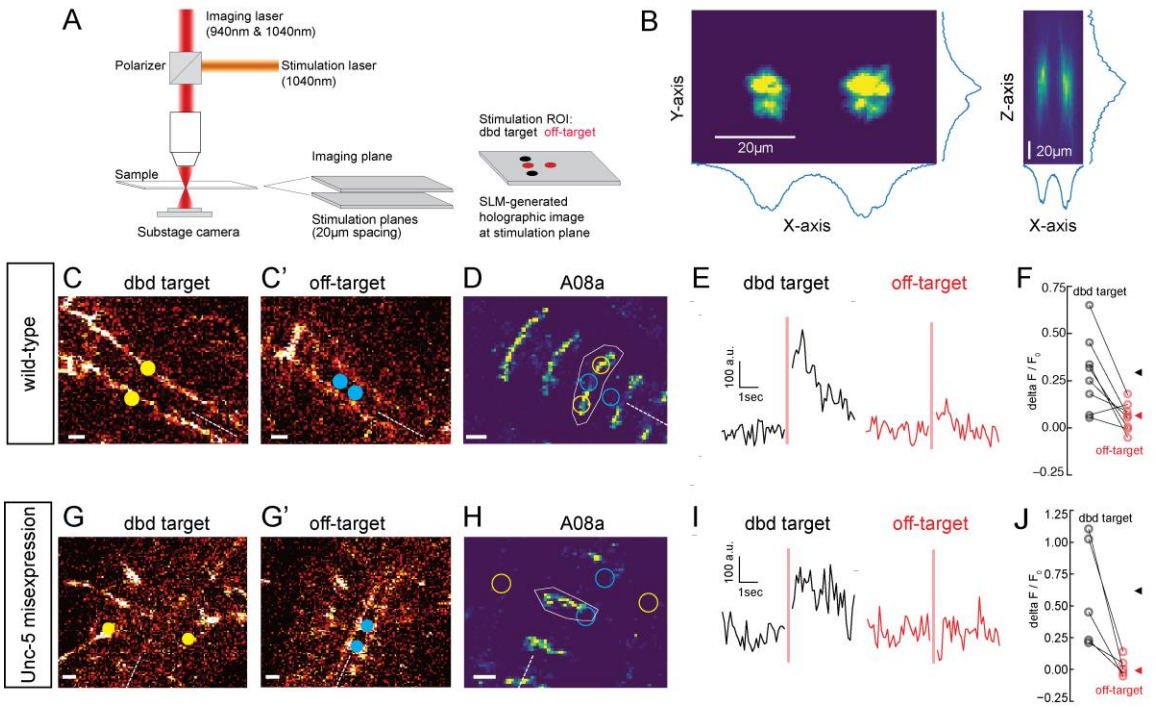

Figure 4.7. Two photon activation of dbd, but not off-target neurons, increases A08a GCaMP6m fluorescence.

(A) Schematic of two photon microscope used for Ca^{+2} imaging and holographic photostimulation. We used a separate imaging (940 or 1040 nm) and stimulation laser (1040 nm). Holographic photostimulation patterns were constructed with a spatial light modulator (SLM). Stimulation targeted either dbd neurons (black circles) or off-target neurons (red circles), separated on average by 20 µm in the z-axis.

(B) XY and XZ profile of fluorescence induced by a holographic stimulation pattern consisting of two 10 µm diameter circles separated center-to-center by 26 µm. Fluorescence profiles were obtained by moving microscope objective systematically relative to a fixed fluorescent rhodamine slide and imaging with a sub-stage camera. Blue lines indicate fluorescence summed across respective axes (arbitrary units).

(C-F) Targeting of Chrimson stimulation and Ca^{+2} imaging of A08a neurons in wild-type 72h ALH larvae. (C-C') Two photon image (1040 nm) of fluorescent mCherry marker at two imaging planes 20 µm apart. Stimulation ROIs used for targeting dbd (C, yellow dots) and off-target (C', cyan dots) neurons are overlaid. Dashed white line indicates midline. Scale bars, 10µm.

(D) Summed GCaMP6m fluorescence in A08a neurons (940 nm). White polygon depicts spatial region used to quantify fluorescence for traces in E. The stimulation regions shown in C are overlaid (outlines: yellow, dbd; cyan, ventral off-targets). Scale bars, 10µm.

(E) Example Ca^{+2} responses from the wild-type larva shown in C, D. Black trace shows raw A08a fluorescence (arbitrary units) prior to and following 150 ms holographic stimulation of dbd targets. Red trace shows A08a fluorescence in response to ventral off-target stimulation. Stimulation timing depicted with pink rectangle.

(F) Mean Ca^{+2} responses ($\Delta F/F_0$) in A08a for each animal to dbd stimulation (black dots) or ventral off-target stimulation (red dots). Triangles are means for each group (dbd, 0.29 +/- .07; off-target, 0.06 +/- 0.07). N= 8 animals. Scale bars, 10µm.

(G-J) Targeting of Chrimson stimulation and Ca^{+2} imaging of A08a neurons in Unc-5 misexpression larvae at 72h ALH. (G-G') Two photon image (1040 nm) of fluorescent mCherry marker at dbd (G) and off-target imaging planes (G'), separated by 20 µm. Stimulation ROIs overlaid (dbd, G, yellow dots; off target, G', cyan dots).

(H) Summed GCaMP6m fluorescence in A08a neurons. Stimulation regions and measurement region plotted as in D.
(I) Example Ca^{+2} responses from Unc-5 larva shown in G, H as in E. Black trace shows raw A08a fluorescence in response to dbd stimulation; red trace is A08a fluorescence in response to off-target stimulation.
(J) Mean Ca^{+2} responses ($\Delta F/F_0$) in A08a for each animal to dbd stimulation (black dots) or ventral off-target stimulation (red dots). Triangles are means for each group (dbd, 0.60+/-.17; off-target, 0.02+/.03). N = 5 animals. Scale bars, 10μm.

To determine whether the lateralized dbd provides monosynaptic input to A08a, we performed the same optogenetic experiments in the presence of tetrodotoxin (TTX), a sodium channel blocker that eliminates neuronal action potentials (Narahashi et al., 1964). First, we applied TTX to isolated larval CNS preparations and observed loss of the spontaneous rhythmic neuronal activity characteristic of fictive locomotion (Pulver et al., 2015), confirming that TTX was effective (Figure 4.8A; Videos 4,5). Next, we assayed the effect of TTX on dbd-A08a connectivity. If dbd-A08a connectivity is monosynaptic, then Chrimson activation of dbd should induce A08a GCaMP activity even in the presence of TTX; in contrast, if dbd-A08a connectivity is indirect (e.g. via feedforward excitation) then A08a GCaMP6m activity should be blocked by TTX (summarized in Figure 4.8B) (Petreanu et al., 2009). We found that TTX does not block dbd-induced A08a activity, in wild-type (Figure 4.8C-C'') or when the dbd axon terminal is lateralized by Unc-5 (Figure 4.8D-D''), showing that the dbd synapses on the lateral dendritic arbor of A08a are functional and monosynaptic. Interestingly, A08a GCaMP responses are significantly greater following TTX application in both wild-type and *unc-5* conditions; this may be due to the elimination of feedforward inhibition (see Discussion). We conclude that the lateralized dbd-A08a synapses are monosynaptic and functional. Our data therefore support a model in which axon guidance cues are the major determinants of dbd-A08a subcellular dendritic synaptic specificity.

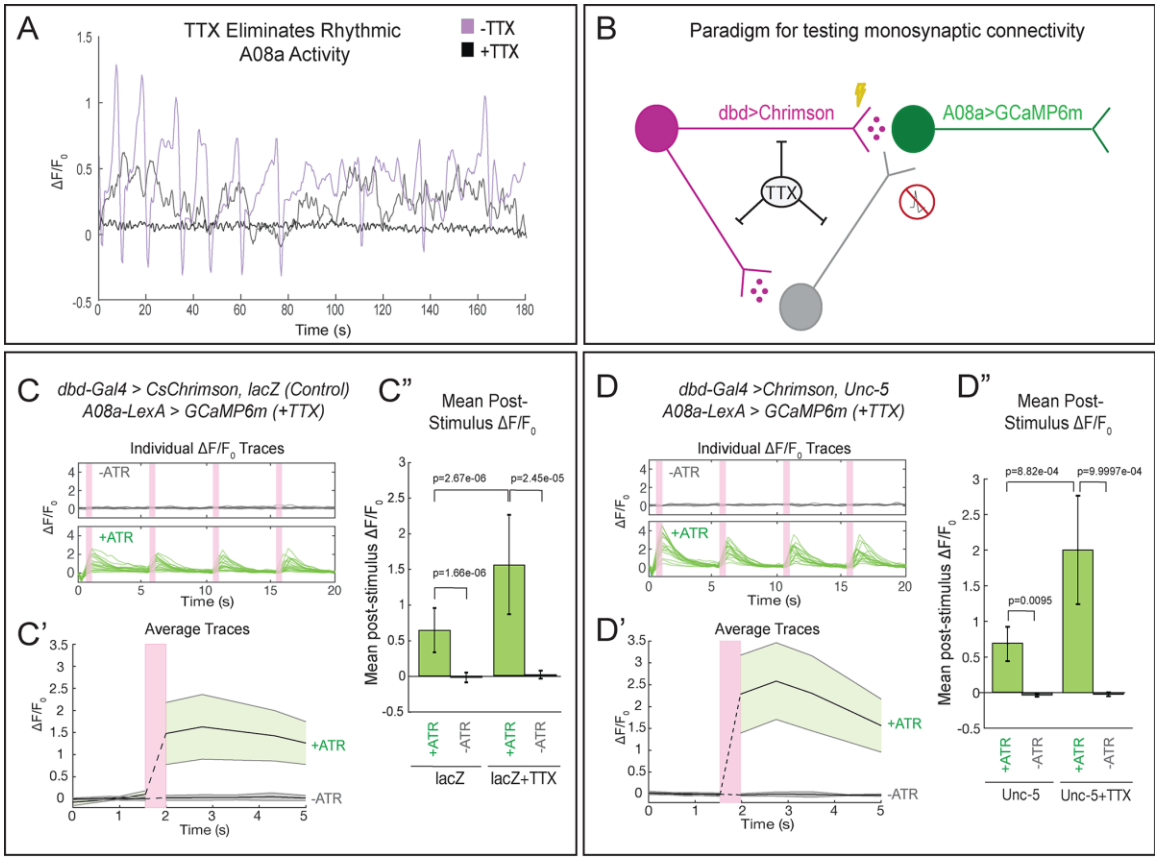

Figure 4.8. Lateralized dbd forms direct, monosynaptic connections with the A08a lateral dendrite.
(A) TTX eliminates spontaneous rhythmic neuronal activity in A08a (in which activity is part of an inter-segmental activity wave moving in the anterior or posterior direction representing fictive motor waves; Itakura et al., 2015). Representative traces show the $\Delta F/F_0$ for individual pairs of A08a neurons over the course of 3 minutes in *lacZ* control animals. Purple trace shows A08a $\Delta F/F_0$ without TTX present. Black trace shows A08a $\Delta F/F_0$ in the presence of 3µM TTX, in which 20/20 A08a pairs from 8 animals where rhythmic activity was eliminated. In 8/20 of these A08a pairs, non-rhythmic, non-intersegmentally coordinated changes in GCaMP6m fluorescence were observed, exemplified by the gray trace (see Discussion).
(B) Experiment to test for monosynaptic dbd-A08a connectivity. TTX eliminates action-potential-mediated activity, preventing stimulation of non-Chrimson expressing neurons. Light-activation of Chrimson induces action-potential-independent neurotransmitter release from dbd. If dbd is monosynaptically connected to A08a, increases in A08a GCaMP fluorescence will result.
(C-C") Wild-type dbd has excitatory, monosynaptic connection to A08a medial dendritic arbor.
(C) A08a GCaMP6m $\Delta F/F_0$ traces from individual A08a pairs resulting from wildtype dbd activation in the presence of TTX.
(C') Average A08a GCaMP6m $\Delta F/F_0$ traces in the presence of 3µM TTX, before and after Chrimson activation of dbd neurons. Solid black lines represent the mean $\Delta F/F_0$. Shaded regions represent the standard deviation from the mean. +ATR, n=20 A08a pairs, from 9 animals; -ATR, n=9 A08a pairs, from 4 animals.
(C") Quantification of the mean post-stimulus $\Delta F/F_0$ for *lacZ* control and *lacZ* +TTX animals. Mean post-stimulus $\Delta F/F_0$: *lacZ* Control +ATR, 0.62 ± 0.28, n=28 A08a pairs, from 10 animals (Data reproduced from Figure 6D); *lacZ* control -ATR, -0.0172 ± 0.07, n=11 A08a pairs, from 5 animals (Data reproduced from

Figure 6D); *lacZ* control +TTX +ATR, 1.48 ± 0.70, n=20 A08a pairs, from 9 animals; *lacZ* control +TTX -ATR, 0.019 ± 0.055, n=9 A08a pairs, from 4 animals.
(D-D") Lateralized dbd has excitatory, monosynaptic connection to A08a lateral dendritic arbor.
(D) GCaMP6m $\Delta F/F_0$ traces from A08a pairs after activation of lateralized dbd in the presence of TTX.
(D') Average A08a GCaMP6m $\Delta F/F_0$ traces in the presence of 3μM TTX, before and after Chrimson activation (pink bar) of dbd neurons. Solid black lines represent the mean $\Delta F/F_0$. Shaded regions represent the standard deviation from the mean. +ATR, n=17 A08a pairs, from 14 animals; -ATR, n=5 A08a pairs, from 4 animals.
(D") Quantification of the mean post-stimulus $\Delta F/F_0$ for Unc-5 and Unc-5 +TTX animals. Mean post-stimulus $\Delta F/F_0$: Unc-5 +ATR, 0.68 ± 0.24, n=6 A08a pairs, from 5 animals (Data reproduced from Figure 6D); Unc-5 -ATR, -0.035 ± 0.02, n=4 A08a pairs, from 3 animals (Data reproduced from Figure 6D); Unc-5 +TTX +ATR, 2.00 ± 0.76, n=17 A08a pairs, from 14 animals; Unc-5 +TTX -ATR, 0.023 ± 0.03, n=5 A08a pairs, from 4 animals. Significance between two groups was determined using a Mann-Whitney test.

Discussion

Achieving subcellular synaptic specificity

The ability of a presynaptic neuron to form synapses with a specific subcellular domain of its post-synaptic partner is well established in mammals (reviewed in Yogev & Shen, 2014), and has been described previously in *Drosophila*, although not at a mechanistic level. For example, the *Drosophila* giant fiber (GF) descending neuron targets a specific dendritic domain of the tergotrochanteral motor neuron, TTMn (Borgen et al., 2017). The transmembrane Sema-1a protein is required for both GF pathfinding to the motor neuropil, but also for establishing synaptic contact with the TTMn (Godenschwege et al., 2002; Godenschwege & Murphey, 2009). However, it remains unknown if Sema-1a protein is restricted to the specific dendritic domain of TTMn chosen by the GF, as predicted by the "labeled arbor" model. Similarly, the Jaam1 and Jaam3 interneurons target different domains of their post-synaptic EL neuron partners (Heckscher et al., 2015), but the mechanism is unknown.

Here, we provide evidence that axon guidance cues are the major determinants of subcellular dendritic synaptic specificity between dbd and A08a neurons, and that all regions of the A08a dendrite are competent to receive dbd synaptic inputs. Our findings expand upon the known mechanisms that generate subcellular synapse specificity to include guidance cues that restrict synaptic inputs to one region of a larger dendritic domain that is competent to receive synaptic input. We observed that the dbd axon is positioned close to the A08a output domain but never forms

presynaptic contacts with this domain, as assayed by light and electron microscopy (data not shown). We speculate that the A08a output domain contains cell surface molecules (CSMs) that locally prevent dbd synapse formation. This is similar to work in *C. elegans* that identified secreted proteins that cluster CSMs to restrict synapse position on the DA9 motor neuron (Klassen & Shen, 2007). Similarly, NF186 expression is confined to the axon initial segment of Purkinje cells and determines the location of basket cell synapses (Ango et al., 2004). These observations suggest that synaptically coupled neurons may utilize both axon guidance cues and arbor-specific molecular cues to achieve subcellular synaptic specificity. We anticipate both "labeled arbors" and "guidance cues" play a role in determining subcellular synaptic specificity – possibly both acting in the same neuron, such as CSMs potentially regulating connectivity between coarse subcellular domains, such as the A08a axon versus dendrite, and guidance cues refining connectivity within a particular subcellular domain, such as the medial and lateral A08a dendritic domains.

Formation of functional lateralized dbd-A08a synapses

We have shown that the lateralized dbd axon not only makes close Brp contacts with the A08a lateral dendrite, but more importantly also makes functional synapses. Interestingly, there appear to be fewer synapse voxels between the lateralized dbd and A08a than between the medial dbd and A08a, yet functional connectivity is indistinguishable. This may be due to homeostatic mechanisms that increase the efficacy of the lateral dbd-A08a synapses. The fact that the dbd-A08a optogenetic activation occurs even in the presence of TTX, together with the observation of direct dbd-A08a synapses in EM, strongly suggests that dbd and A08a have direct, monosynaptic excitatory connectivity. Interestingly, dbd induced activation of GCaMP6m in A08a is greater in the presence of TTX (in both wild-type and after dbd lateralization), suggesting that dbd may activate an inhibitory feed-forward circuit that is silenced by TTX. A good candidate for such feed-forward inhibition is the A02d neuron, which is an inhibitory neuron that receives input from dbd and has output to A08a (Fushiki et al., 2016; Kohsaka et al., 2014) (Figure 4.2G). In some cases, we detected fluctuations in A08a GCaMP6m activity following TTX

application (8/20 A08a pairs; Figure 4.8A); it is unclear if these represent cases of incomplete A08a inactivation, graded Ca^{2+} potentials, or Ca^{2+} release from internal organelles. It is also important to consider that not all insect neurons produce sodium-dependent spikes; therefore, we cannot fully rule out the possibility that the A08a activation we observe in the presence of TTX is due to indirect stimulation from non-spiking interneurons (Pearson & Fourtner, 1975; Pippow et al., 2009).

We also note that animals fed ATR (+ATR) have a statistically significant higher baseline level of calcium activity than -ATR controls (Videos 2,3 and data not shown). This is likely due to our illumination with 488nm light between 561nm stimulus pulses (see optogenetic Methods), because 488nm light was shown previously to weakly activate Chrimson (Klapoetke et al., 2014). It therefore follows that +ATR animals would have a higher baseline level of fluorescence. Importantly, this does not change our interpretation that lateralized dbd neurons form functional synapses with the A08a lateral dendrite.

We have shown that the lateralized dbd maintains synaptic contact with A08a by remapping synaptic connectivity to the lateral arbor of A08a. However, we are unable to determine if dbd still maintains cellular synaptic specificity with its other synaptic partners. In contrast to A08a, other dbd target neurons only have a medial dendritic arbor, such as Jaam-3 (Heckscher et al., 2015). It would be interesting to know how these neurons respond to dbd lateralization; they m ay extend novel dendrite branches laterally, or may simply lose dbd synaptic inputs. The development of genetic tools to specifically label additional dbd target neurons will be required to understand if cellular synaptic specificity of dbd is maintained upon its remapping in the neuropil.

Axonal induction of dendritic arbors

It was proposed ~50 years ago that presynaptic axons can induce or stabilize specific post-synaptic dendritic arbors (Altman & Anderson, 1972; Berry et al., 1980; Kimmel et al., 1982; Morest, 1969; Redmond & Ghosh, 2005). In particular, otic capsule inputs to the Mauthner neuron target a stereotyped lateral dendritic arbor, which is specifically reduced following otic capsule ablation (Kimmel et al., 1982).

Our experiments are consistent with these findings, but involve retargeting of inputs rather than their ablation. We show that in wild-type larvae, the intermediate domain of the A08a dendrite has few or no arborizations, but that partial lateralization of dbd (following Robo-2 or Unc-5 overexpression) results in the induction or stabilization of dendritic arbors in the intermediate domain. It is currently unknown how dbd induces and/or stabilizes A08a dendrites. It is possible that Robo-2 or Unc-5 directly promote dendritogenesis, although we think it is unlikely because we see the same effect following overexpression of two different receptors (Unc-5 and Robo-2). We also think it is unlikely that arbor outgrowth is a homeostatic response to loss of excitatory input, because we have shown that the wild-type and lateralized dbd are both functional at inducing A08a activity, and because the ectopic arbors appear closely associated with the dbd axon terminal. In contrast, it is possible that dbd neural activity positively regulates A08a dendritogenesis, a mechanism that has been reported in *Drosophila* motor neurons (reviewed in Lefebvre et al., 2015). Additional studies are needed to identify the molecular mechanisms used by A08a to achieve the appropriate dendritic morphology during development.

Functional consequences of subcellular synaptic specificity

In other systems, it is well established that subcellular location of synapses has a profound impact on how a neuron propagates information within a circuit (Bloss et al., 2016; Hao et al., 2009; Miles et al., 1996; Pouille et al., 2013; Tobin et al., 2017). From the *Drosophila* larval EM reconstruction, we show that A08a receives distinct input into its medial and lateral dendritic arbors, which is likely to influence how A08a integrates incoming synaptic activity. dbd is a proprioceptive sensory neuron, and A08a is rhythmically active during fictive motor waves (Itakura et al., 2015). Thus, the proper targeting of dbd and A02d to the medial arbor, and A02l and A31x to the lateral arbor, may be important for processing proprioceptive sensory input during locomotion. Although the *dbd-Gal4* line used in our study has ventral sensory "off-target" expression that precludes a behavioral analysis following dbd lateralization, if this off-target expression could be removed, it is possible that the behavioral consequences of dbd lateralization could be determined using recently

developed high resolution quantitative behavior analysis tools (Almeida-Carvalho et al., 2017; Kabra et al., 2013; Klein et al., 2017; Risse et al., 2017). Furthermore, future electrophysiological studies could directly test the functional consequences of the subcellular positioning of A08a inputs on neural processing (e.g. dendritic integration, coincidence detection, and noise suppression).

Materials and Methods

Key Resources Table				
Reagent type (species) or resource	**Designation**	**Source or reference**	**Identifiers**	**Additional information**
Species (*Drosophila melanogaster*)	*26F05-LexA*	BDSC	54702	Expressed in A08a neurons
Species (*D. melanogaster*)	*26F05-Gal4*	BDSC	49192	Expressed in A08a neurons
Species (*D. melanogaster*)	*165-Gal4*	W. Grueber	N/A	Expressed in dbd neurons
Species (*D. melanogaster*)	*UAS-LacZ*	BDSC	8529	Control transgene
Species (*D. melanogaster*)	*UAS-LacZ*	BDSC	8530	Control transgene
Species (*D. melanogaster*)	*UAS-unc-5::HA*	B. Dickson	N/A	UAS drives unc-5
Species (*D. melanogaster*)	*UAS-robo-2::HA*	BDSC	66886	UAS drives robo-2
Species (*D. melanogaster*)	*UAS-bruchpilot(short)-mstrawberry*	S. Sigrist	N/A	UAS drives fluorescently labeled truncated bruchpilot
Species (*D. melanogaster*)	*10xUAS-IVS-myr::smGdP::HA, 13xLexAop2-IVS-myr::smGdP::V5*	BDSC	64092	UAS drives HA membrane tag, LexAop drives V5 membrane tag
Species (*D. melanogaster*)	*UAS-MCFO*	BDSC	64090	UAS drives multi-colored-flip-out
Species (*D. melanogaster*)	*UAS-DenMark, UAS-syt.eGFP*	BDSC	33064	UAS drives DenMark, UAS drives synaptotagmin::GFP
Species (*D. melanogaster*)	*13XLexAop2-IVS-p10-GCaMP6m, 20xUAS-CsChrimson-mCherry*	V. Jayaraman	N/A	LexAop drives GCamp6m, UAS drives Chrimson
Antibody, monoclonal	Mouse anti-V5 tag	Invitrogen, Carlsbad,	Cat. R96025, Lot	(1:1000)

		CA,	1949337	
Antibody, polyclonal	Rabbit anti-mCherry	Novus Biologicals, Littleton, CO	Cat. NBP2-25157, Lot 102816	(1:500)
Antibody, monoclonal	Rat anti-HA tag	Roche Holding, AG, Basel, Switzerland	Cat. 11867423001, Lot 27573500	(1:100, after suggested dilution)
Antibody, monoclonal	Rat anti-OLLAS$^{DyLight-650}$ conjugated antibody	Novus Biologicals, Littleton, CO	Cat. NBP1-06713C, Lot F-090517c	(1:100)
Antibody, polyclonal	Chicken anti GFP	Aves Labs, Inc, Tigard, OR	Cat. GFP-1020, Lot. GFP697986	(1:1000)
Antibody, polyclonal	Rabbit anti-mCherry	Novus Biologicals, Littleton, CO	Cat. NBP2-25157, Lot 102816	(1:500)
Antibody, secondary	Alexa Fluor® 488 AffiniPure Donkey Anti-Mouse IgG (H+L)	Jackson ImmunoResearch, West Grove, PA	Cat. 715-545-151	(1:400)
Antibody, secondary	Rhodamine RedTM-X (RRX) AffiniPure Donkey Anti-Rabbit IgG (H+L)	Jackson ImmunoResearch, West Grove, PA	Cat. 711-295-152	(1:400)
Antibody, secondary	Alexa Fluor® 647 AffiniPure Donkey Anti-Rat IgG (H+L)	Jackson ImmunoResearch, West Grove, PA	Cat. 712-605-153	(1:400)
Antibody, secondary	Alexa Fluor® 488 AffiniPure Donkey Anti-Chicken IgY (IgG) (H+L)	Jackson ImmunoResearch, West Grove, PA	Cat. 703-545-155	(1:400)

Fly stocks

All flies were raised at 25°C on standard cornmeal fly food.

Genotypes	**Figure**
Females containing *10xUAS-IVS-myr::smGdP::HA, 13xLexAop2-IVS-myr::smGdP::V5* (BDSC# 64092); *GMR26F05-LexA* (A08a neurons) (BDSC# 54702), *UAS-bruchpilot (short)-mstraw*; *165-Gal4* (dbd neurons) were crossed to males containing *UAS-lacZ.Exel* (control) (BDSC# 8529)	4.2A-A'; 4.3A-A'', 4.3C-D; 4.4A-A'', 4.4C, 4.4Sup. 1B, E; 4.5A, 4.5D-E
Females containing *10xUAS-IVS-myr::smGdP::HA, 13xLexAop2-IVS-myr::smGdP::V5* (BDSC# 64092); *GMR26F05-LexA* (A08a neurons) (BDSC# 54702), *UAS-bruchpilot(short)-mstraw; 165-Gal4* (dbd neurons) were crossed to males containing *UAS-robo-2::HA* (BDSC# 66886)	4.4Sup 1C, E; 4.5B, 4.5D-E
Females containing *10xUAS-IVS-myr::smGdP::HA, 13xLexAop2-IVS-myr::smGdP::V5* (BDSC# 64092); *GMR26F05-LexA* (A08a neurons) (BDSC# 54702), *UAS-bruchpilot(short)-mstraw; 165-Gal4* (dbd neurons) were crossed to males containing *UAS-unc-5::HA*	4.4B-B'', 4.4D, 4Sup. 1D-E; 4.5C-E
Females containing *GMR57C10-FLPL;; 10xUAS(FRT.stop)myr::smGdP-OLLAS, 10xUAS(FRT.stop)myr::smGdP::HA, 10xUAS(FRT.stop)myr::smGdP::V5-THS-10xUAS(FRT.stop)myr::smGdP-FLAG* (MCFO) (BDSC# 64090) were crossed to males containing *GMR26F05-Gal4* (BDSC# 49192)	4.2B
Females containing *GMR26F05-Gal4* (BDSC# 49192) were crossed to males containing *UAS-DenMark, UAS-syt.eGFP*; *In(3L)D, mirr/TM6C, Sb* (BDSC# 33064)	4.2C-C''
Females containing *GMR26F05-LexA* (BDSC# 54702); *165-Gal4* were crossed to males containing *UAS-lacZ.Exel*; *13XLexAop2-IVS-p10-GCaMP6m, 20xUAS-CsChrimson-mCherry* (control)	4.6A-A', 4.6D, 4.6F, 4.7C-F, 4.8A, 4.8C-C"

Females containing *GMR26F05-LexA* (BDSC# 54702); *165-Gal4, UAS-unc-5::HA* were crossed to males containing *13XLexAop2-IVS-p10-GCaMP6m, 20xUAS-CsChrimson-mCherry*	4.6B-B', 4.6D, 4.7G-J, 4.8D-D"
Females containing *UAS-lacZ.Exel*; *13XLexAop2-IVS-p10-GCaMP6m, 20xUAS-CsChrimson-mCherry* were crossed to males containing *GMR26F05-LexA* (BDSC# 54702) (No Gal4 control)	4.6E-F

Immunohistochemistry and sample preparation

Larval Preparation

Collection of timed larvae: embryos and larvae were raised at 25°C. Embryos were collected on 3.0% agar apple juice caps with yeast paste for 4 hours and then aged for 21 hours. Embryos were transferred to a fresh 3.0% agar apple juice cap and then aged for 4 hours. Hatched larvae were transferred to standard cornmeal fly food vials and aged until dissection.

Immunohistochemistry

Larval brains were dissected in PBS, mounted on 12mm #1.5 thickness poly-L-lysine coated coverslips (Neuvitro Corporation, Vancouver, WA, Cat# H-12-1.5-PLL) and fixed for 23 minutes in fresh 4% paraformaldehyde (PFA) (Electron Microscopy Sciences, Hatfield, PA, Cat. 15710) in PBST. Brains were washed in PBST and then blocked with 2.5% normal donkey serum and 2.5% normal goat serum (Jackson ImmunoResearch Laboratories, Inc., West Grove, PA) in PBST overnight. Brains were incubated in primary antibody for two days at 4°C. The primary was removed and the brains were washed with PBST, then incubated in secondary antibodies overnight at 4°C. The secondary antibody was removed following overnight incubation and the brains were washed in PBST. Brains were dehydrated with an ethanol series (30%, 50%, 75%, 100%, 100%, 100% ethanol; all v/v, 10 minutes each) (Decon Labs, Inc., King of Prussia, PA, Cat. 2716GEA) then incubated in xylene (Fisher Chemical, Eugene, OR, Cat. X5-1) for 2x 10 minutes. Samples were mounted onto slides containing DPX mountant (Millipore Sigma, Burlington, MA, Cat. 06552) and cured for 3 days then stored at 4°C until imaged.

The following primary and secondary antibodies were used:

Primary Antibody (concentration)	Source	Figure
Mouse anti-V5 tag monoclonal antibody (1:1000) Rabbit anti-mCherry polyclonal antibody (1:500) Rat anti-HA tag monoclonal antibody (1:100, after suggested dilution)	Invitrogen, Carlsbad, CA, Cat. R96025, Lot 1949337 Novus Biologicals, Littleton, CO, Cat. NBP2-25157, Lot 102816 Roche Holding, AG, Basel, Switzerland, Cat. 11867423001, Lot 27573500	4.2A-A', 4.3A-A'', 4.3C-C''', 4.4A-B'', 4.4-Sup. 1B-D, 4.5A-C
Rat anti-OLLAS$^{DyLight-650}$ conjugated antibody (1:100)	Novus Biologicals, Littleton, CO, Cat. NBP1-06713C, Lot F-090517c	4.2B
Chicken anti GFP polyclonal antibody (1:1000) (labels Syt:GFP) Rabbit anti-mCherry polyclonal antibody (1:500) (labels DenMark)	Aves Labs, Inc, Tigard, OR, Cat. GFP-1020, Lot. GFP697986 Novus Biologicals, Littleton, CO, Cat. NBP2-25157, Lot 102816	4.2C-C''

Secondary Antibody (concentration)	Source	Figure
Alexa Fluor® 488 AffiniPure Donkey Anti-Mouse IgG (H+L) (1:400) Rhodamine RedTM-X (RRX) AffiniPure Donkey Anti-Rabbit IgG (H+L) (1:400) Alexa Fluor® 647 AffiniPure Donkey Anti-Rat IgG (H+L)	Jackson ImmunoResearch, West Grove, PA, Cat. 715-545-151 Jackson ImmunoResearch, West Grove, PA, Cat. 711-295-152 Jackson ImmunoResearch, West Grove, PA, Cat. 712-605-153	4.2A-A', 4.3A-A'', 4.3C-C''', 4.4A-B'', 4.4-Sup. 1B-D, 4.5A-C
Alexa Fluor® 488 AffiniPure Donkey Anti-Chicken IgY (IgG) (H+L) (1:400) Rhodamine RedTM-X (RRX) AffiniPure Donkey Anti-Rabbit IgG (H+L) (1:400)	Jackson ImmunoResearch, West Grove, PA, Cat. 703-545-155 Jackson ImmunoResearch, West Grove, PA, Cat. 711-295-152	4.2C-C''

Light Microscopy

Fixed larval preparations were imaged with a Zeiss LSM 800 laser scanning confocal (Carl Zeiss AG, Oberkochen, Germany) equipped with an Axio Imager.Z2 microscope. A 63x/ 1.40 NA Oil Plan-Apochromat DIC m27 objective lens and GaAsP photomultiplier tubes were used. Software program used was Zen 2.3 (blue edition) (Carl Zeiss AG, Oberkochen, Germany). For each experiment, all samples were acquired using the same acquisition parameters (see below).

Voxel size	**Excitation wavelength (laser power)**	**Detection wavelength**	**Pinhole size (AU)**	**Figure**
0.090 x 0.090 x 0.280 μm^3	488 nm (0.13%) 561 nm (0.07%) 640 nm (0.14%)	410-541 nm 541-627 nm 656-700 nm	35µm for all channels (488 nm: 0.82AU, 561nm: 0.71AU, 647nm: 0.63AU)	4.2A-A', 4.3A-A'', 4.3C-C''', 4.4A-B'', 4.4-Sup. 1B-D, 4.5A-C'
0.067 x 0.067 x 0.280 μm^3	640 nm (0.65%)	656-700 nm	40µm (0.72AU)	4.2B
0.067 x 0.067 x 0.280 μm^3	488 nm (0.13%) 561 nm (0.25%)	410-540 nm 540-772 nm	43µm (0.99AU) 38µm (0.77AU)	4.2C-C''

Image processing and analyses

Quantification of dbd-A08a synapse voxel distribution

The "synapse voxel" image analyses pipeline identifies Brp voxels that are either one voxel away or already overlapping with membrane containing voxels. Since each voxel size is 90nm, then the "synapse voxels" represent the voxels that have Brp less than 90nm away from membrane voxels.

Image processing and analysis was performed using FIJI (ImageJ 1.50d, https://imagej.net/Fiji). Stepwise, images were rotated

(Image>Transform>Rotate(bicubic)) to align A08a dendrites along the X-axis, then a region of interest was selected in 3D to include A08a dendrites in one hemi-segment (Rectangular selection>Image>Crop). The Brp and A08a dendrite channels were isolated (Image>Color>Split channels). To quantify the amount of voxels containing A08a dendrite signal within 90nm of voxels containing Brp signal, a mask was manually applied to each channel (Image>Adjust>Threshold). The threshold was assigned to include Brp positive voxels and minimize contribution from background. Because of the inherent variability in pixel intensity between different samples (most likely due to the variability of the Gal4 and LexA systems), we could not assign the same threshold to different samples. We found that manually assigning thresholds was a more accurate method of identifying Brp or membrane containing voxels compared to automatic thresholding methods available in FIJI. Importantly, the Brp and membrane thresholds were assigned separately and prior to quantifying the number of overlapping voxels. The Brp mask channel was dilated one iteration (Process>Binary>Dilate). We assigned the 90nm distance threshold to account for the size of the synaptic cleft (~20nm, measured in EM) and the chromatic aberration between 488nm and 555nm wavelengths used to visualize A08a membrane and dbd pre-synapses (~70nm, measured in our light microscope). Then image arithmetic was used to identify the voxels that contain intensity in both the masked A08a dendrite and dilated Brp channels (Process>Image Calculator>Operation "AND"). Images were reduced in the z-dimension (Image>Stacks>Z-project>Sum Slices) and a plot profile was obtained to measure the average voxel intensity across the medial-lateral axis of A08a dendrites (Rectangular selection>Analyze>Plot profile). Distance from the midline was calculated by setting a starting point at the midline and then calculating distance along the medio-lateral axis perpendicular to the midline.

Quantification of A08a dendrite distribution

Image processing and analysis was performed using FIJI (ImageJ 1.50d, https://imagej.net/Fiji). Stepwise, images were rotated (Image>Transform>Rotate(bicubic)) to align A08a dendrites along the X-axis, then a region of interest was selected in 3D to include A08a dendrites in one hemi-segment

(Rectangular selection>Image>Crop). To identify the voxels that contain dendrite intensity a mask was manually applied (Image>Adjust>Threshold). The threshold was assigned to include A08a dendrite positive voxels and minimize contribution from background. To quantify the amount of A08a dendrite positive voxels across the medial-lateral axis, images were reduced in the z-dimension (Image>Stacks>Z-project>Sum Slices) and a plot profile was obtained to measure the average voxel intensity (Rectangular selection>Analyze>Plot profile). An unpaired t-test was used to calculate p-values in Microsoft Excel (Microsoft Corporation, Redmond, WA).

Figure preparation

Images in figures were prepared as either 3D projections in Imaris 9.2.0 (Bitplane AG, Zurich, Switzerland) or maximum intensity projections in FIJI (ImageJ 1.50d, https://imagej.net/Fiji). Scale bars are given for reference on maximum intensity projections and single z-slice micrographs, but do not necessarily represent actual distances, as the tissue samples undergo changes in size during the tissue clearing protocol. Pixel brightness was adjusted in some images for better visualization; all such adjustments were made uniformly over the entire image.

Scale bars were included in all single focal planes and standard maximum intensity projections. In some cases, figures were "3D projected" images exported from the Imaris software, where the scale bars are assigned to match the scale at the "center" of the 3D projection. In these cases, we did not add a scale bar because it would not be accurate for all parts of the image.

Data collection

A power analysis was not performed to determine the appropriate sample size. Many samples were dissected to account for low penetrance of dbd lateralization and to account for damaged samples that were not suitable for image analyses. All sample numbers represent biological replicates. However, we did perform the same experiment on multiple days. We did not exclude any outliers from the data sets. The criteria for excluding samples were as follows. For the fixed tissue preparation, samples with poor dissection quality or poor mounting on slides were excluded as they were unsuitable for

the image analyses pipeline. Samples were also excluded if random "off-target" neuron expression interfered with image analysis. For optogenetic experiments, samples were excluded if sample movement in the z-axis precluded accurate quantification of changes in fluorescence. For lateralized dbd optogenetics, brain segments were excluded from analysis if A08a received input from dbd on the medial dendrite. Samples were allocated into groups by genotype; every genotype was treated as an independent group.

Functional connectivity assays

Newly hatched larvae were aged for 48 ± 4 hours ALH on standard cornmeal fly food at 25°C. At this time, larvae were transferred to apple caps containing wet yeast supplemented with 0.5mM all-*trans* retinal (Sigma-Aldrich, R2500-100MG) and aged at 25°C in the dark. Following another 24 hours (72 ± 4 hours ALH) animals were dissected in HL3.1 saline solution. All dissections were performed in low lighting to prevent premature Chrimson activation. Freshly dissected brains were mounted in HL3.1 saline on 12mm round Poly-L-Lysine coated coverslips.

Confocal experiments (Figures 4.6, 4.8)

GCaMP6m signal in postsynaptic A08a axon terminals was imaged using 0.01% power of the 488nm laser with a 40x objective on a Zeiss LSM800 confocal microscope (NA: 1.4; pinhole size: 32 µm (1AU); detection wavelength: 450-550nm, voxel size: 0.782 x 0.782 x 1μm^3). Chrimson in presynaptic neurons was activated with three pulses of 561 nm laser at 100% power delivered via the same 40x objective using the bleaching function in the ZEN Zeiss software. The total length of the 561nm pulses was about 450msec. After individual recording sessions of *unc-5* expressing samples, Z-stacks of the brain were taken to verify the segments in which A08a exclusively received dbd input onto the lateral dendrite and were therefore permissible for analysis; the few larvae where Chrimson+ off-target neurons were close to A08a neurons were excluded, although due to low signal we can't exclude the possibility of rare or fine contacts. A08a neurons from abdominal segments 3-5 were used for our analyses, as no statistically significant difference in post-stimulus $\Delta F/F_0$ was detected among these neurons.

To quantify $\Delta F/F_0$ traces we used a custom MATLAB script (The MathWorks, Natick, MA). The script first performs rigid registration to correct for movement artifacts during recording, and then allows for ROI selection. ROIs were drawn around A08a axon terminals in individual segments, and ROI size was constant across all experiments (Figure 4.6C). F_0 was set as the average fluorescence of the 3 frames acquired before each 561nm light stimulus. For a single animal, we first average $\Delta F/F_0$ traces for six consecutive 561nm stimuli separated by 20 488nm acquisition frames (4 frames/sec). These 20 frames are enough time to allow GCaMP6m fluorescence to return to baseline. Traces were then averaged across animals to determine the mean $\Delta F/F_0$ for each experimental group. Mean post-stimulus $\Delta F/F_0$ was calculated by first subtracting the mean F_0 from the mean F in the first frame post-stimulus, then dividing the resulting ΔF by the mean F_0. The mean was then calculated for each experimental group.

For demonstrating monosynaptic connectivity between dbd and A08a, brains were dissected and mounted in 3µM TTX (Abcam, Cambridge, MA, ab120055) diluted in HL3.1. Brains were incubated for 5 minutes in the TTX solution prior to the recording session. To first determine the effectiveness of TTX, spontaneous A08a GCaMP6m activity was recorded over 5 minutes with and without TTX (in *lacZ* control animals). Spontaneous GCaMP6m activity was recorded on an LSM800 with a 40X objective (NA: 1.4; excitation wavelength: 488nm; detection wavelength: 492-555nm; pinhole size: 32 µm (1AU)). Once it was established that TTX eliminates spontaneous rhythmic A08a activity, we dissected fresh brains in TTX and performed the same Chrimson activation paradigm (using the same bleaching protocol and image acquisition settings) as described above to test monosynaptic connectivity.

Two photon experiments (Figure 4.7)

Images were generated using a galvanometric and resonant scan mirror-based two-photon microscope (VIVO Multiphoton™ Movable Objective RS+ Microscope and Vector™ resonant galvo scanner, 3i Intelligent Imaging Innovations, Denver, CO). A W Plan-Apochromat 20x/1.0NA Water Dipping Objective (apochromatically corrected 480nm-1300nm) with a working distance of 2.3mm was used for delivery of excitation and stimulation laser excitation. The imaging system utilizes the Chameleon Discovery

duel wavelength laser system (Coherent, Santa Clara, CA) as the pump laser. The pump laser supplies 100fs pulses at an 80MHz repetition with an output power of 1.3W at 940nm and 3.9W at 1040nm. Imaging was accomplished at 40Hz frame rate while averaging 5 frames per image with a scan range of 578um x 571um and a pixel size of 1.47um x 1.42um. GCaMP6m and mCherry were excited using 940 nm (27mW) and 1040nm (200-244mW) radiation respectively while the fluorescence was collected with two fast-gated GaAsP PMTs having filter sets that selectively collect fluorescence between 490-560nm for the green channel and 570-640nm in the red channel.

Sample stimulation was based around a 5W, 192fs, 10MHz laser system for excitation of Chrimson at 1040nm (FemtoTrain 1040-5, Spectra-Physics, Santa Clara, CA). Excitation was delivered through the objective with a phase-only spatial light modulator (SLM) (Phasor, computer—generated holography system, 3i Intelligent Imaging Innovations, Denver, CO) for precise patterned and 3D photomanipulation. Between 21mw and 66mw were used in 100ms stimulation pulses for Chrimson activation. Stimulation ROIs were 10um diameter circles localized over regions of interest. Holographic based stimulation allowed for Chrimson activation at arbitrary depths within the sample while continuously monitoring the imaging plane for an A08a response.

Statistical analyses

Statistical analyses for optogenetic experiments were performed with MATLAB and R. For analyzing the statistical significance of mean post-stimulus $\Delta F/F_0$, an H-test was used to determine whether the data for each experimental group were normally distributed. Because these data were non-normally distributed, a Mann-Whitney test was performed to determine whether there were statistically significant differences in mean $\Delta F/F_0$ among experimental groups. To analyze potential differences in F_0 among + and - ATR groups we used a Pairwise Wilcox Test to calculate comparisons between each experimental group. This was followed by a Benjamini & Hochberg correction for multiple testing. All code for analysis of optogenetic data in Figures 5-7 is deposited at the following GitHub repository https://github.com/timothylwarren/elife_larvae_2019.

Acknowledgements

We thank Larry Scatena for expert technical assistance with the two photon experiments, and for panels 6A and B. Wes Grueber for providing *165-Gal4*, Stephan Sigrist for providing *UAS-brp-short::mstraw*, Vivek Jayaraman for providing optogenetics fly stocks, and Barry Dickson for providing *UAS-unc-5* stocks. We thank Brandon Mark for MATLAB scripts and support with the CATMAID database. We thank Keiko Hirono for assistance with embryo and larval collections. We thank Casey Doe and Cooper Doe for assistance with brain dissections. We thank Aref Zarin and Avinash Khandelwal for annotating neurons in the CATMAID database. We thank lab members, Tory Herman, Shawn Lockery, Judith Eisen, Joseph Brückner, and Adam Miller for comments on the manuscript. We thank Jan Trout for model neuron illustrations in Figure 1. Stocks obtained from the Bloomington Drosophila Stock Center (NIH P40OD018537) were used in this study. Funding was provided by HHMI (CQD, ECS, ELH, TLW), NIH HD27056 (CQD), and NIH Developmental Biology Training Grant T32-HD07348 (ELH). Emily C. Sales is a Howard Hughes Medical Institute Gilliam Fellow.

CHAPTER V

CONCLUSION

Understanding how developing neural circuits assemble with cellular and subcellular precision will impact society through the advancement of technology and medicine. Characterizing the genes that govern synapse specificity will enable the exploration of the underlying cellular mechanisms that mediate this specificity. For example, one can study gene function within the context of particular mechanisms that influence specificity, such as: developmental origins of diverse cell types, neural activity dependent refinement of circuits, or environmental contributions to circuit architecture. The understanding of how these biological processes regulate synapse specificity will support the development of medicinal treatments (eg. biomarkers, drug targets, therapeutics) and the development of novel neural circuits (eg. regeneration of biological circuits, generation of novel computational neural circuits).

The genes underlying synapse specificity have been difficult to identify. Establishing model systems, like the one described here, will be critical to speed up the identification of these genes. Model systems spanning different model organisms, circuit types, and neuron types will provide a more comprehensive understanding of this process. An interdisciplinary approach will also be critical to identify these genes. Single cell RNA sequencing advances will lead to the better characterization of gene expression in individual neurons. Biotechnologies to manipulate genes or entire gene families with precise spatial and temporal control will inform how genetic programs are used by neurons. Computational approaches, such as machine learning algorithms, will better predict relevant cellular pathways and protein interactions. Taken together, these strategies will better define the relationship between genes and neural circuits.

Here, using a novel model system in the *Drosophila* larval nerve cord, I was able to test the role of genes in synapse formation. I took a candidate gene approach, focusing on CSMs with unique and specific binding interactions. I tested the role of genes in the Dpr and DIP families in synaptic partners, dbd and A08a, and did not identify a role for them in synapse formation. Other genes remain to be tested, both in the context of both

synaptically coupled and non-synaptically coupled neurons. For example, an RNAi screen could be performed to identify genes necessary for synapse formation between synaptic partners, and a misexpression screen could be performed to identify genes that are sufficient for synapse formation between neurons that are normally not synaptically coupled, such as dbd and A27j.

The better characterization of Dpr and DIP genes in several neural processes is warranted. Many open questions remain, including: Do Dpr and DIP genes regulate axon fasciculation and contribute to parsing out neuropil domains into anatomical regions that process specific kinds of information? Do neurons that express Dpr and DIP genes early in development act as pioneer neurons? How do neural stem cells assign neurons different Dpr and DIP expression profiles? Can Dpr and DIP proteins mediate mechanotransduction in the peripheral nervous system? Describing the various roles of these gene families will help define their function and also broadly increase our understanding of neural circuit assembly, function, and maintenance.

Understanding how neural circuits assemble at the subcellular level is also important. The studies I presented here, emphasize the role of axon guidance cues in the subcellular positioning of dbd along the dendritic domain of A08a neurons. Most likely there are molecular labels on the axon of A08a that prevent ectopic dbd synapse formation. Future studies might be able to identify these molecular labels and characterize their expression on the subcellular level. For example, how are CSMs localized to particular subcellular domains? Is the subcellular localization of these proteins dependent on non-cell autonomous mechanisms, neural activity, or neural stem cell lineage? Future studies can also focus on how developmental processes to establish synapse specificity contribute to neural circuit structure and function.

It will also be important to characterize the role of dendritogenesis with respect to synapse specificity and neuronal morphology. Manipulations of dbd neuropil position resulted in changes in A08a dendritic morphology, suggesting dbd may actively regulate dendrite formation on its post-synaptic partner, A08a. How these morphological changes of the dendritic structure of A08a impact synaptic input integration remain to be explored. The dbd-A08a model system, coupled with electrophysiological and modeling

approaches, would be a tractable in vivo model system to investigate the functional consequences of subcellular synaptic specificity.

REFERENCES CITED

Allensworth, E. M., Healey, K., Gwynne, J. A., & Crespin, R. (n.d.). *High School Graduation Rates through Two Decades of District Change The Influence of Policies, Data Records, and Demographic Shifts?* Retrieved from https://files.eric.ed.gov/fulltext/ED568549.pdf

Almeida-Carvalho, M. J., Berh, D., Braun, A., Chen, Y., Eichler, K., Eschbach, C., … Zlatic, M. (2017). The Ol $_1$ mpiad: concordance of behavioural faculties of stage 1 and stage 3 *Drosophila* larvae. *The Journal of Experimental Biology*, *220*(13), 2452–2475. https://doi.org/10.1242/jeb.156646

Altman, J., & Anderson, W. J. (1972). Experimental reorganization of the cerebellar cortex. I. Morphological effects of elimination of all microneurons with prolonged x-irradiation started at birth. *The Journal of Comparative Neurology*, *146*(3), 355–405. https://doi.org/10.1002/cne.901460305

Ango, F., di Cristo, G., Higashiyama, H., Bennett, V., Wu, P., & Huang, Z. J. (2004). Ankyrin-Based Subcellular Gradient of Neurofascin, an Immunoglobulin Family Protein, Directs GABAergic Innervation at Purkinje Axon Initial Segment. *Cell*, *119*(2), 257–272. https://doi.org/10.1016/j.cell.2004.10.004

Ashley, J., Sorrentino, V., Lobb-Rabe, M., Nagarkar-Jaiswal, S., Tan, L., Xu, S., … Carrillo, R. A. (2019). Transsynaptic interactions between IgSF proteins DIP-α and Dpr10 are required for motor neuron targeting specificity. *ELife*, *8*. https://doi.org/10.7554/eLife.42690

Berry, M., McConnell, P., & Sievers, J. (1980). Chapter 4 Dendritic Growth and The Control of Neuronal Form. *Current Topics in Developmental Biology*, *15*, 67–101. https://doi.org/10.1016/S0070-2153(08)60117-9

Bloss, E. B., Cembrowski, M. S., Karsh, B., Colonell, J., Fetter, R. D., & Spruston, N. (2016). Structured Dendritic Inhibition Supports Branch-Selective Integration in CA1 Pyramidal Cells. *Neuron*, *89*(5), 1016–1030. https://doi.org/10.1016/j.neuron.2016.01.029

Borgen, M., Rowland, K., Boerner, J., Lloyd, B., Khan, A., & Murphey, R. (2017). Axon Termination, Pruning, and Synaptogenesis in the Giant Fiber System of *Drosophila melanogaster* Is Promoted by Highwire. *Genetics*, *205*(3), 1229–1245. https://doi.org/10.1534/genetics.116.197343

Brand, A. H., & Perrimon, N. (1993). Targeted gene expression as a means of altering cell fates and generating dominant phenotypes. *Development (Cambridge, England)*, *118*(2), 401–415. Retrieved from http://www.ncbi.nlm.nih.gov/pubmed/8223268

Carrillo, R. A., Özkan, E., Menon, K. P., Nagarkar-Jaiswal, S., Lee, P. T., Jeon, M., … Zinn, K. (2015). Control of Synaptic Connectivity by a Network of Drosophila IgSF Cell Surface Proteins. *Cell*, *163*(7), 1770–1782. https://doi.org/10.1016/j.cell.2015.11.022

Cheng, S., Park, Y., Kurleto, J. D., Jeon, M., Zinn, K., Thornton, J. W., … analyzed data, E. (2019). *Family of neural wiring receptors in bilaterians defined by phylogenetic, biochemical, and structural evidence Data deposition: The atomic coordinates and structure factors have been deposited in the Protein Data Bank, www.wwpdb.org (PDB ID codes 6ON6, 6O*. https://doi.org/10.1073/pnas.1818631116

Chisholm, A. D., Hutter, H., Jin, Y., & Wadsworth, W. G. (2016). The Genetics of Axon Guidance and Axon Regeneration in Caenorhabditis elegans. *Genetics*, *204*(3), 849–882. https://doi.org/10.1534/genetics.115.186262

Christensen, R., Shao, Z., & Colón-Ramos, D. A. (2013). The cell biology of synaptic specificity during development. *Current Opinion in Neurobiology*, *23*(6), 1018–1026. https://doi.org/10.1016/j.conb.2013.07.004

Colon-Ramos, D. A., Margeta, M. A., & Shen, K. (2007). Glia Promote Local Synaptogenesis Through UNC-6 (Netrin) Signaling in C. elegans. *Science*, *318*(5847), 103–106. https://doi.org/10.1126/science.1143762

Cosmanescu, F., Katsamba, P. S., Sergeeva, A. P., Zipursky, S. L., Honig, B., & Shapiro Correspondence, L. (2018). Neuron-Subtype-Specific Expression, Interaction Affinities, and Specificity Determinants of DIP/Dpr Cell Recognition Proteins. *Neuron*, *100*, 1385-1400.e6. https://doi.org/10.1016/j.neuron.2018.10.046

Dickson, B. J. (2002). Molecular Mechanisms of Axon Guidance. *Science*, *298*(5600), 1959–1964. https://doi.org/10.1126/science.1072165

Fouquet, W., Owald, D., Wichmann, C., Mertel, S., Depner, H., Dyba, M., … Sigrist, S. J. (2009). Maturation of active zone assembly by Drosophila Bruchpilot. *The Journal of Cell Biology*, *186*(1), 129–145. https://doi.org/10.1083/jcb.200812150

Fuller Torrey, E., Lamb, R., & Pavle, J. (2010). *More Mentally Ill Persons Are in Jails and Prisons Than Hospitals: A Survey of the States*. Retrieved from https://www.treatmentadvocacycenter.org/storage/documents/final_jails_v_hospitals_study.pdf

Fushiki, A., Zwart, M. F., Kohsaka, H., Fetter, R. D., Cardona, A., & Nose, A. (2016). A circuit mechanism for the propagation of waves of muscle contraction in Drosophila. *ELife*, *5*, e13253. https://doi.org/10.7554/eLife.13253

Gerhard, S., Andrade, I., Fetter, R. D., Cardona, A., & Schneider-Mizell, C. M. (2017). *Conserved neural circuit structure across Drosophila larval development revealed by comparative connectomics*. https://doi.org/10.7554/eLife.29089.001

Giovedí, S., Corradi, A., Fassio, A., & Benfenati, F. (2014). Involvement of synaptic genes in the pathogenesis of autism spectrum disorders: the case of synapsins. *Frontiers in Pediatrics*, *2*, 94. https://doi.org/10.3389/fped.2014.00094

Godenschwege, T. A., Hu, H., Shan-Crofts, X., Goodman, C. S., & Murphey, R. K. (2002). Bi-directional signaling by Semaphorin 1a during central synapse formation in Drosophila. *Nature Neuroscience*, *5*(12), 1294–1301. https://doi.org/10.1038/nn976

Godenschwege, T. A., & Murphey, R. K. (2009). Genetic Interaction of Neuroglian and Semaphorin1a during Guidance and Synapse Formation. *Journal of Neurogenetics*, *23*(1–2), 147. https://doi.org/10.1080/01677060802441380

Gohl, D. M., Silies, M. A., Gao, X. J., Bhalerao, S., Luongo, F. J., Lin, C.-C., … Clandinin, T. R. (2011). A versatile in vivo system for directed dissection of gene expression patterns. *Nature Methods*, *8*(3), 231–237. Retrieved from http://www.ncbi.nlm.nih.gov/pubmed/21473015

Hao, J., Wang, X., Dan, Y., Poo, M., & Zhang, X. (2009). An arithmetic rule for spatial summation of excitatory and inhibitory inputs in pyramidal neurons. *Proceedings of the National Academy of Sciences of the United States of America*, *106*(51), 21906–21911. https://doi.org/10.1073/pnas.0912022106

Heckscher, E. S., Zarin, A. A., Faumont, S., Clark, M. Q., Manning, L., Fushiki, A., … Doe, C. Q. (2015). Even-Skipped+ Interneurons Are Core Components of a Sensorimotor Circuit that Maintains Left-Right Symmetric Muscle Contraction Amplitude. *Neuron*, 1–16. https://doi.org/10.1016/j.neuron.2015.09.009

Huang, Z. J., Di Cristo, G., & Ango, F. (2007). Development of GABA innervation in the cerebral and cerebellar cortices. *Nature Reviews Neuroscience*, *8*(9), 673–686. https://doi.org/10.1038/nrn2188

Itakura, Y., Kohsaka, H., Ohyama, T., Zlatic, M., Pulver, S. R., & Nose, A. (2015). Identification of inhibitory premotor interneurons activated at a late phase in a motor cycle during drosophila larval locomotion. *PLoS ONE*, *10*(9), 1–24. https://doi.org/10.1371/journal.pone.0136660

Kabra, M., Robie, A. A., Rivera-Alba, M., Branson, S., & Branson, K. (2013). JAABA: interactive machine learning for automatic annotation of animal behavior. *Nature Methods*, *10*(1), 64–67. https://doi.org/10.1038/nmeth.2281

Keleman, K., & Dickson, B. J. (2001). Short- and long-range repulsion by the Drosophila Unc5 netrin receptor. *Neuron*, *32*(4), 605–617. Retrieved from http://www.ncbi.nlm.nih.gov/pubmed/11719202

Kimmel, C. B., Powell, S. L., & Kimmel, R. J. (1982). Specific reduction of development of the Mauthner neuron lateral dendrite after otic capsule ablation in Brachydanio rerio. *Developmental Biology*, *91*(2), 468–473. https://doi.org/10.1016/0012-1606(82)90053-7

Klapoetke, N. C., Murata, Y., Kim, S. S., Pulver, S. R., Birdsey-Benson, A., Cho, Y. K., … Boyden, E. S. (2014). Independent optical excitation of distinct neural populations. *Nature Methods*, *11*(3), 338–346. https://doi.org/10.1038/nmeth.2836

Klassen, M. P., & Shen, K. (2007). Wnt Signaling Positions Neuromuscular Connectivity by Inhibiting Synapse Formation in C. elegans. *Cell*, *130*(4), 704–716. https://doi.org/10.1016/j.cell.2007.06.046

Klein, M., Krivov, S. V, Ferrer, A. J., Luo, L., Samuel, A. D., & Karplus, M. (2017). Exploratory search during directed navigation in C. elegans and Drosophila larva. *ELife*, *6*. https://doi.org/10.7554/eLife.30503

Kohsaka, H., Takasu, E., Morimoto, T., & Nose, A. (2014). A Group of Segmental Premotor Interneurons Regulates the Speed of Axial Locomotion in Drosophila Larvae. *Current Biology*, *24*(22), 2632–2642. https://doi.org/10.1016/j.cub.2014.09.026

Kubick, N., Brösamle, D., & Mickael, M.-E. (2018). Molecular Evolution and Functional Divergence of the IgLON Family. *Evolutionary Bioinformatics Online*, *14*, 1176934318775081. https://doi.org/10.1177/1176934318775081

Lai, S.-L., & Lee, T. (2006). Genetic mosaic with dual binary transcriptional systems in Drosophila. *Nature Neuroscience*, *9*(5), 703–709. https://doi.org/10.1038/nn1681

Lefebvre, J. L., Sanes, J. R., & Kay, J. N. (2015). Development of Dendritic Form and Function. *Annual Review of Cell and Developmental Biology*, *31*(1), 741–777. https://doi.org/10.1146/annurev-cellbio-100913-013020

Li-Kroeger, D., Kanca, O., Lee, P.-T., Cowan, S., Lee, M. T., Jaiswal, M., … Bellen, H. J. (2018). An expanded toolkit for gene tagging based on MiMIC and scarless CRISPR tagging in Drosophila. *ELife*, *7*, 1–27. https://doi.org/10.7554/elife.38709

Merikangas, K. R., He, J.-P., Burstein, M., Swanson, S. A., Avenevoli, S., Cui, L., … Swendsen, J. (2010). Lifetime prevalence of mental disorders in U.S. adolescents: results from the National Comorbidity Survey Replication--Adolescent Supplement (NCS-A). *Journal of the American Academy of Child and Adolescent Psychiatry*, *49*(10), 980–989. https://doi.org/10.1016/j.jaac.2010.05.017

Meyer, R. L. (1998). Roger Sperry and his chemoaffinity hypothesis. *Neuropsychologia*, *36*(10), 957–980. https://doi.org/10.1016/S0028-3932(98)00052-9

Miles, R., Tóth, K., Gulyás, A. I., Hájos, N., & Freund, T. F. (1996). Differences between somatic and dendritic inhibition in the hippocampus. *Neuron*, *16*(4), 815–823. https://doi.org/10.1016/S0896-6273(00)80101-4

Mizumoto, K., & Shen, K. (2013). Interaxonal Interaction Defines Tiled Presynaptic Innervation in C. elegans. *Neuron*, *77*(4), 655–666. https://doi.org/10.1016/J.NEURON.2012.12.031

Morest, D. K. (1969). The growth of dendrites in the mammalian brain. *Zeitschrift Fur Anatomie Und Entwicklungsgeschichte*, *128*(4), 290–317. Retrieved from http://www.ncbi.nlm.nih.gov/pubmed/4899901

Nakamura, M., Baldwin, D., Hannaford, S., Palka, J., & Montell, C. (2002). Defective proboscis extension response (DPR), a member of the Ig superfamily required for the gustatory response to salt. *The Journal of Neuroscience : The Official Journal of the Society for Neuroscience*, *22*(9), 3463–3472. https://doi.org/20026336

Narahashi, T., MOORE, J. W., & SCOTT, W. R. (1964). Tetrodotoxin Blockage of Sodium Conductance Increase in Lobster Giant Axons. *The Journal of General Physiology*, *47*(5), 965–974. https://doi.org/10.1085/jgp.47.5.965

Nicolaï, L. J. J., Ramaekers, A., Raemaekers, T., Drozdzecki, A., Mauss, A. S., Yan, J., … Hassan, B. A. (2010). Genetically encoded dendritic marker sheds light on neuronal connectivity in Drosophila. *Proceedings of the National Academy of Sciences of the United States of America*, *107*(47), 20553–20558. https://doi.org/10.1073/pnas.1010198107

Owald, D., Fouquet, W., Schmidt, M., Wichmann, C., Mertel, S., Depner, H., … Sigrist, S. J. (2010). A Syd-1 homologue regulates pre- and postsynaptic maturation in *Drosophila*. *The Journal of Cell Biology*, *188*(4), 565–579. https://doi.org/10.1083/jcb.200908055

Özkan, E., Carrillo, R. a, Eastman, C. L., Weiszmann, R., Waghray, D., Johnson, K. G., … Garcia, K. C. (2013). An extracellular interactome of immunoglobulin and LRR proteins reveals receptor-ligand networks. *Cell*, *154*, 228–239. https://doi.org/10.1016/j.cell.2013.06.006

Pearson, K. G., & Fourtner, C. R. (1975). Nonspiking interneurons in walking system of the cockroach. *Journal of Neurophysiology*, *38*(1), 33–52. https://doi.org/10.1152/jn.1975.38.1.33

Petreanu, L., Mao, T., Sternson, S. M., & Svoboda, K. (2009). The subcellular organization of neocortical excitatory connections. *Nature*, *457*(7233), 1142–1145. https://doi.org/10.1038/nature07709

Pfeiffer, B. D., Ngo, T.-T. B., Hibbard, K. L., Murphy, C., Jenett, A., Truman, J. W., & Rubin, G. M. (2010). Refinement of tools for targeted gene expression in Drosophila. *Genetics*, *186*(2), 735–755. https://doi.org/10.1534/genetics.110.119917

Pippow, A., Husch, A., Pouzat, C., & Kloppenburg, P. (2009). Differences of Ca2+ handling properties in identified central olfactory neurons of the antennal lobe. *Cell Calcium*, *46*(2), 87–98. https://doi.org/10.1016/j.ceca.2009.05.004

Pouille, F., Watkinson, O., Scanziani, M., & Trevelyan, A. J. (2013). The contribution of synaptic location to inhibitory gain control in pyramidal cells. *Physiol Rep*, *1*(5), 67. https://doi.org/10.1002/phy2.67

Prahlad, A., Spalthoff, C., Kong, D., Großhans, J., Göpfert, M. C., & Schmidt, C. F. (2017). Mechanical Properties of a Drosophila Larval Chordotonal Organ. *Biophysical Journal*, *113*(12), 2796–2804. https://doi.org/10.1016/j.bpj.2017.08.061

Pulver, S. R., Bayley, T. G., Taylor, A. L., Berni, J., Bate, M., & Hedwig, B. (2015). Imaging fictive locomotor patterns in larval *Drosophila*. *Journal of Neurophysiology*, *114*(5), 2564–2577. https://doi.org/10.1152/jn.00731.2015

Redmond, L., & Ghosh, A. (2005). Regulation of dendritic development by calcium signaling. *Cell Calcium*, *37*(5), 411–416. https://doi.org/10.1016/j.ceca.2005.01.009

Risse, B., Berh, D., Otto, N., Klämbt, C., & Jiang, X. (2017). FIMTrack: An open source tracking and locomotion analysis software for small animals. *PLOS Computational Biology*, *13*(5), e1005530. https://doi.org/10.1371/journal.pcbi.1005530

Rostron, B. L., Boies, J. L., & Arias, E. (2010). Education reporting and classification on death certificates in the United States. *Vital and Health Statistics. Series 2, Data Evaluation and Methods Research*, (151), 1–21. Retrieved from http://www.ncbi.nlm.nih.gov/pubmed/25093685

Saalfeld, S., Fetter, R., Cardona, A., & Tomancak, P. (2012). Elastic volume reconstruction from series of ultra-thin microscopy sections. *Nature Methods*, *9*(7), 717–720. https://doi.org/10.1038/nmeth.2072

Sakurai, T. (2017). The role of cell adhesion molecules in brain wiring and neuropsychiatric disorders. *Molecular and Cellular Neuroscience*, *81*, 4–11. https://doi.org/10.1016/J.MCN.2016.08.005

Samhsa. (2009). *Current Statistics on the Prevalence and Characteristics of People Experiencing Homelessness in the United States*. Retrieved from https://www.samhsa.gov/sites/default/files/programs_campaigns/homelessness_programs_resources/hrc-factsheet-current-statistics-prevalence-characteristics-homelessness.pdf

Schneider-Mizell, C. M., Gerhard, S., Longair, M., Kazimiers, T., Li, F., Zwart, M. F., … Cardona, A. (2016). *Quantitative neuroanatomy for connectomics in Drosophila*. https://doi.org/10.7554/eLife.12059.001

Schrader, S., & Merritt, D. J. (2000). Central projections ofDrosophila sensory neurons in the transition from embryo to larva. *The Journal of Comparative Neurology*, *425*(1), 34–44. https://doi.org/10.1002/1096-9861(20000911)425:1<34::AID-CNE4>3.0.CO;2-G

Simpson, J. H., Bland, K. S., Fetter, R. D., & Goodman, C. S. (2000). Short-range and long-range guidance by Slit and its Robo receptors: a combinatorial code of Robo receptors controls lateral position. *Cell*, *103*(7), 1019–1032. Retrieved from http://www.ncbi.nlm.nih.gov/pubmed/11163179

Simpson, J. H., Kidd, T., Bland, K. S., & Goodman, C. S. (2000). Short-range and long-range guidance by slit and its Robo receptors. Robo and Robo2 play distinct roles in midline guidance. *Neuron*, *28*(3), 753–766. Retrieved from http://www.ncbi.nlm.nih.gov/pubmed/11163264

Soni, A. (2009). *The Five Most Costly Conditions, 1996 and 2006: Estimates for the U.S. Civilian Noninstitutionalized Population*. Retrieved from http://www.meps.ahrq.gov/mepsweb/data_files/publications/mr2/mr2.shtml

Sperry, R. W. (1963). Chemoaffinity in the Orderly Growth of Nerve Fiber Patterns and Connections*. *Proceedings of the National Academy of Sciences of the United States of America*, *50*, 703–710. https://doi.org/10.1073/pnas.50.4.703

Suslak, T. J., & Jarman, A. P. (2016). *Stretching the imagination beyond muscle spindles-stretch-sensitive mechanisms in arthropods*. https://doi.org/10.1111/joa.12329

Suslak, T. J., Watson, S., Thompson, K. J., Shenton, F. C., Bewick, G. S., Armstrong, J. D., & Jarman, A. P. (2015). Piezo Is Essential for Amiloride-Sensitive Stretch-Activated Mechanotransduction in Larval Drosophila Dorsal Bipolar Dendritic Sensory Neurons. *PLOS ONE*, *10*(7), e0130969. https://doi.org/10.1371/journal.pone.0130969

Tan, L., Zhang, K. X., Matthew, Y., Bellen, H. J., Morey, M., Tan, L., … Takemura, S. (2015). Ig Superfamily Ligand and Receptor Pairs Expressed in Synaptic Partners in Drosophila Article Ig Superfamily Ligand and Receptor Pairs Expressed in Synaptic Partners in Drosophila. *Cell*, *163*(7), 1756–1769. https://doi.org/10.1016/j.cell.2015.11.021

Telley, L., Cadilhac, C., Cioni, J.-M., Saywell, V., Jahannault-Talignani, C., Huettl, R. E., … Ango, F. (2016). Dual Function of NRP1 in Axon Guidance and Subcellular Target Recognition in Cerebellum. *Neuron*, *91*(6), 1276–1291. https://doi.org/10.1016/j.neuron.2016.08.015

Tessier-Lavigne, M., & Goodman, C. S. (1996). The molecular biology of axon guidance. *Science (New York, N.Y.)*, *274*(5290), 1123–1133. Retrieved from http://www.ncbi.nlm.nih.gov/pubmed/8895455

Tobin, W. F., Wilson, R. I., & Lee, W.-C. A. (2017). Wiring variations that enable and constrain neural computation in a sensory microcircuit. *ELife*, *6*. https://doi.org/10.7554/eLife.24838

Van't Hof, W., & Resh, M. D. (2000). Targeting proteins to plasma membrane and membrane microdomains by N-terminal myristoylation and palmitoylation. *Methods in Enzymology*, *327*, 317–330. https://doi.org/10.1016/S0076-6879(00)27287-X

Venkatasubramanian, L., Guo, Z., Xu, S., Tan, L., Xiao, Q., Nagarkar-Jaiswal, S., & Mann, R. S. (2019). Stereotyped terminal axon branching of leg motor neurons mediated by IgSF proteins DIP-α and Dpr10. *ELife*, *8*. https://doi.org/10.7554/eLife.42692

Venken, K. J. T., Schulze, K. L., Haelterman, N. a, Pan, H., He, Y., Evans-Holm, M., … Bellen, H. J. (2011). MiMIC: a highly versatile transposon insertion resource for engineering Drosophila melanogaster genes. *Nature Methods*, *8*(9), 737–743. https://doi.org/10.1038/nmeth.1662

Viswanathan, S., Williams, M. E., Bloss, E. B., Stasevich, T. J., Speer, C. M., Nern, A., … Looger, L. L. (2015). High-performance probes for light and electron microscopy. *Nature Methods*, *12*(6), 568–576. https://doi.org/10.1038/nmeth.3365

Vogel, C., & Chothia, C. (2006). Protein Family Expansions and Biological Complexity. *PLoS Computational Biology*, *2*(5), e48. https://doi.org/10.1371/journal.pcbi.0020048

Wang, X., Shaw, W. R., Tsang, H. T. H., Reid, E., & O'Kane, C. J. (2007). Drosophila spichthyin inhibits BMP signaling and regulates synaptic growth and axonal microtubules. *Nature Neuroscience*, *10*(2), 177–185. https://doi.org/10.1038/nn1841

Washbourne, P. (2004). Cell Adhesion Molecules in Synapse Formation. *Journal of Neuroscience*, *24*(42), 9244–9249. https://doi.org/10.1523/jneurosci.3339-04.2004

Washbourne, Philip. (2015). Synapse assembly and neurodevelopmental disorders. *Neuropsychopharmacology : Official Publication of the American College of Neuropsychopharmacology*, *40*(1), 4–15. https://doi.org/10.1038/npp.2014.163

Yogev, S., & Shen, K. (2014). Cellular and Molecular Mechanisms of Synaptic Specificity. *Annual Review of Cell and Developmental Biology*, *30*, 417–437. https://doi.org/10.1146/annurev-cellbio-100913-012953

Zhan, H., Bruckner, J., Zhang, Z., & O'Connor-Giles, K. (2016). Three-dimensional imaging of Drosophila motor synapses reveals ultrastructural organizational patterns. *Journal of Neurogenetics*, *30*(3–4), 237–246. https://doi.org/10.1080/01677063.2016.1253693

Zlatic, M., Landgraf, M., & Bate, M. (2003). Genetic specification of axonal arbors: atonal regulates robo3 to position terminal branches in the Drosophila nervous system. *Neuron*, *37*(1), 41–51. Retrieved from http://www.ncbi.nlm.nih.gov/pubmed/12526771

Zlatic, M., Li, F., Strigini, M., Grueber, W., & Bate, M. (2009). Positional Cues in the Drosophila Nerve Cord: Semaphorins Pattern the Dorso-Ventral Axis. *PLoS Biology*, *7*(6), e1000135. https://doi.org/10.1371/journal.pbio.1000135